SECOND QUARTERLY PROGRESS REPORT

14 August 1964 to 14 November 1964

Contract NAS 8-11204

FEASIBILITY STUDY FOR DEVELOPMENT OF A HYPERVELOCITY GUN

for

National Aeronautics and Space Administration
George C. Marshall Space Flight Center

8 December 1964

MB-R-64/86

MB ASSOCIATES
San Ramon
(near San Francisco)
California
837-7201

I. INTRODUCTION

The work statement for the second quarter of this contract specified six tasks of two general kinds: those concerned with answering some remaining questions about the operation of the rail gun and those concerned with setting up an auxiliary field system. The following sections describe our progress in carrying out these tasks.

II. VOLTAGE MEASUREMENTS ACROSS THE MUZZLE AND BREECH

The voltage differences shown in Figure 1 are related in the following way:

$$V_b = V_m + \frac{d}{dt}(LI) \qquad (1)$$

where I is the total current through the arc and L is the inductance included between the breech and the arc. By decomposing

we have:

$$V_b = V_m + L'\dot{x}I + L\dot{I} \qquad (2)$$

where L' is the inductance per unit length of the rails. (V_m, which is the voltage across the arc, may be measured anywhere across the rails in front of the arc.)

The following actual measurement of I, L', V_b, V_m, and $\dot{x}$ taken at peak current ($\dot{I}$ =0) were consistent with equation (2):

$$I = 290 \text{ k amp}$$

$$L' = .28\,\mu\text{h/m}$$

$$\dot{x} = 3.2 \text{ km/sec}$$

$$V_b = 700 \text{ v}$$

$$V_m = 440 \text{ v}$$

The total electric power into the gun is $V_b I$. Of this, $V_m I$ is irretrievably dissipated in the arc, $L\dot{I}I$ goes into increasing the magnetic field in the region between the breech and the arc, $\frac{1}{2}L'I^2\dot{x}$ into creating field in the region being uncovered by the motion of the arc, and $\frac{1}{2}L'I^2\dot{x}$ into the kinetic energy of the arc-projectile system. The fraction V_m/V_b is, therefore, a minimum measure of the energy inefficiency of the gun.

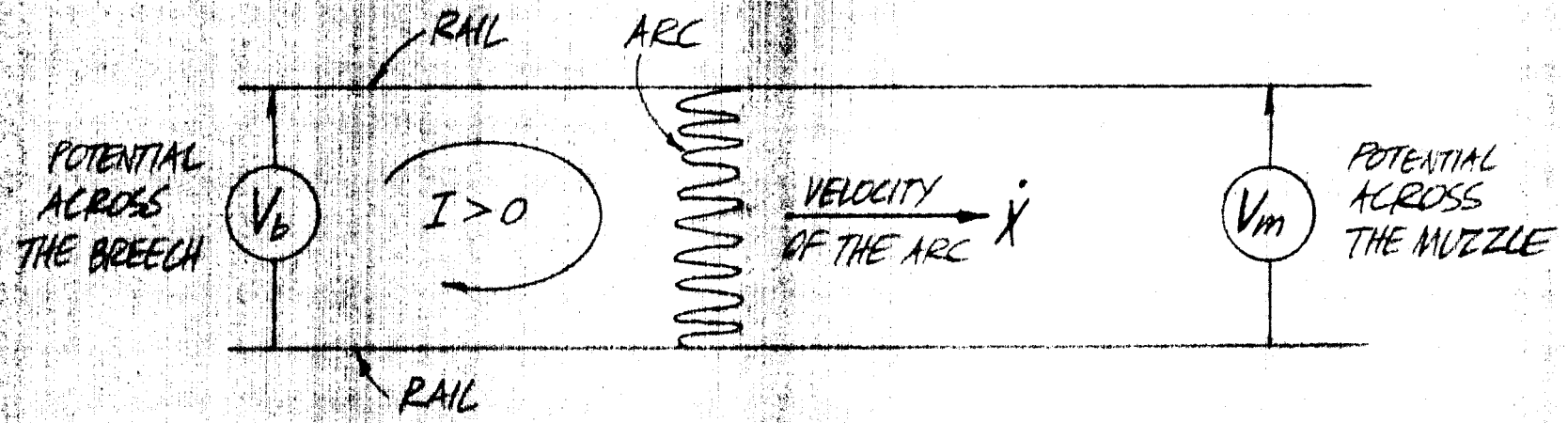

Figure 1. Voltage Measurements Across The Rails

In previous experiments with no projectile, V_m / V_b appeared to be greater than 90% indicating a very poor energy efficiency of the gun. During this quarter, the experiment was repeated with a projectile (a 1/8 inch nylon cube), and V_m / V_b was found to be roughly 60% during almost the entire acceleration. Since the magnetic field energy is always at least as great as the arc-projectile kinetic energy, the net energy efficiency must be less than half the complement of 60%, i.e. less than 20%. The gross energy efficiency computed from the projectile mass and velocity and the condenser bank capacity and voltage was 2.0% — less than the 20% upper limit on the gun's efficiency, as it must be.

III. VARIATION OF BARREL CROSS-SECTION

At the last planning meeting, we made the conjecture that the mass-input would be proportional to the gap surface width of the rails, and that, since the total Lorentz force, for the magnetic field constant, is proportional to the cross-sectional area of the barrel, the effect of the mass-input would be inversely proportional to the width of the barrel. Experiments were carried out with 1/8, 1/16, and 1/32 inch square and 5/32 inch round barrels to test this conjecture. The result was that the effect of mass-input may have been reduced by larger barrels, so that the velocity of the free arc was enhanced (up to 16 km/sec at 1 atm.), but, for the correspondingly heavier projectile the velocities were roughly the same (about 5.5 km/sec), the only improvement being in energy efficiency.

This may have some possible use in a two-stage drag-operated device, in which the velocity of the second-stage free arc must be greater than that of the first.

IV. VOLTAGE DROP MEASUREMENTS OF TOTAL RAIL CURRENT

Six attempts were made to measure the total current into the rails by recording the voltage drop along a segment of the input lead to the gun. (The method we usually use is magnetic pick-up.) Unfortunately, the results were rendered unintelligible by what seems to be inductive effects. These arose from the close proximity of the input lead to the gun. This arrangement was necessary because of the short, thick leads, for low inductance, between the secondary of the transformer and the gun. The circuit used (Figure 2) was designed to cancel out the inductive effects due to the uniform field of the input leads; however, it could not balance the non-uniform fields of the gun and secondary output terminals.

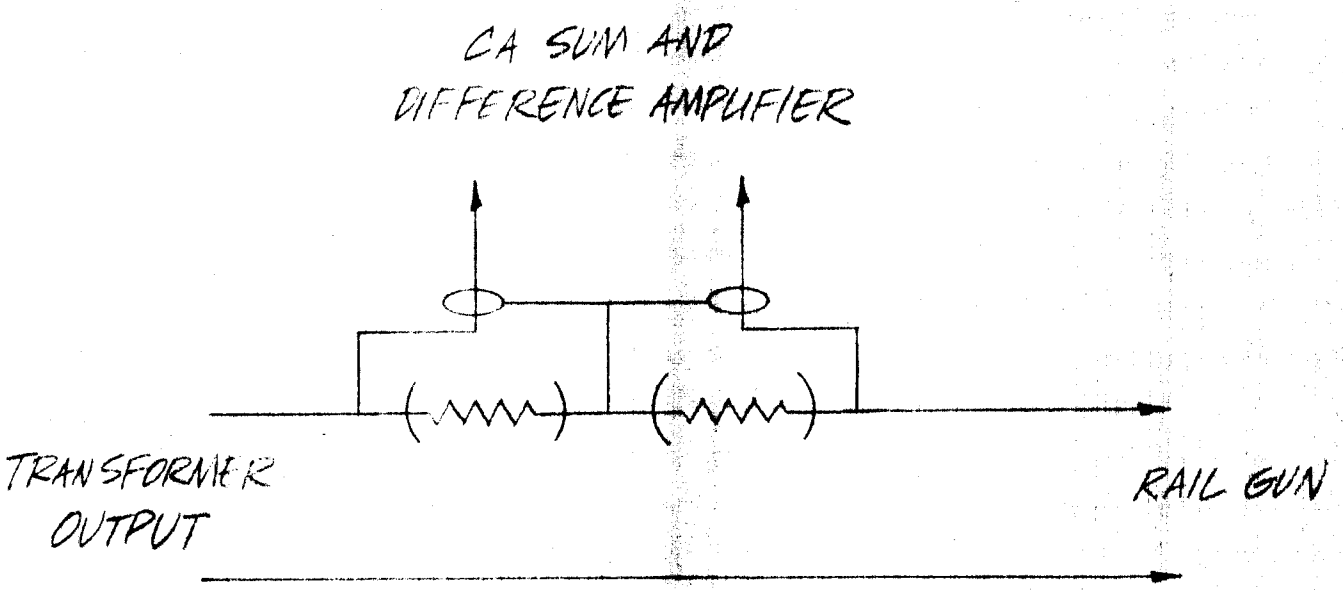

Figure 2. Inductively Balanced Circuit For Measuring The Voltage Drop Along The Leads To The Rail-Gun

V. AUXILIARY FIELD RAIL GUN SYSTEM

In accordance with the planning meeting for the second quarter, we have assembled and made preliminary tests on an auxiliary field rail gun system. (See Figure 3. The considerations leading to this approach are discussed in "Study of a Rail-Type Hypervelocity Projectile Accelerator" by D.E. Brast and D.R.Sawle in the Proceedings of the Seventh Hypervelocity Impact Symposium, Tampa, Nov. 17-19, 1964, AFSC, USABRL, USNRL). Copy attached.

In addition to already existing equipment, the following were made to complete the system:

1. a condenser bank for driving the auxiliary field turns
2. a circuit for charging both banks in parallel
3. a triggered spark gap for discharging the new bank
4. an impedance matching transformer for the auxiliary field circuit
5. a rail gun with auxiliary field turns

The new condenser bank consists of ten 14 μfd, 20 kv capacitors of the same type as used in the old bank (Sangamo, type EDC, Class B). (In addition to these, an eleventh capacitor was bought to replace a damaged one in the old bank). These ten capacitors were strapped together in pairs and each pair placed on a separate, four wheel dolly. Each capacitor is connected to the spark gap switch by separate coaxial cables. These provisions will allow for easy moving of a pair of capacitors from the auxiliary to the gun circuit or vice-versa as the need arises.

A remote control charging and automatic crowbar mechanism was attached to the new bank. The charging leads are connected to the same power supply as the old bank so that both banks may be charged in parallel, each being disconnected from the charging supply as it reaches the desired voltage. The banks are discharged through their respective spark gaps in a controlled time sequence provided by an Abtronix delay chassis. We tested this arrangement and found it reliable.

The gun itself, shown in Figure 4, is of the usual sandwich construction. The steel dowel pins give lateral support, and the whole assembly is clamped from above and below by two one-inch thick melamine-fiberglass blocks (not shown) drawn together on each side of the gun by 3/8 inch high-tensile-strength steel bolts.

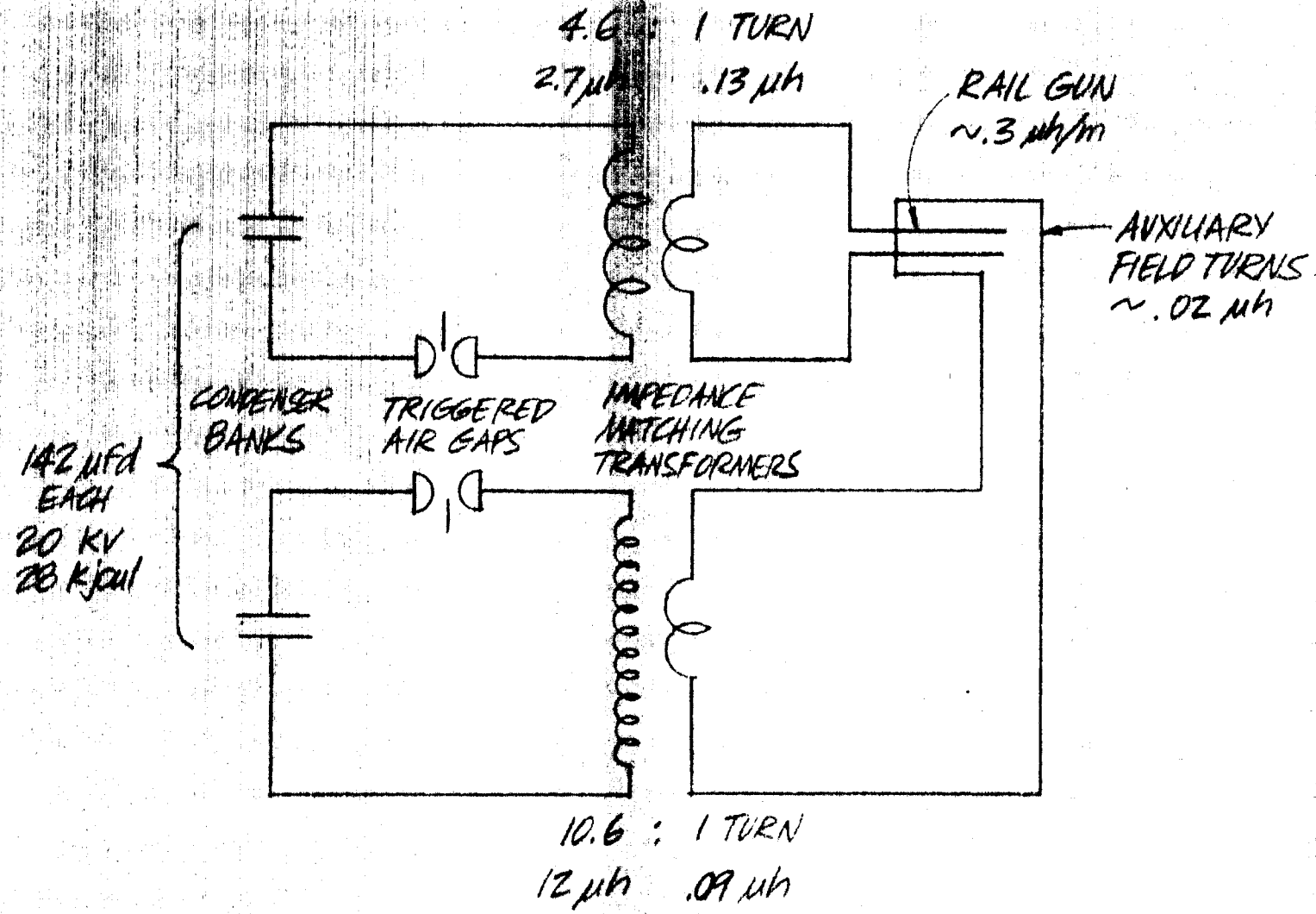

Figure 3. Auxiliary-Field Rail-Gun System

The two auxiliary turns are connected at the muzzle of the gun in parallel to the secondary terminals of one transformer. The rails are connected at the breech of the gun to the secondary of the other transformer. The field produced in the rail gap by the auxiliary turns is about 3 gauss/amp. For modest auxiliary and rail currents of 100k amps, the resulting Lorentz force will accelerate a 5 mg projectile to 30 km/sec in 10 μsec.

Preliminary tests with a prototype of the gun shown in Figure 4 were made with only one capacitor in the rail circuit. With a much lower auxiliary field than would be produced in the present gun, a velocity of about 2 km/sec was achieved.

During the next quarter, we plan to complete the preliminary testing of the components and perform the final testing of the entire system.

David E. Brast
Project Engineer

Approved:

Arthur T. Biehl
Technical Director

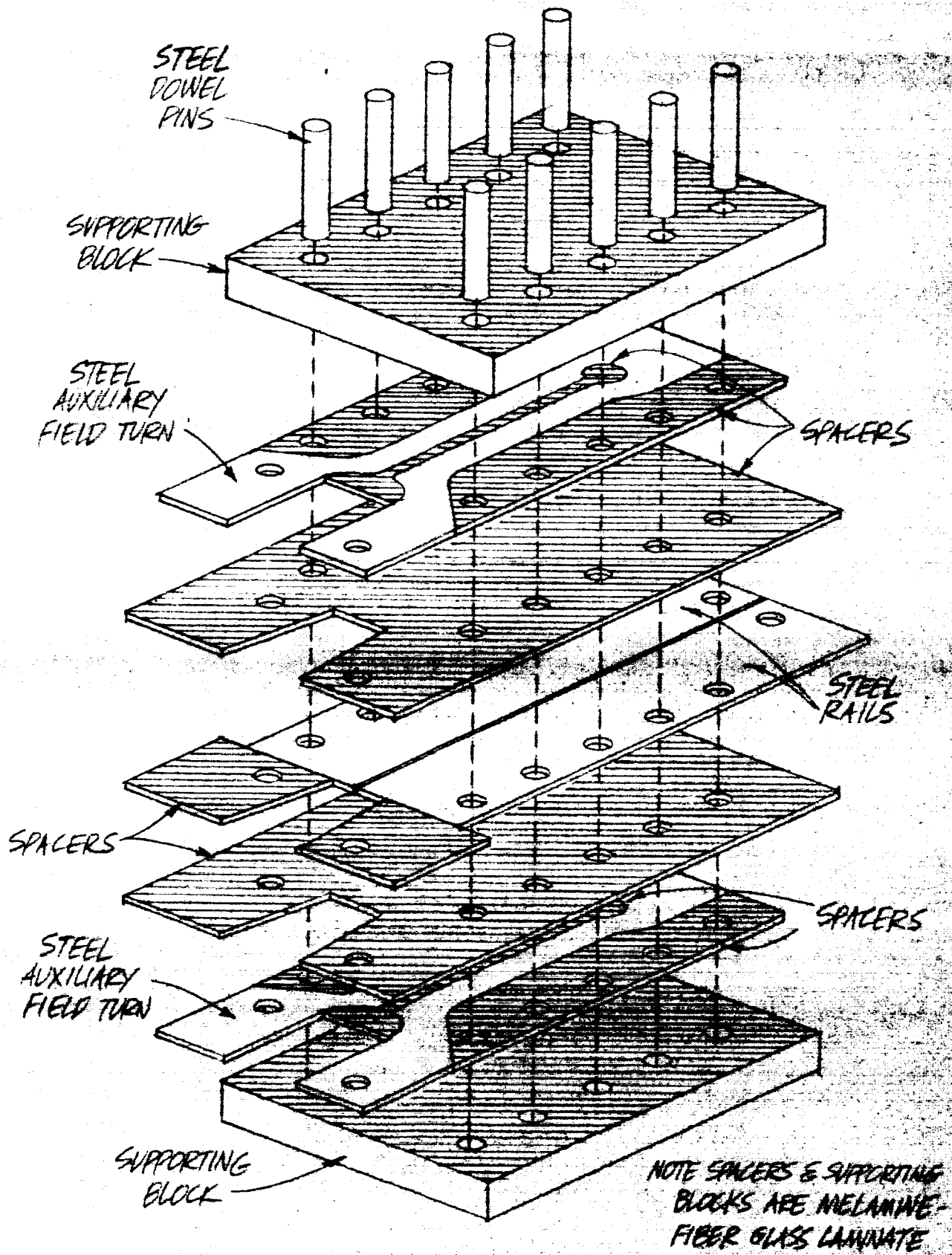

Figure 4. Exploded View Of The Auxiliary-Field Rail-Gun

STUDY OF A RAIL-TYPE MHD HYPERVELOCITY PROJECTILE ACCELERATOR

D. E. Brast
D. R. Sawle

MB Associates
San Ramon, California

MHD RAIL-TYPE ACCELERATOR

ABSTRACT

A rail gun with an electric arc as the armature was used to accelerate a 2.4 milligram nylon sphere to a velocity of 6.0 km/sec and 5 and 31 milligram nylon cubes to velocities of from 5 to 6 km/sec. The energy source was a 28 k joule, 142 μfd condenser bank. The authors describe the system used, analyse the Lorentz force and the limiting phenomena of ion sputtering and high-field skin heating, and propose a slow auxiliary field as a means of overcoming these limitations.

MHD RAIL-TYPE ACCELERATOR

SYMBOLS

$\sim$	is of the order of
$\mathcal{O}$	something of the order of
$b, g, r, z, \rho, \Delta\rho, R, \delta$	see figure 1
B	magnetic induction
I	instantaneous current
I_p	peak current
j	current density
L'	inductance per unit length
M	mass of the projectile
m_I	mass-input per unit charge
r_{ml}	radius of the outer electrode of a coaxial rail gun
S	surface of integration
t	time
V	velocity of the arc
V	volume of integration
1	unit tensor
δ	skin depth
σ	electrical conductivity
ω	angular frequency

MHD RAIL-TYPE ACCELERATOR

INTRODUCTION

The defining features of a rail gun are (See Figure 1) a pair of conducting rails and across them a conducting armature. Electric current is passed through the rails and armature so that the magnetic field produced by the current in the rails (and possibly in auxiliary field coils) interacts with the current in the armature. The resulting Lorentz force (jxB) tends to accelerate the armature away from the end of the rails at which the current is introduced.

Practically, two kinds of armature have been used, electric arc plasmas[1,2] and solid conductors.[3-7] In most projectile accelerators, the projectile is itself conductive and serves as the armature. In our gun, the projectile is nonconductive (usually nylon) and the armature that drives it is an arc plasma.[8] This circumvents the problem of ohmic heating in the projectile.

By this means, we have succeeded in accelerating 2.4 milligram nylon spheres to velocities of 6.0 km/sec and 5 and 31 milligram nylon cubes to velocities of about 5 or 6 km/sec.

The system used consists of a 28 k joule, 142 μfd condenser bank, which is discharged by a triggered spark gap either directly into the gun or into an impedance matching pulse transformer giving peak currents up to 700 k amp at ringing frequencies as high as 25 k c The arc is initiated by a small bit of aluminum foil behind the projectile and travels the entire length of the gun during the first half-cycle of the discharge. When a pulse transformer is used, about three fourths of the bank energy is dissipated in that time. Of the total bank energy, however, at most about 3% goes into the kinetic energy of the projectile.

The gun itself is anywhere from three to eight inches or so in length and consists of a pair of metal rails, usually copper, sandwiched between two insulating slabs. A cubic projectile can be fitted snugly into the resulting square barrel. Alternatively, a cylindrical barrel can be fabricated by machining or molding and a spherical projectile fitted to it.

Routine diagnostics include magnetic flux loops very close to the barrel to record the progress of the arc, a photoelectric muzzle-watcher

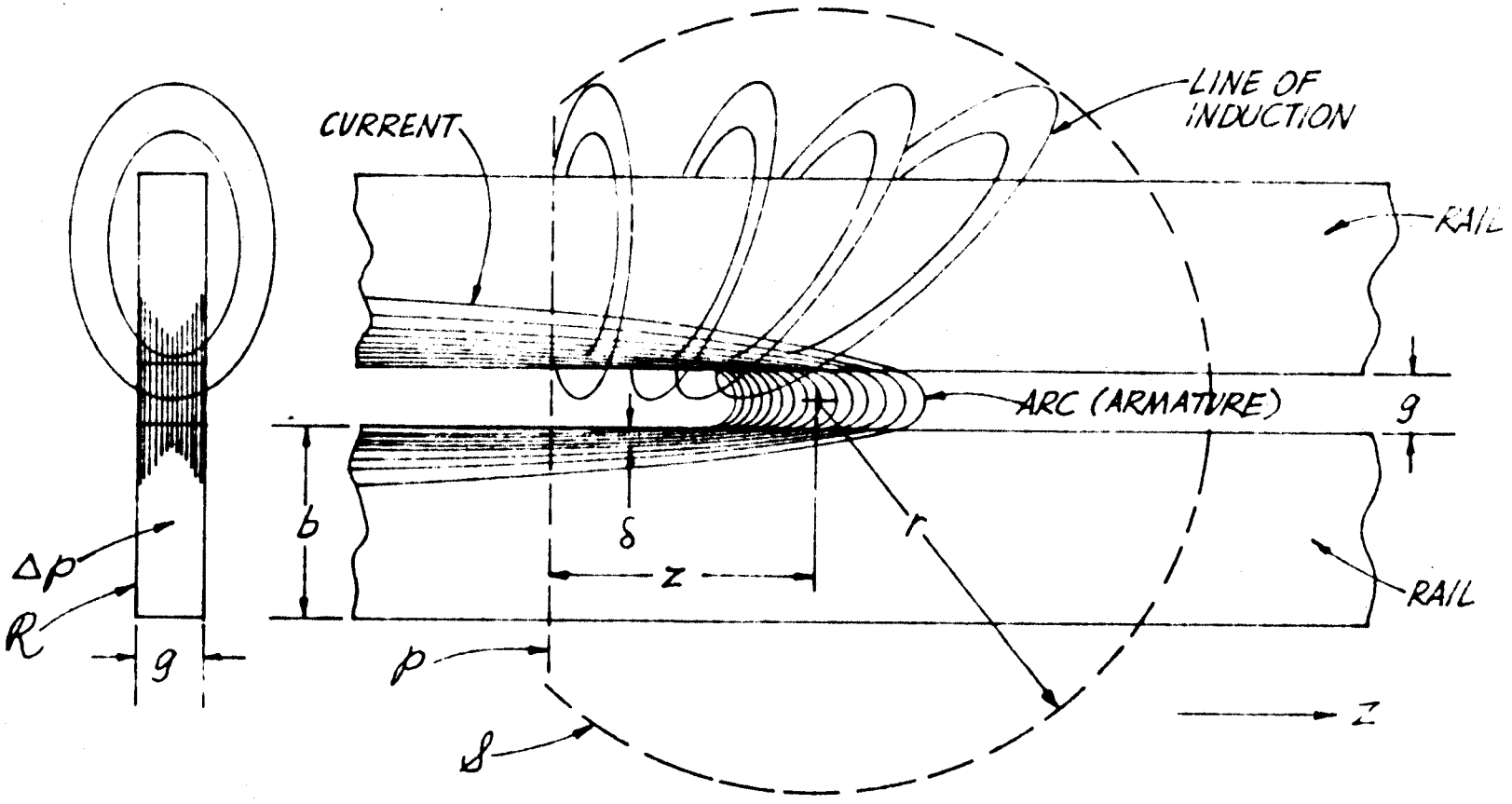

Figure 1. The Arc Discharge Between Parallel Rails

to record the appearance of the luminous arc plasma at the muzzle (this always coincides with the current front as determined by the flux loop at the muzzle)[9] a flux loop to record the total instantaneous current, and transit time and crater depth measurements to determine velocity. Occasionally, we have measured directly the voltage across the muzzle and breech of the gun to determine the resistive voltage of the arc (about 200 v) and the rate of change of flux.

In the rail gun acceleration of plasmas, velocities upwards of 100 km/sec have been achieved[1,2] Offhand, one would, with some modesty, hope to use the same techniques and more energy to achieve somewhat lower velocities for small projectiles. However, because even a 1 mg nylon sphere has an areal mass density 10^6 times that of rail gun plasma bodies (10 gm/cm^2 versus 10 μgm/cm^2) the magnetic pressure required to produce the same acceleration in the projectiles as in the plasmas is correspondingly higher. Smaller accelerations of longer duration over greater distance lead to (1) greater loss of energy into unusable magnetic fields due to lateral diffusion and forward expansion and into mass sputtered off the rails by current carrying ions, (2) heating of even a nonconducting projectile by the arc through thermal conduction, (3) such a large impedance that a second arc strikes at the breech even before the first one reaches the muzzle.

The magnetic fields needed for large accelerations are of the order of a megagauss. The ohmic heat per unit volume produced by such high fields (turned on fast enough to be contained by good conductors) is sufficient to melt the current carrying portion of the rails,[4] and momentum then goes into the molten rail material. Also the pressures are so high that the rails suffer plastic flow.

The way out of the dilemma seems to us to be a slow auxiliary field. This, of course, wastes more energy in the magnetic field and does not decrease the force on the rails, but it does eliminate sputtering and skin heating

The following is a more detailed description and analysis of the operation of the rail gun including some relevant experimental results.

MHD RAIL-TYPE ACCELERATOR

OPERATION OF THE RAIL GUN

The Lorentz Force On The Arc

The Lorentz force on an arc in a rail gun without an auxiliary field can always be written as $\frac{1}{2} L' I^2$, where I is the instantaneous total current in the rails, and L' is some inductance per unit length. The total momentum produced by this force will then be $\int \frac{1}{2} L' I^2 dt$. If L' is nearly constant in time, and if we know its value, we have a very useful expression for the momentum in terms of an easily measured quantity, I. In general this will not be the case, because L' is dependent on the current distribution in the rails, and, except in special cases, for example, the case of infinitely thin wire rails, this current distribution will vary with time in an unknown way.

Fortunately, the rail gun considered here falls under on of those special cases, at least to an approximation, and we can get an estimate of L' by means of the Maxwell stress tensor, $BB - \frac{1}{2}|B|^2 1$ (1 is the unit tensor) in the following way.

The Lorentz force on an arbitrary volume, V, is given by

$$F = \int j \times B \, dV$$
$$= \oint_S \frac{1}{\mu_0} (BB - \tfrac{1}{2}|B|^2 1) \cdot dS \qquad (1)$$

where S is the surface enclosing V, and dS is outward. For S (See Figure 1) we take the truncated spherical surface $\mathcal{S}$ of radius r centered about the arc and the disc P perpendicular to the axis of symmetry at a distance z from the arc. The integral over S is the Lorentz force on the portion of the rails enclosed by S and upon the arc.

We now let $\mathcal{S}$ go to infinity. On $\mathcal{S}$, B is proportional to $1/r^2$. Therefore, the integral on $\mathcal{S}$ is proportional to $1/r^2$ and goes to zero. P is now the entire plane. For $z^2 \gg g^2$, the forward component of the Lorentz force will be given by the integral of $\frac{1}{2\mu_0}|B|^2$ over this plane. The integral of $B_z B \cdot dS$ will be negligible for the following reasons. B_z is due solely to the

current in and near the arc, so that

$$\begin{aligned} &B_z|_P \sim \mu_0 I\, g/z^2 \\ &\tfrac{1}{\mu_0} B_z B \cdot dS \sim \mu_0 I^2 g^2/z^4 \\ &\int_P \tfrac{1}{\mu_0} B_z B \cdot dS \sim \mu_0 I^2 g^2/z^2 \end{aligned} \tag{2}$$

On the other hand, in the gap

$$\begin{aligned} &|B| \sim \mu_0 I/g \quad \text{so that} \\ &\int_P \tfrac{1}{2\mu_0} |B|^2 |dS| \sim \mu_0 I^2 \end{aligned} \tag{3}$$

If one compares the approximate expressions in (2) and (3), one sees that, for $z^2 \gg g^2$, $\int_P \frac{1}{\mu_0} B_z B \cdot dS$ can be ignored, and that the total forward force on the rails and arc is given by

$$F_{total} = \int_{P(z^2 \gg g^2)} \tfrac{1}{2\mu_0} |B|^2 |dS|$$

The forward force on the rails alone is given by

$$F_{rails} = \int_{\Delta P} \tfrac{1}{2\mu_0} |B|^2 |dS| + \int_K \tfrac{1}{\mu_0} B_z B \cdot dS \tag{4}$$

where ΔP is the cross section of the rails, K is the surface of the rails, and dS is now outward from the rails. The forward force on the arc, F_{arc} is just $F_{total} - F_{rails}$ or,

$$F_{arc} = \int_{P-\Delta P} \tfrac{1}{2\mu_0} |B|^2 |dS| - \int_K \tfrac{1}{\mu_0} B_z B \cdot dS \tag{5}$$

The first integral in Equation (5) is the external magnetic energy per unit length behind the arc.

In the case of an azimuthally symmetrical discharge in a coaxial-cylinder rail gun, the first integral is just $\frac{\mu_0}{4\pi} I^2 \ln \frac{r_{outer}}{r_{inner}}$, which is just $I^2/2$ times the geometric external inductance. The second integral is zero in this case, because both B_z and $B \cdot dS_K$ are zero. Therefore, for azimuthal symmetry, L' is just the

geometrical external inductance per unit length, independent of the radial distribution of the current in the electrodes.

The same result holds for the previously mentioned special case of infinitely fine wire rails and for the case of infinite conductivity. This can be derived from Equation (4) or from the conservation of energy and Faraday's Law. Both of these derivations depend on the fact that, in these special cases, we can define a unique magnetic flux through the circuit.

In the case of interest, the discharge is not azimuthally symmetrical, the cross sectional size of the rails is comparable to the size of the gap so that the rails cannot be considered infinitely thin, and the electrical skin depth in the rails for typical transit times is considerable compared to the other dimensions so that the rails cannot offhand be considered of infinite conductivity. Near the arc, lines of induction which cut the rails because of their finite conductivity have components both normal to the surface of the rails and along the z - direction. Therefore, the second integral in Equation (5) may no longer be negligible.

In order to estimate this integral, we again make use of the fact that, away from the arc, only the current in the arc and not the current in the rails contributes to B_z. B_z will, therefore, be roughly proportional to the inverse square distance from the arc, $1/z^2$, and to the sine of the angle between the rail-surface normal and the radius vector from the surface to the center of the arc. This sine is approximately g/z so that B_z is proportional to $1/z^3$. At a given distance, z, from the arc, the width of the area on the rails cut by B will be the skin depth, δ, corresponding to the time for the arc to travel that distance. Letting v be the velocity of the arc and σ the conductivity of the rails, we have

$$\delta \sim \sqrt{T/\mu_0 \sigma} \qquad T \sim z/v$$

$$\int_R \frac{1}{\mu_0} B_z \, B \cdot dS \qquad (6)$$

$$\sim \int_0^g \frac{1}{\mu_0} |B|^2 \sqrt{\frac{z}{\mu_0 \sigma v}}\, dz + \int_g^a \frac{1}{\mu_0} |B|^2 \frac{g^2}{z^2} \frac{g}{z} \sqrt{\frac{z}{\mu_0 \sigma v}}\, dz$$

$$\sim \frac{1}{\mu_0} |B|^2 g \sqrt{\frac{g}{\mu_0 \sigma v}}$$

If we let the first integral in Equation (5) be $\frac{1}{2} L' I^2$ and the second integral a correction to it, then, whatever the exact value of L' is, it will be roughly true that $L' \sim \mu_0$ and near the gap, $|B| \sim L' I / g$.

Substituting these expressions into Equation (6), we have

$$\frac{1}{\mu_0}\int_R B_z B \cdot dS \sim \left(\tfrac{1}{2}L'I^2\right)/\sqrt{\mu_0\sigma v g}$$

Putting in the typical values

g = 1.5 mm

v = 5 km/sec

σ = 5.8×10^7 mho/m for copper

we have $1/\sqrt{\mu_0\sigma v g} \sim 0.04$.

This is the order of magnitude of the fractional negative correction that will have to be made in the expression for the Lorentz force derived from the first integral of Equation (5). From the above calculation, we see that, for copper, it is perhaps small enough to be neglected. For steel with a conductivity of, say, 5.8×10^6 mho/m, the correction is about 0.12, perhaps large enough to be considerable.

As long as this correction is not too large, the skin depth at P will be small enough so that we can get a fair approximation to L' from the high frequency inductance per unit length. Even for $\delta \ll g$, this may still be somewhat innaccurate because the surface current distribution in this problem is not exactly that of the steady state alternating current problem. However, when it is accurate enough, the high frequency inductance per unit length can be measured directly in a ringing circuit or indirectly by means of a two-dimensional electrical analog.

To summarize, the Lorentz force on the arc is given by

$$F_{arc} = \tfrac{1}{2}L'I^2\left[1 - \mathcal{O}\left(\frac{1}{\sqrt{\mu_0\sigma v g}}\right)\right] \qquad (7)$$

where L' is roughly the high-frequency inductance per unit length and $\mathcal{O}\left(\frac{1}{\sqrt{\mu_0\sigma v g}}\right)$ is a negative correction of the order of the ratio between the skin depth near the arc to the width of the gap.

MHD RAIL-TYPE ACCELERATOR

Mass-Input Limitation On The Projectile Velocity

The momentum as calculated from Equation (7) using the measured values of L' and I is actually about three times greater than the mass of the projectile times its measured velocity. As a tentative explanation for this we proposed a mass-input to the arc proportional to the total charge through the arc. This is the sort of thing one would expect if sputtering were taking place.[9]

For experiments without an impedance matching transformer, the current had the form of a slightly damped sine wave. Putting $I_p \sin \omega t$ for the current, M for the mass of the projectile, and m_I for the mass-input per unit charge, we get the following expression for velocity

$$v = \frac{L' I_p}{4 m_I} \frac{\omega t - \frac{1}{2} \sin 2\omega t}{\frac{\omega M}{I_p m_I} + 1 - \cos \omega t} \qquad (8)$$

by equating the momentum of the projectile and arc plasma to the momentum calculated from Equation (7).

Figure 2 shows a plot of position versus time based on Equation (8). The curve was made to fit through a set of experimental points by setting $m_I = 4.6$ Cu atoms/ion. In order to show the seriousness of including mass input, another curve with $m_I = 0$ was made to fit through the experimental point at 30 μ sec by setting L' equal to about one-third its measured value. It is hardly possible that the measurement of L' could be so much in error, but, even if it were, the curve for $m_I = 0$ has the wrong shape. It, therefore, seems that phenomenologically, at least, a charge proportional mass-input describes the situation. The following section indicates how the description may be more than phenomenological.

Ion Sputtering

In the present range of temperatures (10 to 100 ev)[2] and magnetic fields (10^5 to 10^6 gauss), the electron and ion cyclotron frequencies and radii will be roughly

$\omega_e \sim 10^{12}$/sec $\omega_i \sim 10^7$/sec

$r_e \sim .0001$ mm $r_i \sim .01$ mm

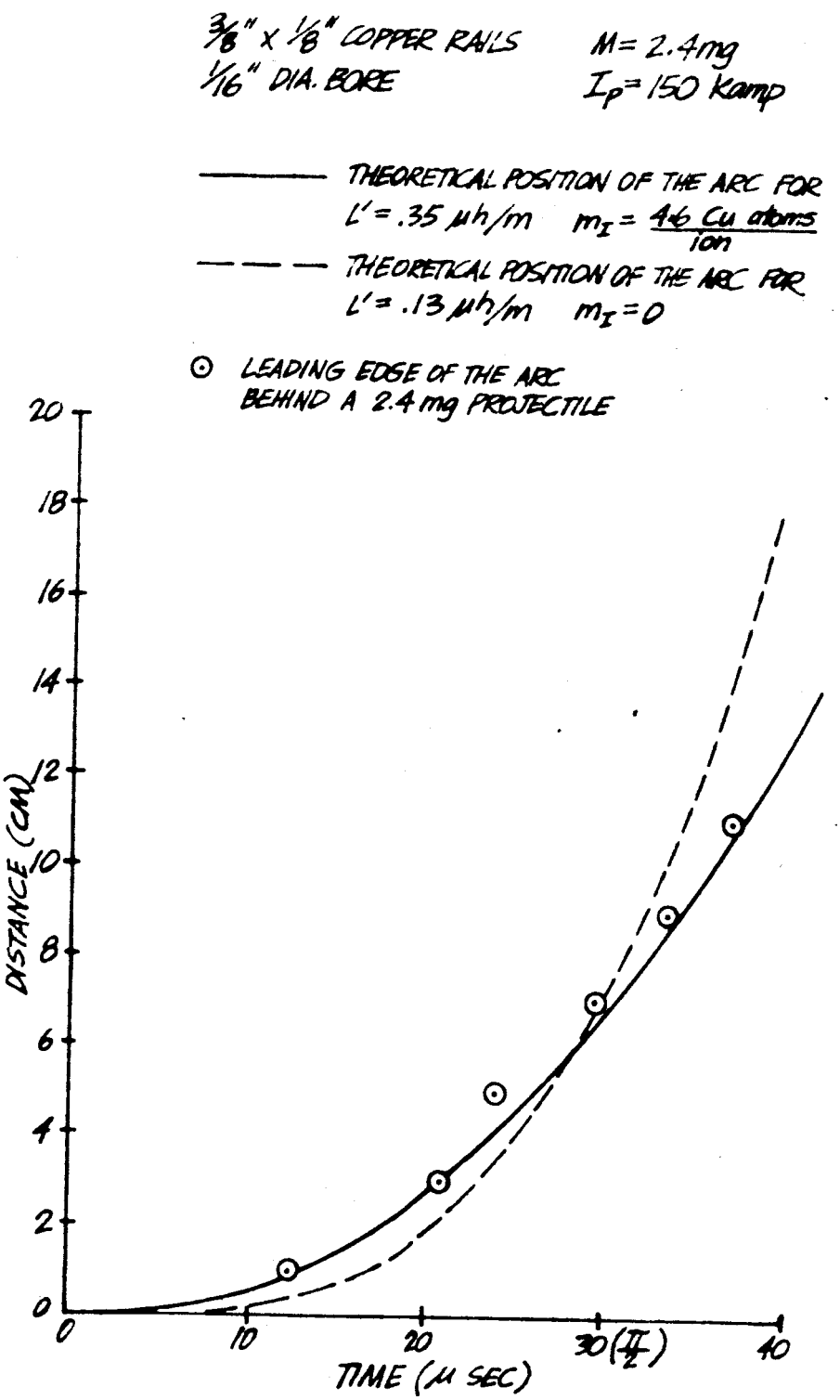

Figure 2. Distance vs Time For The Projectile Theoretical and Experimental

Since these radii are much less than the inter-electrode spacing of 1.5 mm, if the electron collision frequency for current producing collisions (electron-ion or electron-neutral) is much less than ω_e, which is probable, then the arc current will be carried predominantly by ions.

The total resistive voltage drop across the arc has been measured as roughly 200 v. Current carrying copper ions impinging on the copper with the corresponding energy of 200 ev would sputter roughly 0.9 copper atoms/ion (61 atomic mass units; see the included table).

The discrepancy between 0.9 and 4.6 may be accounted for by skin heating, which certainly does melt rail material and may even enhance the sputtering yield. The next section discusses this effect.

Ohmic Skin Heating

During the transit of the arc down the rails, current and magnetic field diffuse into the rail due to the finite conductivity of the rail material. As we will show, the average energy density deposited by ohmic heating in the region of the arc is approximately the magnetic energy density in the gap. If this energy density is greater than the heat content of the rail material from its initial temperature, say, room temperature, to just above its melting point, then rail material will be melted in that region.[4] Since there is a forward component of the Lorentz force on the rails near the arc, this molten material will be carried forward and will, therefore, contribute to the mass of the arc-projectile system. (Although heating continues in the rails behind the arc, the Lorentz force is outward, and the molten material there will only be pressed against the rails, not carried forward.)

The heating in the region of the arc is determined as follows. The average power per unit volume is j^2/σ where j is the average current density and σ the conductivity. The volume under consideration has the thickness of the rails, g, and an average depth $\sqrt{2t/\mu\sigma}$, the electrical skin depth corresponding to the length of time, t, for the arc to travel its own length. The current density is, therefore, $(I/g)\sqrt{\mu\sigma/2t}$, where I is the total current. The average power is $\mu I^2/2g^2t$, and, since this power is applied in the region of the arc only over the time t, the heat developed is $\mu I^2/2g^2$, which is roughly the magnetic energy

MHD RAIL-TYPE ACCELERATOR

IMPORTANT PHYSICAL CHARACTERISTICS OF ELEMENTAL RAIL MATERIALS

Element	Number	Total heat content 20°C through M.P. $\frac{\text{k joule}}{\text{cm}^3}$	Self sputtering yield at 200 ev* $\frac{\text{a m u}}{\text{ion}}$	Electrical Resistivity $\mu\Omega$ cm	Tensile Strength 10^3 psi
Be	4	6.9	11	4.3	50
C	6	>15.0	0.4	800	-
Mg	12	1.9	8	4.6	30
Al	13	2.7	8	2.8	40
Ti	22	> 6.0	11	3.2	100
V	23	> 6.7	17	25	100
Cr	24	>12.0	37	13	60
Fe	26	9.2	34	10	100
Co	27	10.5	39	9.8	100
Ni	28	9.2	43	7.8	160
Cu	29	5.6	61	1.7	70
Zn	30	2.1	35	5.8	30
Y	39	> 3.5	24	65	20
Zr	40	> 5.1	20	39	100
Nb	41	>10.0	20	14	50
Mo	42	>11.0	31	5.7	60
Ru	44	>10.0	38	7.6	-
Rh	45	> 8.5	52	4.5	100
Pd	46	6.8	98	10.8	40
Ag	47	> 3.3	127	1.59	40
Hf	72	>5.0	33	36	100
Ta	73	11.0	33	12.4	150
W	74	>12.0	28	5.5	200
Re	75	15.0	46	19.1	150
Os	76	11.0	54	9.5	150
Ir	77	11.0	88	5.3	-
Pt	78	8.2	97	9.8	50
Au	79	5.4	171	2.2	20

* Not much data exists on the sputtering of cathodes by ions of the same element; therefore, the self-sputtering yields listed here have been based on data for sputtering by noble gases.[10] Since sputtering at those energies is thought to be predominantly a momentum transfer process, the yield for each element has been taken from the data for the noble gas of most nearly the same atomic weight.[11]

density in the gap, as stated. For

I = 200 k amp and

g = 1.5 mm,

$\frac{\mu_0 I^2}{2g^2} \sim$ 10 k joule/cm^3

The averages above are very loosely defined, and the consequent results are only good to an order of magnitude. The actual heating will depend upon the details of the current distribution in the rails. Even so, one can see from the table, that this is the right order of magnitude to melt the current carrying part of the rail.

From flux loop data, we have a typical value for τ of 10 μ sec. The corresponding electrical skin depth is 0.7 mm, and the thermal skin depth is 0.03 mm. It would, therefore, be impossible for the heat generated to dissipate by conduction during the passage of the arc. The appearance of the rails after the shot bears this out. In fact, for a steel rail with 8 mil copper cladding, the entire copper face was melted in the region of highest current. The total amount of copper melted over a 6 cm length has a mass of from 0.1 to 1 gm. Ten or so milligrams of this carried forward against the projectile would account for the mass-input effect.

For a given energy density the amount of material melted will increase in direct proportion to the skin depth and hence the square root of the resistivity in the rail material. In addition to the decrease in inductance, this may have contributed to the poorer performance of steel compared to copper even though the steel rails showed less deformation.

Mechanical Effects

Lorentz Force On The Rails

In the region behind the arc, the Lorentz force density is outward from the gap in the plane of the rails. The equivalent pressure at the gap surface of the rails is just the magnetic energy density in the gap. For the case described in the last section, this is a pressure of about 10^6 psi, enough to cause plastic flow in the solid rail material.

MHD RAIL-TYPE ACCELERATOR

In addition to plastic flow at the gap surface, the Lorentz force causes gross motion of the rails in the lateral direction. This begins to occur after the shock wave created at the gap surface travels to the outside edge of the rails and back. Since the rails are restrained in this direction by bolts or steel dowel pins, this motion causes plastic flow of the rail around the bolts.

The appearance of the rails after the shot shows that considerable plastic flow and gross motion of the rails do occur. Depending upon the rail material, the peak current, and upon the insulator, which serves to prevent relief perpendicular to the plane of the rails, the gap may be enlarged by a factor of from 1.5 to 3. The effect of this spreading is to lower the Lorentz force on the arc. This can be seen either as a decrease in inductance or, equivalently, a drop in magnetic pressure due to expansion.

The Pressure And Length Of The Arc

The arc is contained at the front by the inertial forces of the projectile and of its own mass, from the sides by the rails and insulator, and from behind by what may be thought of as a magnetic pressure, (typically 10^6 psi). In the steady state, the ordinary kinetic pressure in the arc will just balance this magnetic pressure. For temperatures of 10 to 100 ev this corresponds to the following:

10^{22} to 10^{21} atoms/cm^3 particle density

1 to .1 gm/cm^3 mass density

Given the mass of the arc and the cross section of the barrel, the arc length is completely specified by this density. Flux loop measurements give this length as very roughly 1 cm. The corresponding mass range is 2 to 20 mg, consistent with the observed mass-input limitation.

The mechanical effect of the arc pressure is to stress the insulator over the arc. This stress is followed by another due to the plastic deformation of the rails, as described above. One-half inch thick cloth-phenolic insulators have been broken in two along the barrel by this shock. Melamine-glass cloth laminate blocks, which we now use, show some separation of the laminations but seem to be more than strong enough to withstand the pressures in the present current

regime. This sort of failure helps to lower the Lorentz force on the arc by allowing the rails to spread.

Experimental Results

Rail Materials

Experiments with rails of

copper
mild steel
tool steel
pure aluminum
aluminum 6061
aluminum 7075
magnesium
tungsten

which were designed to test the sputtering characteristics of these metals, seemed merely to show the strength and melting characteristics described earlier. An attempt was made to separate these characteristics by using a composite rail with a hard core, in one case of melamine fiberglass laminate and of tool steel in another, and a cladding of the metal under consideration. We also used a rail of mild steel with a copper edge attached by hard soldering. The cladding technique showed the best results.

Insulator Material

Experiments with guns of identical construction except for the thin insulating liner next to the rails were done at a relatively low current to minimize mechanical effects. The results were as follows:

Insulator	Projectile Velocity
glass	3.8 km/sec
melamine-fiberglass laminate	3.8 km/sec
epoxy-fiberglass laminate	2.0 km/sec

The glass and melamine showed much less erosion compared with the epoxy.

MHD RAIL-TYPE ACCELERATOR

Current Variation

Two series of shots at various currents with guns of identical construction within each series showed an increase in velocity with current up to an optimum current, after which the velocity fell off. The optimum current was higher in the gun of stronger construction.

CONCLUSIONS

The explanation of these results in terms of the preceding discussion is that the ideal operation, with L' constant and mass-input due to sputtering, takes place at lower magnetic field intensities. In this regime, velocity increases with increasing magnetic field. Beyond some critical field intensity, L' is reduced by deformation of the rails, and large scale melting of the rails takes place. In this regime, velocity actually decreases with increasing magnetic field.

This limitation can be overcome with auxiliary field turns. However, these turns cannot be in series with the rails, because, although such an arrangement reduces the effect of sputtering by increasing L' it does not eliminate the problem of skin heating. As long as the skin depth corresponding to the rise time of the auxiliary field is small compared to the width of the rails, the ohmic heat per unit volume will be roughly the same as the magnetic energy density. This obstacle can be circumvented by turning on the auxiliary field slowly. For rails of centimeter width, ten or so milliseconds would be long enough.

In light of the foregoing, a rail gun should be constructed and operated as follows.

The rail material should have high yield strength, high electrical conductivity, a low self-sputtering yield, and a high heat content from room temperature through the melting point. The included table shows that molybdenum, rhodium, tungsten, and iridium might be the best rail materials. This rail material should either be used in its toughest state or else used as cladding over a very strong core.

The insulating support structure should be as strong as possible to prevent spreading of the rails.

A slow (ten milliseconds) auxiliary magnetic field of the highest possible intensity should be used.

Given the best rail material and the strongest supporting structure, the energy density in the gap should be as high as possible without melting or spreading the rails.

ACKNOWLEDGMENTS

Dr. Harold P Furth has been of invaluable help in his capacity as consultant to this program. We owe thanks to Dr. Gottfried K. Wehner for kindly supplying us with data and information concerning sputtering.

This work was performed for NASA, Marshall Space Flight Center, Huntsville, Alabama, contract NAS 8-11204, under the active supervision of Dr. O. K. Hudson.

REFERENCES

1. J. Marshall, Phys. Fluids 3, 134 (1960)

2. P. J. Hart, Phys. Fluids 5, 38 (1962)

3. W. W. Salisbury, Proc. of 1st Symp. on Hypervelocity Impact

4. K. W. Miller and R. M. Bergslien, Proc. 2nd Hypervelocity and Impact Effects Symp., Vol. 1, USNRL, Washington (1957) p. 127

5. C. Mannal and Y. A. Yoler, Proc. 2nd Hypervelocity and Impact Effects Symp., p. 169

6. D. L. Wennersten, Proc. 3rd Symp. on Hypervelocity Impact, Vol. 1, US Army, Chicago (1958) p. 475

7. R. L. Chapman, D. E. Harms, and G. P. Sorenson, Proc. 6th Symp. on Hypervelocity Impact, Vol. 1, US Army, Cleveland, (1963) p. 317

8. J. J. Baruch et al., High Velocity Electric Accelerator Systems, WADD 60-468, USAF (1960)

9. L. Leibing, Phys. Fluids 6, 1035 (1963)

10. "Sputtering Yield Data in the 100 - 600 ev Energy Range", General Mills Report No. 2309, July 15, 1962, Minneapolis

11. G. K. Wehner, Advances in Electronics and Electron Physics, Vol. 7, Academic Press, New York (1955) pp. 292-296

NSG-132

THE UNIVERSITY OF MICHIGAN

UNPUBLISHED PRELIMINARY DATA

Vibrations and Stability of Buckled Rectangular Plates

YAO W. CH[redacted]

November 1964

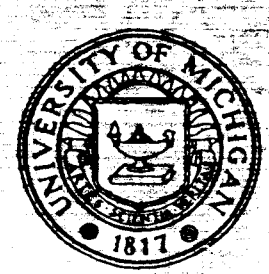

ANN ARBOR

THE UNIVERSITY OF MICHIGAN

COLLEGE OF ENGINEERING

DEPARTMENT OF ENGINEERING MECHANICS

VIBRATIONS AND STABILITY OF BUCKLED RECTANGULAR PLATES

Yao W. Chang
Ernest F. Masur

Under Contract with

National Aeronautics and Space Administration

Grant N_sG-132-61

Washington 25, D.C.

October, 1964

TABLE OF CONTENTS

LIST OF FIGURES

CHAPTER I

INTRODUCTION

Current structural design practice calls for decreasing structural thickness as a result of weight limitations; as a consequence, many structures are permitted to buckle and are then used in the post-buckled state. Members that previously served only in a nonstructural capacity are used to sustain loads greater than those predicted in the usual "Euler load" sense. In addition, structures subjected to these high static loads are frequently expected to survive dynamic disturbances. This is particularly true in aircraft and space structures where the stiffness and dynamic characteristics of a buckled rectangular panel have become important with increasing flight speeds. The buckling of the skin panels, whether caused by air loads or by thermal expansion, will cause a marked reduction in the stiffness of the structure. The changes in frequencies and mode shapes that take place as a result of thermal expansion affect the various static and dynamic instabilities considerably. The purpose of the present study is to determine the dynamic characteristics, that is, the natural frequencies and mode shapes of vibration of a rectangular plate, in terms of a load parameter both before and after buckling.

The free vibrations of elastic bodies or structures about the unbuckled equilibrium configuration have been studied extensively before. The natural frequency and the mode shape of vibration are obtained from the solution of an eigenvalue problem. If such a body or structure is first preloaded statically, then the resulting frequency of vibration is increased by tensile stresses or forces and decreased

by compressive forces. In the case of compressive loading, it goes to zero when the compressive force reaches the buckling load.

The most familiar example of such a problem is the lateral vibration of a simply supported bar which is axially loaded. The square of the frequency of the vibration is linearly related to the axial force. Willers[1] has calculated the decrease in the natural frequency of a clamped circular plate under uniform radial compressive forces. Massonnet[2] and Lurie[3] have shown the existence of an intimate relationship between normal vibrations and instability. A definitive discussion can be found in the book by Bolotin.[4] In general, within the framework of linear theories, whenever the mode shape of buckling and of vibration in the presence of axial load are the same, the square of the natural frequency varies linearly with increasing axial load until it vanishes at the corresponding buckling load. This property is often used to predict the buckling load by extrapolation of a few points obtained experimentally at relatively low loads on the frequency squared-load curve.

The buckling of a simply supported plate under edge compression was first studied by Bryan[5] in 1891. The buckling loads for plates that are not simply supported have been investigated extensively by Timoshenko.[6] These problems are all solved within the framework of linear classical theory under the assumption that the deflection of the plate is small in comparison with its thickness; therefore the solution applies only to the incipient state of buckling. It is obvious that the linear theory of plates no longer applies when the behavior of the plate above the buckling load is to be investigated.

A set of nonlinear differential equations for plates with large deflections was introduced in 1910 by von Kármán.[7] Owing to the nonlinearity of the equations, there exist relatively few exact solutions. However, various approximate solutions have been presented by Cox[8] and Timoshenko,[6] and a more accurate solution of the problem of large deflections has been given by Marguerre.[9] By means of Fourier series Levy[10] has obtained an "exact" solution to the large deflection equations of von Kármán for square plates. Friedrichs and Stoker[11,12] have used methods of perturbation, power series and asymptotic expansions to solve, in a very exhaustive manner, the problem of a simply supported circular plate subjected to radial compressive loading. Alexeev,[13] using a method of successive approximations, has obtained a solution for the square plate buckling into both one buckle and two buckles. Masur[14] has utilized a stress function space together with a minimum energy principle to obtain a sequence of solutions with error estimates for the post-buckling behavior of plates. With the exception of the analysis of Alexeev,[13] all of the above studies of the post-buckling behavior of plates are concerned with primary buckling.

Secondary buckling has been observed through experiments,[15,16,17] and in the case of circular plates, the instability of the primary buckling mode has been pointed out by several authors.[11,14] Further, Stein[18] has used a perturbation technique to convert the nonlinear large deflection equations of von Kármán into a set of linear equations and to investigate the post-buckling behavior of simply supported rectangular plates by solving the first few of the equations. His investigation

indicates possible changes in buckle pattern; the same has also been noted by Koiter.[19]

Bisplinghoff and Pian[20] have treated the case of vibration of a thermally stressed rectangular plate which is simply supported and free to displace laterally. Shulman[21] has considered the case of a uniformly heated plate with two opposite edges simply supported and with generalized support conditions on the other two edges. Both papers consider the small vibrations of the plate in its pre- and post-buckling states, the analysis of the latter being approximate. Herzog and Masur[22] have treated the case of vibration of a buckled circular plate by means of both perturbation techniques and power series expansions. Their analysis is "exact" within the limits of classical plate theory, small amplitude vibration and in the sense of a converging series which has been truncated.

The present study is concerned with the linearized vibrations of a rectangular plate relative to a static buckled configuration, and with the instability of the buckling modes. Both the static and dynamic equations of equilibrium are solved by perturbation techniques. If perturbation coefficients up to the third order are included, the results are acceptable for a significant range of the loading parameter. For large values of the latter the frequency of vibration of the plate is obtained by means of the Galerkin method while the static problem is solved by a method similar to the one due to Marguerre.

CHAPTER II

FORMULATION OF THE PROBLEM

In what follows we consider the xy plane to be the middle plane of an elastic, isotropic plate and z the direction of the lateral deflection. The plate is subjected to membrane forces in the plane of the plate. For the sake of convenience, the index notation is used for the general discussion of the problem, with Latin subscripts i, j and k taking the values of x and y, a repeated subscript representing the sum of all allowable values of that subscript, and a comma followed by a Latin subscript denoting appropriate differentiation.

Let a plate of thickness h be subjected to prescribed edge thrusts λT_i on B' and to displacements λU_i on B'', in which $B = B' + B''$ forms the boundary of the region R of the middle plane and λ is a parameter assuming increasing positive values. The membrane displacements and stresses u_i and t_{ij}, respectively, may then be conveniently characterized by

$$\begin{aligned} u_i &= \lambda u_i^o + U_i' \\ t_{ij} &= \lambda t_{ij}^o + T_{ij}' \end{aligned} \tag{2.1}$$

In Equations (2.1) the first terms on the right side correspond to the unbuckled state and are governed by the customary "generalized plane stress" equations

$$\begin{aligned} t_{ij}^o &= \frac{E}{1-\nu^2}\left[\frac{1-\nu}{2}(u_{i,j}^o + u_{j,i}^o) + \nu u_{k,k}^o \delta_{ij}\right] = t_{ji}^o \qquad \text{in R} \\ t_{ij,j}^o &= 0 \end{aligned} \tag{2.2}$$

$$t^{o}_{ij}n_j = T_i \qquad \text{on } B'$$
$$u^{o}_{i} = U_i \qquad \text{on } B'' \tag{2.3}$$

in which E and ν are Young's modulus and Poisson's ratio, respectively, δ_{ij} is the Kronecker delta, and n_i are the components of the unit outer normal.

The second (primed) terms in Equations (2.1) represent the changes induced by buckling and satisfy the set of equations

$$T'_{ij} = \frac{E}{1-\nu^2}\left[\frac{1-\nu}{2}(U'_{i,j} + U'_{j,i} + W_{,i}W_{,j}) + \nu(U'_{k,k} + \frac{1}{2}W_{,k}W_{,k})\delta_{ij}\right] = T'_{ji} \qquad \text{in R}$$

$$T'_{ij,j} = 0 \tag{2.4}$$

$$T'_{ij}n_j = 0 \qquad \text{on } B'$$
$$U'_i = 0 \qquad \text{on } B'' \tag{2.5}$$

in which the static deflection W satisfies the additional equation

$$D\Delta\Delta W - h(\lambda t^{o}_{ij} + T'_{ij})W_{,ij} = 0 \quad \text{in R} \tag{2.6}$$

and appropriate boundary conditions on B. In Equation (2.6) Δ stands for the Laplacian operator and D, the bending stiffness, is given by

$$D = \frac{Eh^3}{12(1-\nu^2)} \tag{2.7}$$

The separation of the solution into two parts in line with Equation (2.1) has been found convenient because of the linear homogeneity of Equations (2.4) and (2.5) in U'_i and T'_{ij}. That is, for a given function $W(x,y)$ these equations represent a boundary value problem whose solution may be expressed symbolically by means of

$$T'_{ij} = \frac{1}{2} \left\langle W_{,i}W_{,j} \right\rangle \tag{2.8}$$

The operator so defined obeys appropriate superposition principles, e.g.,

$$\langle W^1_{,i}+W^2_{,i}, W^1_{,j}+W^2_{,j}\rangle = \langle W^1_{,i}W^1_{,j}\rangle + \langle W^2_{,i}W^1_{,j}\rangle + \langle W^1_{,i}W^2_{,j}\rangle + \langle W^2_{,i}W^2_{,j}\rangle \quad (2.9)$$

It is also noted that for sufficiently small values of λ (say, $\lambda \leqq \lambda_o$), Equations (2.4), (2.5), and (2.6) admit only trivially vanishing solutions. For $\lambda > \lambda_o$ these represent unstable configurations. Other (i.e. buckled) configurations exist in that case, although not all of these may be stable.

If a small vibration $w(x,y)e^{i\omega t}$ is superimposed on W, then, after linearization with respect to w, the governing equation of motion is

$$D\Delta\Delta w - h(\lambda t^o_{ij} + T'_{ij})w_{,ij} - ht'_{ij}W_{,ij} - h\mu w = 0 \quad (2.10)$$

in which

$$\mu = \rho\omega^2 \quad (2.11)$$

with ρ representing the mass density. The dynamic membrane stress t'_{ij} (or rather its amplitude) is given symbolically by

$$t'_{ij} = \frac{1}{2}\langle W_{,i}w_{,j} + w_{,i}W_{,j}\rangle \quad (2.12)$$

if in-plane inertia is ignored.*

We consider now a rectangular, simply supported plate covering the region $0 \leqq x \leqq a$, $0 \leqq y \leqq b$. It is postulated that the edges are made to approach one another by a specified amount and are then held fixed during the vibration. This seemingly artificial type of boundary

*For the case of shallow shells this has been justified in Ref. 23.

condition is equivalent to fixing* the boundary while the plate is heated uniformly; this is considered to be a reasonably realistic representation of actual conditions.

The complete set of boundary conditions for the static case is therefore as follows:

$$B_1(W) \equiv W(0,y) = W(a,y) = W(x,0) = W(x,b) = 0 \tag{2.13}$$

$$B_2(W) \equiv W_{,xx}(0,y) = W_{,xx}(a,y) = W_{,yy}(x,0) = W_{,yy}(x,b) = 0 \tag{2.14}$$

$$\begin{aligned} &u^o(0,y) = v^o(x,0) = 0;\ u^o(a,y) = U_E,\ v^o(x,b) = V_E \\ &v^o_{,x}(0,y) = v^o_{,x}(a,y) = u^o_{,y}(x,0) = u^o_{,y}(x,b) = 0 \end{aligned} \tag{2.15}$$

$$\begin{aligned} &U'(0,y) = U'(a,y) = V'(x,0) = V'(x,b) = 0 \\ &V'_{,x}(0,y) = V'_{,x}(a,y) = U'_{,y}(x,0) = U'_{,y}(x,b) = 0 \end{aligned} \tag{2.16}$$

U_E and V_E are the magnitude of the displacements which are required to cause the plate to buckle in the linear sense; thus the value of λ determines the extent to which the critical deformation (or temperature increase) has been exceeded.

For the dynamic case the boundary conditions are

$$B_1(w) \equiv w(0,y) = w(a,y) = w(x,0) = w(x,b) = 0 \tag{2.17}$$

$$B_2(w) \equiv w_{,xx}(0,y) = w_{,xx}(a,y) = w_{,yy}(x,0) = w_{,yy}(x,b) = 0 \tag{2.18}$$

$$\begin{aligned} &u'(0,y) = u'(a,y) = v'(x,0) = v'(x,b) = 0 \\ &v'_{,x}(0,y) = v'_{,x}(a,y) = u'_{,y}(x,0) = u'_{,y}(x,b) = 0 \end{aligned} \tag{2.19}$$

in which u' and v' are the dynamic displacement amplitudes of a point in the x and y directions, respectively.

---

* Actually, fixity is assumed only in the normal direction, while the plate is free to slide in the direction of the boundary. This type of shearless constraint reduces the computational labor enormously, yet is believed to introduce no significant deviation from the computationally far more intractable condition of full fixity.

CHAPTER III

THE PERTURBATION SOLUTION

In this chapter we obtain a solution to both the static and dynamic problem through a perturbation expansion. As usual this method is operative only within a limited range of the perturbation parameter; for large values the series converges too slowly to be handled without excessive labor. In the present case the results obtained appear to be acceptable up to a value of at least ten of the post-buckling parameter λ. The static portion is similar to previous work by Stein,[18] but has had to be rederived in order to make the dynamic portion comprehensible.

We consider first the static case. It is required to solve Equation (2.6), in which t^o_{ij} and u^o_i satisfy Equations (2.2) and T'_{ij}, U'_i and W satisfy Equations (2.4), with the associated boundary conditions Equations (2.13), (2.14), (2.15) and (2.16).

Equations (2.2) and (2.15) represent the usual problem of plane elasticity, whose well-known solution for a rectangular plate is

$$\begin{aligned} u^o(x,y) &= U_E \frac{x}{a} \\ v^o(x,y) &= V_E \frac{y}{b} \end{aligned} \tag{3.1}$$

where U_E and V_E are found later on.

We now assume the functions W and λ to be expandable in a power series in terms of an arbitrary parameter ϵ in the neighborhood of the point of buckling $\epsilon = 0$, that is, with $W \equiv W(x,y,\epsilon)$,

$$W = \epsilon W^{(1)} + \epsilon^3 W^{(3)} + \epsilon^5 W^{(5)} + \ldots \tag{3.2}$$

$$\lambda = \lambda_o + \epsilon^2 \lambda_2 + \epsilon^4 \lambda_4 + \ldots . \tag{3.3}$$

Here $W^{(n)*}$ are functions of x,y only and ϵ, the perturbation parameter, will be assumed to be monotonely increasing as buckling progresses. The fact that W is odd and λ is even in ϵ may be easily verified upon substitution in the relevant equations. For the sake of brevity these steps are omitted here. Since at the point of buckling, $\epsilon = 0$, λ_o is identified as the load parameter for the Euler buckling load. In view of Equations (2.8) and (2.9) T'_{ij} can be expressed in terms of the arbitrary parameter ϵ as follows:

$$T'_{ij} = \sum_{p=1}^{\infty} \epsilon^p T_{ij}^{(p)} \tag{3.4}$$

in which

$$T_{ij}^{(p)} = \frac{1}{2} \left\langle W_{,i}^{(p-1)} W_{,j}^{(1)} + W_{,i}^{(p-2)} W_{,j}^{(2)} + \ldots + W_{,i}^{(1)} W_{,j}^{(p-1)} \right\rangle \tag{3.5}$$

The membrane stress equilibrium equations can be written in terms of the additional displacements as

$$\begin{aligned} U'_{,xx} + \frac{1-\nu}{2} U'_{,yy} + \frac{1+\nu}{2} V'_{,xy} &= -W_{,x}W_{,xx} - \frac{1+\nu}{2} W_{,y}W_{,xy} - \frac{1-\nu}{2} W_{,x}W_{,yy} \\ V'_{,yy} + \frac{1-\nu}{2} V'_{,xx} + \frac{1+\nu}{2} U'_{,xy} &= -W_{,y}W_{,yy} - \frac{1+\nu}{2} W_{,x}W_{,xy} - \frac{1-\nu}{2} W_{,y}W_{,xx} \end{aligned} \tag{3.6}$$

In view of this the additional displacements U' and V' can also be expanded in a power series of the same arbitrary parameter ϵ, and the series is expected to start with the second power of ϵ and to contain

---

* Superscripts in parentheses are intended to identify the variable and not to act as an exponent. Whenever possible, however, parentheses will be omitted where there is no possible confusion and will be included only if necessary.

only even expansions. Thus,

$$U' = \epsilon^2 U^{(2)} + \epsilon^4 U^{(4)} + \ldots. \tag{3.7}$$

$$V' = \epsilon^2 V^{(2)} + \epsilon^4 V^{(4)} + \ldots. \tag{3.8}$$

When these expansions are substituted in Equation (2.6) and other relevant equations, the requirement that each coefficient in the power series vanish individually leads to a set of linear differential equations with associated boundary conditions. These equations can be solved in sequence.

For ϵ^1 the differential equation is

$$L_1(W^1) \equiv D\triangle\triangle W^1 - h\lambda_o t^o_{ij} W^1_{,ij} = 0 \tag{3.9}$$

and the boundary conditions are

$$B_1(W^1) = 0 \tag{3.10}$$

$$B_2(W^1) = 0 \tag{3.11}$$

This is the linear eigenvalue problem for the buckling of a rectangular plate subject to edge compressions or displacements. It is now assumed that the edge displacements are such as to induce a hydrostatic plane stress,* that is,

$$U_E = -\frac{1-\nu}{E} a$$

$$V_E = -\frac{1-\nu}{E} b \tag{3.12}$$

$$t^o_{ij} = -\delta_{ij}$$

There exist an infinite number of eigenvalues and eigenfunctions. The normalized deflection function

$$W^1 = h \sin \frac{m\pi x}{a} \sin \frac{n\pi y}{b} \tag{3.13}$$

---

* This corresponds to the case of uniform heating of a thermally isotropic plate.

in which m and n are integers, automatically satisfies the boundary conditions. This fixes the physical meaning of ϵ as representing the amplitude of the first term in the perturbation expansion. The associated eigenvalue takes the familiar form

$$\lambda_o = \frac{D}{h}\left(\frac{m^2\pi^2}{a^2} + \frac{n^2\pi^2}{b^2}\right) \tag{3.14}$$

Any combination of m and n in the above expression can be identified as an eigenvalue of the differential equation. If only the first buckling mode is of interest, the lowest eigenvalue associated with the first buckling mode is obtained by choosing $m = n = 1$ regardless of the aspect ratio $\frac{a}{b}$ of the plate.

For ϵ^3 the differential equation is

$$L_1(W^3) = h\lambda_2 t^o_{ij} W^1_{,ij} + hT^2_{ij} W^1_{,ij} \tag{3.15}$$

in which

$$T^2_{ij} = \frac{1}{2}\left\langle W^1_{,i} W^1_{,j} \right\rangle \tag{3.16}$$

with W^1 given by Equation (3.13).

The associated boundary conditions are

$$B_1(W^3) = 0 \tag{3.17}$$

$$B_2(W^3) = 0 \tag{3.18}$$

The differential Equation (3.15) here is nonhomogeneous, but the associated homogeneous equation is identical with Equation (3.9). This homogeneous system has the nontrivial solution W^1. The nonhomogeneous differential equation therefore has a solution if and only if the right hand side of Equation (3.15) is orthogonal to W^1.[24] When Equation (3.9) is multiplied by W^3 and Equation (3.15) by W^1, after

integration by parts and in view of the boundary conditions, this orthogonality condition becomes

$$\lambda_2 = - \frac{\int T^2_{ij} W^1_{,i} W^1_{,j} dA}{\int t^o_{ij} W^1_{,i} W^1_{,j} dA} \tag{3.19}$$

Furthermore, the solution is not unique. Any arbitrary multiple of W^1 added to a particular solution is also a solution of the differential Equation (3.15). Let $\bar{W}^3$ be a particular solution. Then W^3 is, in general, given by

$$W^3 = \bar{W}^3 + \alpha_3 W^1 \tag{3.20}$$

The choice of the value of α_3 is arbitrary. For convenience of computation let

$$\int t^o_{ij} W^1_{,i} W^3_{,j} = 0 \tag{3.21}$$

then

$$\alpha_3 = - \frac{\int t^o_{ij} W^1_{,i} \bar{W}^3_{,j} dA}{\int t^o_{ij} W^1_{,i} W^1_{,j} dA} \tag{3.22}$$

This is always possible, since in the present case

$$\int t^o_{ij} W^1_{,i} W^1_{,j} dA = - \int W^1_{,i} W^1_{,i} dA < 0 \tag{3.23}$$

Let the vector $\vec{T}$ denote any stress field T_{ij} symbolically, and let the inner product of two vectors $\vec{T}^\alpha$ and $\vec{T}^\beta$ be defined by

$$\vec{T}^\alpha \cdot \vec{T}^\beta = h \int T^\alpha_{ij} E^\beta_{ij} dA \tag{3.24}$$

in which E^β_{ij} is the strain associated with the stress T^β_{ij}. In view of the positive definiteness of the strain energy and of the symmetry of the stress-strain coefficients, it follows that $\vec{T}^\alpha \cdot \vec{T}^\alpha$ is positive definite and that $\vec{T}^\alpha \cdot \vec{T}^\beta = \vec{T}^\beta \cdot \vec{T}^\alpha$.

By Equation (3.16), through the application of Green's theorem, and in view of the boundary conditions, it can be shown that

$$\vec{T}^1 \cdot \vec{T}^2 = \frac{1}{2} h \int T^1_{ij} W^1_{,i} W^1_{,j} dA \tag{3.25}$$

Likewise we define

$$\vec{T} \cdot (W^m W^n) = h \int T_{ij} W^m_{,i} W^n_{,j} dA \tag{3.26}$$

Equation (3.19) can be written

$$\lambda_2 = - \frac{\vec{T}^2 \cdot \vec{T}^2}{\vec{T}^o \cdot \vec{T}^2} \tag{3.27}$$

Since, for positive λ, $\vec{T}^o \cdot \vec{T}^2$ is negative, [see (3.23)], and since $\vec{T}^2 \cdot \vec{T}^2$ is positive definite, λ_2 is always positive. This, in turn, confirms the well-known fact that the load parameter increases with increasing buckling amplitudes near the buckling point; the latter therefore represents a point of stable equilibrium.

For ϵ^5 the governing differential equation is

$$L_1(W^5) = h\lambda_2 t^o_{ij} W^3_{,ij} + h\lambda_4 t^o_{ij} W^1_{,ij} + h T^2_{ij} W^3_{,ij} + h T^4_{ij} W^1_{,ij} \tag{3.28}$$

in which

$$T^4_{ij} = \frac{1}{2} \left\langle W^1_{,i} W^3_{,j} + W^3_{,i} W^1_{,j} \right\rangle \tag{3.29}$$

with associated boundary conditions

$$B_1(W^5) = 0 \tag{3.30}$$

$$B_2(W^5) = 0 \tag{3.31}$$

As before, the right hand side of Equation (3.28) must satisfy the orthogonality condition if the equations has a solution for W^5. Thus,

$$\lambda_4 = - \frac{\int T^2_{ij} W^3_{,i} W^1_{,j} dA + \int T^4_{ij} W^1_{,i} W^1_{,j} dA}{\int t^o_{ij} W^1_{,i} W^1_{,j} dA} \tag{3.32}$$

Let $\overline{W}^5$ be a particular solution of Equation (3.28), then

$$W^5 = \overline{W}^5 + \alpha_5 W^1 \tag{3.33}$$

Let, for convenience,

$$\int t^o_{ij} W^1_{,i} W^5_{,j} dA = 0 \tag{3.34}$$

from which

$$\alpha_5 = - \frac{\int t^o_{ij} W^1_{,i} \overline{W}^5_{,j} dA}{\int t^o_{ij} W^1_{,i} W^1_{,j} dA} \tag{3.35}$$

In terms of the inner product notation, Equation (3.32) reduces to

$$\lambda_4 = - \frac{3\vec{T}^4 \cdot \vec{T}^2}{2\vec{T}^o \cdot \vec{T}^2} \tag{3.36}$$

in which Equation (3.29) has been utilized. Since $\vec{T}^4 \cdot \vec{T}^2$ can be either positive or negative, no conclusion can be drawn relative to the sign of the value of λ_4 .

The equations which contain higher powers of ϵ can be solved in the same manner; however, the calculations become exceedingly cumbersome. For the range of values considered here no further expansion has been found necessary.

We now consider the vibratory motion of the plate. It is noted that the method of solution in the dynamic case is similar to the one used above and hence only the essential points are presented.

The equation governing the motion of the plate is Equation (2.10). For the sake of convenience, it is presented again:

$$D\Delta\Delta W - h(\lambda t^o_{ij} + T'_{ij}) w_{,ij} - h t'_{ij} W_{,ij} - \mu h w = 0 \tag{2.10}$$

with

$$t'_{ij} = \frac{1}{2} \left\langle W_{,i} w_{,j} + w_{,i} W_{,j} \right\rangle \tag{2.12}$$

subject to the boundary conditions

$$B_1(w) = 0 \tag{2.17}$$

$$B_2(w) = 0 \tag{2.18}$$

Here, λ, t^o_{ij}, T'_{ij} and W are now assumed to be known. The differential equations and the boundary conditions are linearly homogeneous in w, and once again we have an eigenvalue problem in which μ represents the eigenvalue. For each eigenvalue ${}_{pq}\mu$, there exists an eigenfunction ${}_{pq}w(x,y)$ which satisfies the differential equation as well as the boundary conditions. The prescripts p,q denote the pq^{th} mode of vibration.

We assume that the eigenfunction ${}_{pq}w$ and the associated eigenvalue ${}_{pq}\mu$ can be expanded in a power series in terms of the same parameter ϵ as in the static case, that is,

$${}_{pq}w = {}_{pq}w^{(o)} + \epsilon^2 \, {}_{pq}w^{(2)} + \epsilon^4 \, {}_{pq}w^{(4)} + \ldots. \tag{3.37}$$

$${}_{pq}\mu = {}_{pq}\mu^{(o)} + \epsilon^2 \, {}_{pq}\mu^{(2)} + \epsilon^4 \, {}_{pq}\mu^{(4)} + \ldots. \tag{3.38}$$

The fact that ${}_{pq}w$ and ${}_{pq}\mu$ are even expansions in ϵ may be easily verified upon substitution in the relevant equations. For the sake of brevity these steps are omitted here. In view of Equation (2.12) ${}_{pq}t'_{ij}$ can be expressed as

$${}_{pq}t'_{ij} = \epsilon \, {}_{pq}t^{(1)}_{ij} + \epsilon^3 \, {}_{pq}t^{(3)}_{ij} + \epsilon^5 \, {}_{pq}t^{(5)}_{ij} + \ldots. \tag{3.39}$$

with

$${}_{pq}t^{(n)}_{ij} = \frac{1}{2} \left\langle \sum_{s=1,3}^{n} \left(W^{(s)}_{,i} \; {}_{pq}w^{(n-s)}_{,j} + {}_{pq}w^{(s)}_{,i} \; W^{(n-s)}_{,j} \right) \right\rangle$$

Upon substitution of these perturbation expansions in Equation (2.10) a new sequence of differential equations is obtained whose solution follows procedures analogous to those presented for the static case.

From here on the prescripts p,q will be omitted, it being understood that $w^{(n)}$, $\mu^{(n)}$ and $t_{ij}^{(n)}$ denote the nth perturbation coefficients of the deflection, frequency squared and membrane stresses functions, respectively, for the pq^{th} mode of vibration of the plate. Whenever there is a possibility of confusion, or a specific mode of vibration is referred to, the prescripts will be added.

For ϵ^o the differential equation is

$$L_2(w^o) \equiv D\triangle\triangle w^o - h\lambda_o t_{ij}^o w_{,ij}^o - \mu^o h w^o = 0 \tag{3.40}$$

with the associated boundary conditions

$$B_1(w^o) = 0 \tag{3.41}$$

$$B_2(w^o) = 0 \tag{3.42}$$

This is satisfied by the normalized* function

$$w^o = \sin \frac{p\pi x}{a} \sin \frac{q\pi y}{b} \tag{3.43}$$

in which p and q are integers, provided that

$$\mu^o = \left(\frac{p^2\pi^2}{a^2} + \frac{q^2\pi^2}{b^2}\right) \left[\frac{D}{h}\left(\frac{p^2\pi^2}{a^2} + \frac{q^2\pi^2}{b^2}\right) - \lambda_o\right] \tag{3.44}$$

The membrane stresses t_{ij}^1 can now be obtained from

$$t_{ij}^1 = \frac{1}{2} \left\langle w_{,i}^1 w_{,j}^o + w_{,i}^o w_{,j}^1 \right\rangle \tag{3.45}$$

---

* Naturally the linearized vibration solution is subject to an arbitrary amplitude factor.

For ϵ^2 the differential equation is

$$L_2(w^2) = h(\lambda_2 t^o_{ij} + T^2_{ij})w^o_{,ij} + ht^1_{ij}W^1_{,ij} + \mu^2 hw^o \tag{3.46}$$

and the boundary conditions are

$$B_1(w^2) = 0 \tag{3.47}$$

$$B_2(w^2) = 0 \tag{3.48}$$

As before, the right hand side of Equation (3.46) must satisfy an orthogonality condition* if a solution is to exist. After some manipulation this leads to

$$\mu^2 = \frac{(\lambda_2 \vec{T}^o + \vec{T}^2) \cdot (w^o w^o) + \vec{t}^1 \cdot \vec{t}^1}{h \int (w^o)^2 dA} \tag{3.49}$$

The solution of the differential Equation (3.46) is not unique; any multiple of w^o added to the particular solution is also a solution of the differential equation. For the sake of convenience we let

$$\int w^2 w^o dA = 0 \tag{3.50}$$

Thus, w^2 is determined and t^3_{ij} can now be obtained from

$$t^3_{ij} = \frac{1}{2}\left\langle W^1_{,i}w^2_{,j} + w^2_{,i}W^1_{,j} + W^3_{,i}w^o_{,j} + w^o_{,i}W^3_{,j}\right\rangle \tag{3.51}$$

For ϵ^4 the differential equation is

$$\begin{aligned} L_2(w^4) = {} & ht^o_{ij}(\lambda_4 w^o_{,ij} + \lambda_2 w^2_{,ij}) + hT^4_{ij}w^o_{,ij} + hT^2_{ij}w^2_{,ij} \\ & + ht^3_{ij}W^1_{,ij} + ht^1_{ij}W^3_{,ij} + \mu^4 hw^o + \mu^2 hw^2 \end{aligned} \tag{3.52}$$

---

* Note that this orthogonality condition is different from the one pertaining to the static case.

and the associated boundary conditions are

$$B_1(w^4) = 0 \tag{3.53}$$

$$B_2(w^4) = 0 \tag{3.54}$$

Again, the orthogonality condition determines the value of

$$\mu^4 = \frac{(\lambda_4\vec{T}^0 + \vec{T}^4)\cdot(w^0w^0) + (\lambda_2\vec{T}^0 + \vec{T}^2)\cdot(w^2w^0) + 2\vec{t}^3 \cdot \vec{t}^1 - \vec{t}^1 \cdot (w^1w^2)}{h \int (w^0)^2 dA} \tag{3.55}$$

while the deflection function w^4 satisfies

$$\int w^4 w^0 dA = 0 \tag{3.56}$$

Since the static deflection is truncated at the coefficient w^5, there is no sense in pursuing the solution of the dynamic problem beyond this point.

The results of these calculationsare given in Appendix A for the general case of a rectangular plate. The first part deals with the static problem. Algebraic expressions are given for the expansion terms in the deflection $W(x,y)$, the additional stresses $T'_{ij}(x,y)$, the load parameter λ, and the additional membrane displacements $U'(x,y)$ and $V'(x,y)$. These are not necessarily based on the assumption that the plate buckles freely immediately after its unbuckled equilibrium configuration becomes unstable; however, the case of $m = n = 1$ is the only one which has practical significance.

The dynamic response for the same case is computed next. Again general algebraic expressions are given for the vibration modes, membrane stresses, and frequency parameters. Only the lowest two modes $p = 1$, $q = 1$ and $p = 2$, $q = 1$ are considered; an obvious, and trivial,

extension is easily obtained for $p = 1$, $q = 2$ through a suitable exchange of variables.

Higher buckling modes (say, $m = 2$, $n = 1$) are of course associated with larger critical buckling parameters; however, as the lowest buckling parameter λ_o is exceeded, at least one frequency becomes imaginary and the associated unbuckled equilibrium configuration becomes unstable and hence physically meaningless. Nevertheless it is conceivable that if the plate were forced into one of these higher buckling modes (perhaps through the application of kinematic constraints), its equilibrium may again become stable for sufficiently large buckling amplitude. A necessary and sufficient criterion for such a condition is that the square of the smallest frequency of vibration becomes again positive.

This may be physically significant. As has been observed and commented on repeatedly, buckled plates often snap from their original buckling configuration into another one. Just when this type of "secondary buckling" takes place is conjectural and has been the object of some speculation; for example it has been postulated that a suitable criterion is obtained when the energies in the primary and secondary states are equated.[25] In any event it is safe to state that a snap-through from a stable configuration into an unstable one can be ruled out. The lowest loading parameter at which the secondary configuration becomes stable may therefore be considered a lower bound to the secondary buckling parameter.

Charts showing the frequencies of vibration for specific cases are given in the present paper for several such higher buckling modes,

and in Appendix A are included the general algebraic expressions for the vibration modes, membrane stresses and frequency parameters of the lowest two modes $p = 1, q = 1$ and $p = 2, q = 1$ if the plate has buckled into the second mode $m = 2, n = 1$. The general algebraic expressions of μ^0 and μ^2 are given for any vibration mode and for any buckling mode. These expressions are generally rather complex and have therefore been deleted from the main body of the paper.

For the special (and, near the buckling point, most important) condition of $m = n = p = q = 1$, the formulas become much simpler. Since, for that case, $w^0 = W^1$, it follows from Equation (3.40) that

$$\mu^0 = 0 \tag{3.57}$$

as expected, which in turn implies that $\vec{t}^1 = 2\vec{T}^2$ and $w^2 = 3w^3$. When these relations are substituted in Equations (3.49) and (3.55), it follows, after some manipulation, that

$$\mu^2 = \frac{4\vec{T}^2 \cdot \vec{T}^2}{h \int (W^1)^2 dA} = 2\left(\frac{\pi^2}{a^2} + \frac{\pi^2}{b^2}\right) \lambda_2 \tag{3.58}$$

$$\mu^4 = \frac{2\lambda_4 \vec{T}^0 \cdot \vec{T}^2 + 3\lambda_2 \vec{T}^0 \cdot (W^3 W^1) + 15\vec{T}^4 \cdot \vec{T}^2}{h \int (W^1)^2 dA} = 4\left(\frac{\pi^2}{a^2} + \frac{\pi^2}{b^2}\right) \lambda_4 \tag{3.59}$$

For the rate of change of frequency of vibration with respect to the load parameter in the neighborhood of buckling ($\epsilon = 0$) one obtains

$$\lim_{\epsilon \to 0} \frac{d\mu}{d\lambda} = \lim_{\epsilon \to 0} \frac{d\mu}{d\epsilon} \Big/ \frac{d\lambda}{d\epsilon} = \frac{\mu^{(2)}}{\lambda_2} \tag{3.60}$$

For the vibration mode $p = q = 1$, $\mu^{(2)}$ is positive and so is the value of $\frac{d\mu}{d\lambda}$ at the point of buckling, as anticipated since the plate is stable in the immediate post-buckling neighborhood. A similar, though less important, conclusion is reached for any vibration mode satisfying $p=m$, $q=n$.

CHAPTER IV

THE ENERGY METHOD SOLUTION

In the perturbation method, the rapidity of convergence of the perturbation series is always an issue. In some problems the series converges fairly rapidly, in others it converges only for a rather small range of values of the load parameter λ. An indication (though not fully conclusive) of the convergence of the perturbation series is the agreement between the results obtained from the truncation at the term ϵ^n and ϵ^{n-1}. The present calculations show satisfactory convergence for a technically significant range of the load parameter. Nevertheless the truncated expressions become unreliable, as expected, when the buckling amplitudes reach very large values. To cover this range at least approximately an energy method is employed in this chapter.

The static condition is analyzed by a method similar to the one of Marguerre-Papkovitch.[9] The deflection of the plate is assumed to be expressed by means of

$$W = C_1 W^1 + C_2 W^2 + C_3 W^3 \tag{4.1}$$

in which W^1, W^2 and W^3 are geometrically admissible functions and C_1, C_2 and C_3 are parameters whose values are to be determined from the theorem of minimum potential energy. With this assumed deflection function, the additional membrane stresses T'_{ij} can be obtained from Equation (2.8), that is,

$$T'_{ij} = C_1^2 T_{ij}^{11} + C_2^2 T_{ij}^{22} + C_3^2 T_{ij}^{33} + C_1 C_2 T_{ij}^{12} + C_1 C_3 T_{ij}^{13} + C_2 C_3 T_{ij}^{23} \tag{4.2}$$

in which

$$T_{ij}^{11} = \frac{1}{2} \left\langle W^1_{,i} W^1_{,j} \right\rangle$$

$$T_{ij}^{22} = \frac{1}{2} \left\langle W^2_{,i} W^2_{,j} \right\rangle$$

$$T_{ij}^{33} = \frac{1}{2} \left\langle W^3_{,i} W^3_{,j} \right\rangle$$

$$T_{ij}^{12} = \frac{1}{2} \left\langle W^1_{,i} W^2_{,j} + W^2_{,i} W^1_{,j} \right\rangle$$

$$T_{ij}^{13} = \frac{1}{2} \left\langle W^1_{,i} W^3_{,j} + W^3_{,i} W^1_{,j} \right\rangle$$

$$T_{ij}^{23} = \frac{1}{2} \left\langle W^2_{,i} W^3_{,j} + W^3_{,i} W^2_{,j} \right\rangle$$

The additional potential energy V, that is the difference in the potential energies of the buckled and unbuckled states, is defined by

$$V = U_b + U_m - \lambda W_e \tag{4.3}$$

in which

$$U_b \equiv \frac{D}{2} \int [(1-\nu) W_{,ij} W_{,ij} + \nu W_{,ii} W_{,jj}] dA$$

$$U_m \equiv \frac{h}{2} \int T'_{ij} E'_{ij} dA = \frac{1}{2} \vec{T}' \cdot \vec{T}'$$

$$W_e \equiv - \frac{h}{2} \int t^o_{ij} W_{,i} W_{,j} dA$$

After application of Green's theorem, membrane stress equilibrium equations ($T'_{ij,j} = 0$) and boundary conditions, the membrane strain energy U_m is now given by

$$U_m = \frac{h}{4} \int T'_{ij} W_{,i} W_{,j} dA \tag{4.4}$$

If the edges of the plate are simply supported, the bending strain energy U_b reduces to

$$U_b = \frac{D}{2} \int W_{,ii} W_{,jj} dA \tag{4.5}$$

Since $t^{o}_{ij} = -\delta_{ij}$, W_e becomes

$$W_e = \frac{h}{2} \int W_{,i} W_{,i} dA \tag{4.6}$$

Upon substitution of Equations (4.1) and (4.2) into Equation (4.3) we have

$$\begin{aligned} V = {} & (U_b^{11} - \lambda W_e^{11}) C_1^2 + (U_b^{22} - \lambda W_e^{22}) C_2^2 + (U_b^{33} - \lambda W_e^{33}) C_3^2 \\ & + \frac{1}{2} (C_1^2 \vec{T}^{11} + C_2^2 \vec{T}^{22} + C_3^2 \vec{T}^{33} + C_1 C_2 \vec{T}^{12} + C_1 C_3 \vec{T}^{13} + C_2 C_3 \vec{T}^{23}) \\ & \cdot (C_1^2 \vec{T}^{11} + C_2^2 \vec{T}^{22} + C_3^2 \vec{T}^{33} + C_1 C_2 \vec{T}^{12} + C_1 C_3 \vec{T}^{13} + C_2 C_3 \vec{T}^{23}) \end{aligned} \tag{4.7}$$

in which*

$$U_b^{11} \equiv \frac{D}{2} \int W^1_{,ii} W^1_{,jj} dA$$

$$U_b^{22} \equiv \frac{D}{2} \int W^2_{,ii} W^2_{,jj} dA$$

$$U_b^{33} \equiv \frac{D}{2} \int W^3_{,ii} W^3_{,jj} dA$$

$$W_e^{11} \equiv \frac{h}{2} \int W^1_{,i} W^1_{,i} dA$$

$$W_e^{22} \equiv \frac{h}{2} \int W^2_{,i} W^2_{,i} dA$$

$$W_e^{33} \equiv \frac{h}{2} \int W^3_{,i} W^3_{,i} dA$$

Setting the first variation of the potential energy equal to zero leads

---

* Terms such as U_b^{12}, W_e^{12} etc. may also appear; however, if $W^{(n)}$ are chosen to be orthogonal functions, these terms vanish from the above expression.

to

$$2(U_b^{11} - \lambda W_e^{11})C_1 + 2(\vec{T}^{11} \cdot \vec{T}^{11})C_1^3 + (\vec{T}^{12} \cdot \vec{T}^{12} + 2\vec{T}^{11} \cdot \vec{T}^{22})C_1C_2^2$$
$$+ (\vec{T}^{13} \cdot \vec{T}^{13} + 2\vec{T}^{11} \cdot \vec{T}^{33})C_1C_3^2 + 3(\vec{T}^{11} \cdot \vec{T}^{12})C_1^2C_2 + 3(\vec{T}^{11} \cdot \vec{T}^{13})C_1^2C_3$$
$$+ 2(\vec{T}^{11} \cdot \vec{T}^{23} + \vec{T}^{12} \cdot \vec{T}^{13})C_1C_2C_3 + (\vec{T}^{22} \cdot \vec{T}^{12})C_2^3 + (\vec{T}^{22} \cdot \vec{T}^{13} + \vec{T}^{12} \cdot \vec{T}^{23})C_2^2C_3$$
$$+ (\vec{T}^{33} \cdot \vec{T}^{12} + \vec{T}^{13} \cdot \vec{T}^{23})C_1C_3^2 + (\vec{T}^{33} \cdot \vec{T}^{13})C_3^3 = 0 \qquad (4.8a)$$

$$2(U_b^{22} - \lambda W_e^{22})C_2 + 2(\vec{T}^{22} \cdot \vec{T}^{22})C_2^3 + (\vec{T}^{12} \cdot \vec{T}^{12} + 2\vec{T}^{11} \cdot \vec{T}^{12})C_1^2C_2$$
$$+ (\vec{T}^{23} \cdot \vec{T}^{23} + 2\vec{T}^{22} \cdot \vec{T}^{33})C_2C_3^2 + 3(\vec{T}^{22} \cdot \vec{T}^{12})C_1C_2^2 + 3(\vec{T}^{22} \cdot \vec{T}^{23})C_2^2C_3$$
$$+ 2(\vec{T}^{22} \cdot \vec{T}^{13} + \vec{T}^{12} \cdot \vec{T}^{23})C_1C_2C_3 + (\vec{T}^{33} \cdot \vec{T}^{23})C_3^3 + (\vec{T}^{33} \cdot \vec{T}^{12} + \vec{T}^{13} \cdot \vec{T}^{23})C_1C_3^2$$
$$+ (\vec{T}^{11} \cdot \vec{T}^{23} + \vec{T}^{12} \cdot \vec{T}^{13})C_1^2C_3 + (\vec{T}^{11} \cdot \vec{T}^{12})C_1^3 = 0 \qquad (4.8b)$$

$$2(U^{33} - \lambda W^{33})C_3 + 2(\vec{T}^{33} \cdot \vec{T}^{33})C_3^3 + (\vec{T}^{13} \cdot \vec{T}^{13} + 2\vec{T}^{11} \cdot \vec{T}^{33})C_1^2C_3$$
$$+ (\vec{T}^{23} \cdot \vec{T}^{23} + 2\vec{T}^{22} \cdot \vec{T}^{33})C_2^2C_3 + 3(\vec{T}^{33} \cdot \vec{T}^{13})C_1C_3^2 + 3(\vec{T}^{33} \cdot \vec{T}^{23})C_2C_3^2$$
$$+ 2(\vec{T}^{33} \cdot \vec{T}^{12} + \vec{T}^{13} \cdot \vec{T}^{23})C_1C_2C_3 + (\vec{T}^{11} \cdot \vec{T}^{13})C_1^3 + (\vec{T}^{11} \cdot \vec{T}^{23} + \vec{T}^{12} \cdot \vec{T}^{13})C_1^2C_2$$
$$+ (\vec{T}^{22} \cdot \vec{T}^{13} + \vec{T}^{12} \cdot \vec{T}^{23})C_1C_2^2 + (\vec{T}^{22} \cdot \vec{T}^{23})C_2^3 = 0 \qquad (4.8c)$$

C_1, C_2 and C_3 can be solved in terms of the load parameter λ from Equations (4.8).

The deflection functions of the lowest buckling mode can be assumed to be of the following form

$$W^1 = \sin \frac{\pi}{a} x \sin \frac{\pi}{b} y$$
$$W^2 = \sin \frac{3\pi}{a} x \sin \frac{\pi}{b} y \qquad (4.9)$$
$$W^3 = \sin \frac{\pi}{a} x \sin \frac{3\pi}{b} y$$

This assumption is not without justification. W^1 is the buckling mode as predicted in the linear theory. The formation of a W^2 wave along the unloaded edges and in the direction of the loads has been observed experimentally in the buckling of a simply supported plate subjected to longitudinal edge compressions. It is therefore reasonable to include both W^2 and W^3 functions in the present problem. Note that W^1 is also the first term of the perturbation series for W and $(W^2 + W^3)$ is the second term of the perturbation series for a square plate.

An exact solution to the dynamic problem is generally out of the question, in spite of its linearity, because of the presence of functions of x and y as coefficients in the relevant differential equations. For this type of problem the Galerkin method (which, for conversative systems of the present kinds, represents essentially a modified energy method) yields comparatively good approximations which are known to constitute upper bounds to the exact eigenvalues.*

If the vibration mode is assumed to be of the form

$$w = \sum_{n=1}^{N} a_n w_n(x,y) \tag{4.10}$$

then this technique leads to the linear system

$$\sum_{n=1}^{N} a_n P_{mn} = 0 \quad (m = 1, 2, \ldots, N) \tag{4.11}$$

in which

$$P_{mn} = P_{nm} = D \int (\Delta w^n)(\Delta w^m) dA + \lambda \vec{T}^o \quad (w^n w^m) + \vec{T}' \cdot (w^n w^m) + \vec{t}^n \cdot (W\, w^m) - \mu h \int w^n w^m dA \tag{4.12}$$

with

$$t^n_{ij} \equiv \frac{1}{2} \left\langle W_{,i} w^n_{,j} + w^n_{,i} W_{,j} \right\rangle \tag{4.13}$$

* No such statement can be made here, of course, as long as the static problem itself has been solved only approximately.

These equations have a non-trivial solution for a_n if

$$\text{determinant } |P_{mn}| = 0 \tag{4.14}$$

from which μ is computed.

In the present analysis four terms have been used in the approximating series, namely,

$$\begin{aligned} w^1 &= \sin \frac{\pi x}{a} \sin \frac{\pi y}{b} \\ w^2 &= \sin \frac{\pi x}{a} \sin \frac{3\pi y}{b} \\ w^3 &= \sin \frac{2\pi x}{a} \sin \frac{\pi y}{b} \\ w^4 &= \sin \frac{2\pi x}{a} \sin \frac{3\pi y}{b} \end{aligned} \tag{4.15}$$

The squares of the frequencies of the various modes are plotted as functions of the load parameter λ, with the results shown in the chart.

To determine the stability and instability of the buckling modes it is necessary to examine the second variation of the potential energy V. The latter is given in Equation (4.3), which, for convenience, may be written symbolically

$$V = U_b(W,W) + U_m \langle WW \rangle \langle WW \rangle - \frac{1}{2} \lambda \vec{T}^o \cdot (WW) \tag{4.16}$$

The following expansions identities are also useful:

$$\begin{aligned} U_b(W+w) &= U_b(W,W) + 2U_b(W,w) + U_b(w,w) \\ U_m(W+w) &= U_m \langle WW \rangle \langle WW \rangle + 4U_m \langle WW \rangle \langle Ww \rangle \\ &\quad + 2U_m \langle WW \rangle \langle ww \rangle + 4U_m \langle Ww \rangle \langle Ww \rangle \\ &\quad + 4U_m \langle Ww \rangle \langle ww \rangle + U_m \langle ww \rangle \langle ww \rangle \\ \vec{T}^o \cdot (W+w) &= \vec{T}^o \cdot (WW) + 2\vec{T}^o \cdot (Ww) + \vec{T}^o \cdot (ww) \end{aligned} \tag{4.17}$$

A configuration is in equilibrium if the potential energy assumes a stationary value. By standard methods this leads to Equation (2.6) in the present problem. The second variation of the potential energy, which determines the stability or instability of the buckled state, takes the form

$$\delta^2 V(WW;\eta\eta) = U_b(\eta,\eta) + 2U_m \langle WW \rangle \langle \eta\eta \rangle + 4U_m \langle W\eta \rangle \langle W\eta \rangle - \frac{1}{2} \lambda \vec{T}^o \cdot (\eta\eta) \tag{4.18}$$

After some integrations by parts and upon application of the boundary conditions, this leads to

$$\delta^2 V(WW;\eta\eta) = \int [\frac{D}{2} \eta_{,iijj} - \frac{h}{2}(\lambda t^o_{ij} + T'_{ij})\eta_{,ij} - \frac{h}{2} \tau'_{ij} W_{,ij}]\eta \, dA \tag{4.19}$$

in which

$$\tau'_{ij} \equiv \frac{1}{2} \langle W_{,i}\eta_{,j} + \eta_{,i}W_{,j} \rangle \tag{4.20}$$

It may be of interest to note that in view of Equation (2.10) the eigenvalues μ_n are equal to the stationary values of this expression provided the function $\eta(x,y)$ is chosen to be the associated normalized vibration mode $w_n(x,y)$. Since positive values for all μ_n have previously been identified with stability this confirms the familiar connection between stability and the positive definiteness of the second variation of the potential energy.

It is recalled that λ is the ratio of the edge displacement to that required for the initial instability. Now let γ be the ratio of the edge compressive force caused by the prescribed edge displacement to that required for initial instability. Then γ is related to λ

by the equation

$$\gamma = \frac{\int (\lambda t^{o}_{ij} + T^{i}_{ij})ds}{\int \lambda_{o} t^{o}_{ij}\, ds} \tag{4.21}$$

in which the integrals are along a loaded edge. The buckled state is often characterized by its γ versus λ curve, i.e., the load-shortening curve. The intersection of the load-shortening curve of one mode (say the symmetric mode which corresponds to the lowest buckling load) with the load-shortening curve of another mode (the antisymmetric mode which corresponds to the next lowest buckling load) usually indicates a possibility of the change of buckling modes. Just when and where this type of secondary buckling takes place is conjectural. Various authors[25,26] consider it reasonable to apply the equal energy criterion to determine the change of buckling modes. Hence, the primary buckling mode may change to the secondary buckling mode when

$$V_1 = V_2 \tag{4.22}$$

in which V_1 is the potential energy associated with the primary buckling mode and V_2 that associated with the secondary buckling mode.

In the present analysis, the vibration method and equal energy criterion are used to determine the stability of the buckling modes and changes of buckling modes. In addition to the problem stated in Chapter II, the stability and change of buckling modes of a simply supported rectangular plate subjected to uniaxial edge compression is also investigated by the present method. The details of this analysis are presented in Appendix B.

CHAPTER V

RESULTS AND DISCUSSION

Charts showing the frequencies of vibration and the load-shortening curves are given in nondimensional quantities μ', λ' and λ'', in which $\mu' = \mu/4(\frac{\pi}{a})^4 \frac{D}{h} \rho$, $\lambda' = \lambda/2(\frac{\pi}{a})^2 \frac{D}{h}$ and $\lambda'' = \lambda/4(\frac{\pi}{a})^2 \frac{D}{h}$. All calculations are based upon the value of Poisson's ratio $\nu = .30$.

Figure 1a shows the relation between μ' and λ' for small values of λ' for a square plate subjected to plane hydrostatic pressure. The results are obtained from the perturbation series which converges satisfactorily for $\lambda' < 16$. Only the two lowest vibration modes, i.e., $p = 1$, $q = 1$ and $p = 2$, $q = 1$, about the lowest buckling configuration ($m = n = 1$) are plotted. It is interesting to note that μ' increases practically linearly with λ' in the vicinity of initial instability for both the symmetric ($p = q = 1$) and antisymmetric ($p = 2$, $q = 1$) vibration modes.

The frequency of the symmetric vibration mode is strongly affected by the increase of λ', the rate of increase of μ' after buckling being twice as much as the rate of decrease before buckling. For example, with $\lambda' = 4$ and $\mu' = 5.8$, the "stiffness" of the plate has increased to 2.41 times that of the unbuckled state while the maximum deflection at the center of the plate is only 1.5 h. This rapid increase in the stiffness after buckling is important in flutter analysis. In general, the vibration mode associated with the initial buckling mode, that is, $p = m$ and $q = n$, is the mode affected most strongly by the increase of λ'. For further increase of λ' the frequency of the symmetric vibration mode becomes higher than that of the antisymmetric

mode. This is not unreasonable since the antisymmetric vibration is primarily inextensional while the symmetric vibration is primarily extensional.

The results of the same problem as shown in Figure 1a but for a larger range of values of λ' are shown in Figure 1b. The solid lines represent the perturbation solution up to $\lambda' = 50$; however, the results become less reliable since, for $\lambda' > 20$, the perturbation series for the symmetric vibration mode converges rather poorly. In contrast, for the antisymmetric vibration mode it still converges satisfactorily for values of λ' up to 40. The dashed lines represent the results of Equation (4.14) when the approximating series takes the form of Equation (4.15). It is noted that after a further increase of λ', the frequency of the symmetric vibration mode increases less rapidly and eventually becomes again less than that of the antisymmetric vibration mode. This is due to the fact that for large values of λ' two nodal lines appear in the symmetric vibration mode, which therefore becomes more nearly inextensional. Figure 2 shows the shapes of the symmetric and antisymmetric vibration modes for various values of λ'.

Figures 3a and 3b show the relation between γ and λ' for the same case of a square plate subjected to plane hydrostatic pressure. The perturbation results are shown in Figure 3a, the energy method results in Figure 3b. The rate of increase of γ after buckling is only one fourth as much as that before buckling (as against one half in the case of uniaxial edge compression).

Figure 4 shows the relations between μ' and λ' for rectangular plates of various aspect ratios. The plates are assumed to be forced

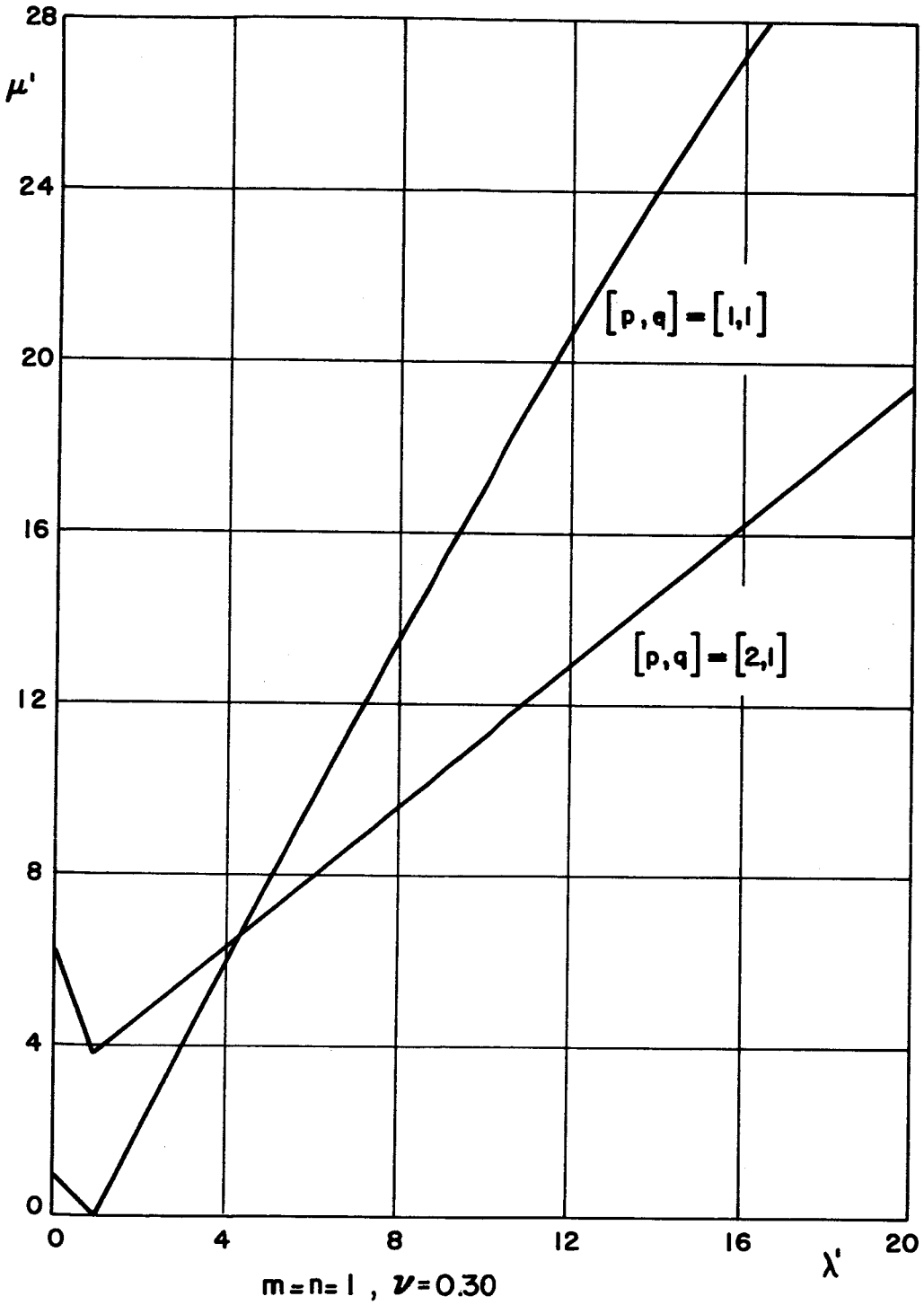

Figure 1a. Nondimensional Frequency Squared-Load Curves for Square Plate under Hydrostatic Pressure.

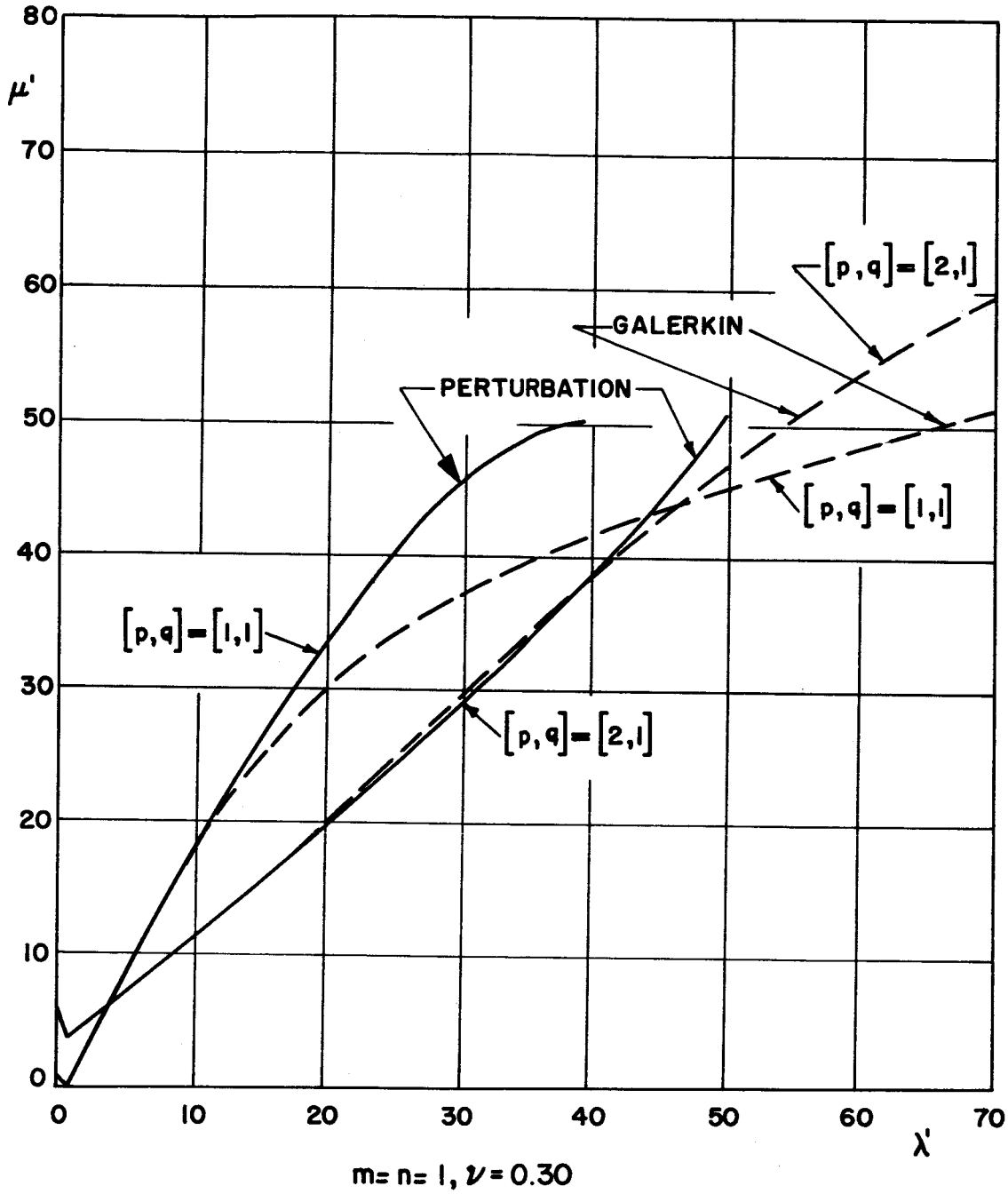

Figure 1b. Nondimensional Frequency Squared-Load Curves for Square Plate under Hydrostatic Pressure (same as Figure 1a but extended range).

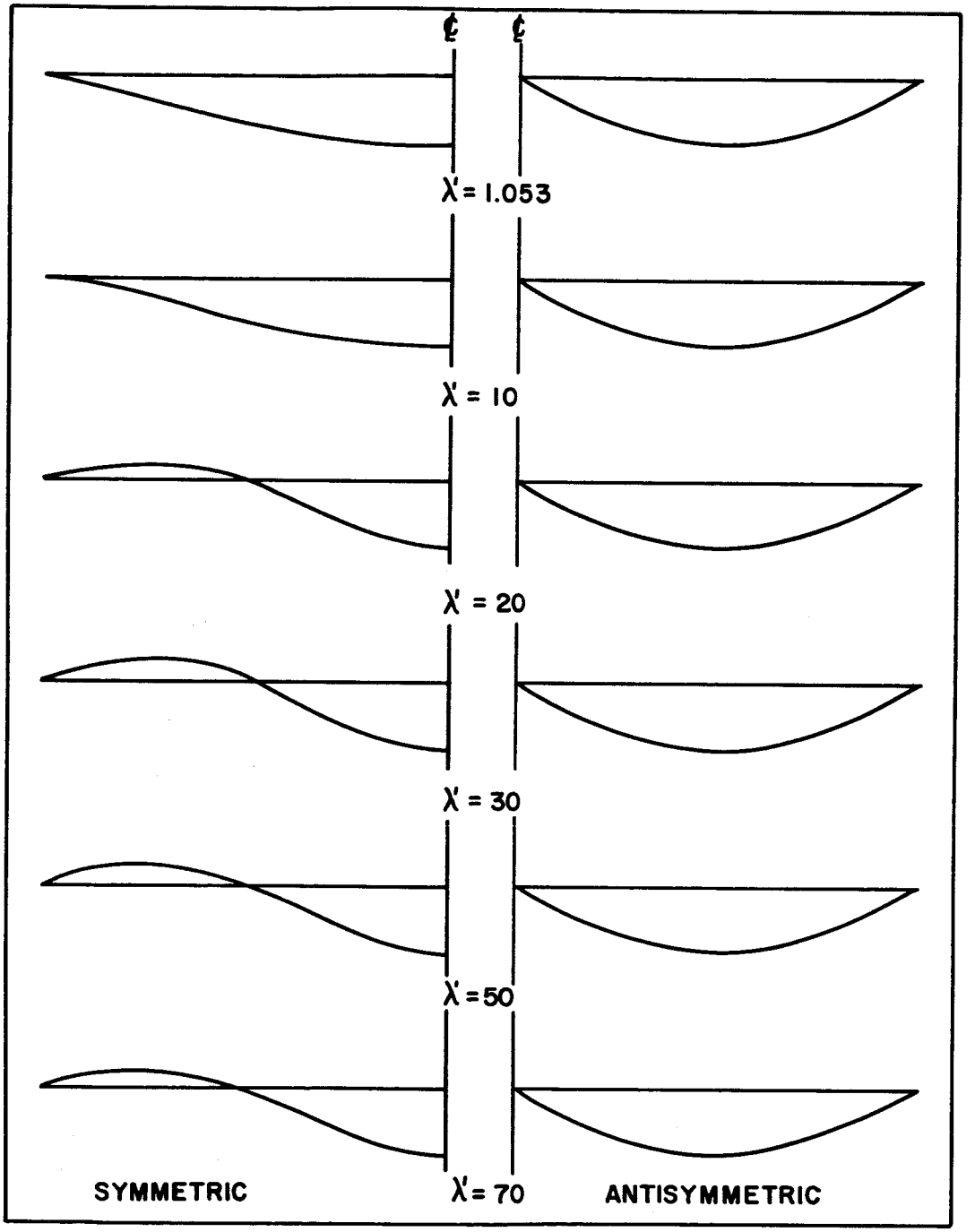

Figure 2. Modes of Vibration for Square Plate under Hydrostatic Pressure (only half plate is shown).

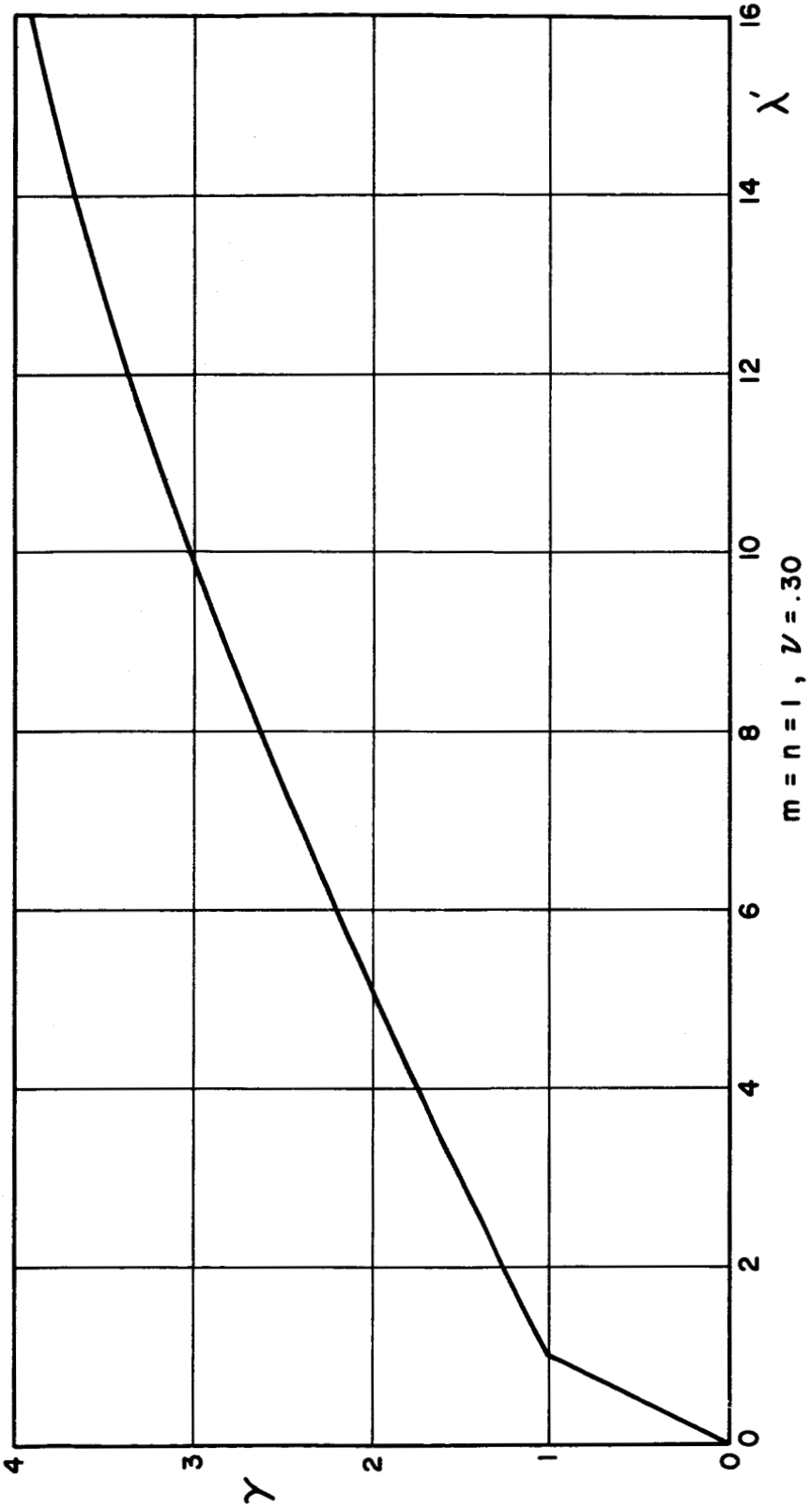

Figure 3a. Nondimensional Load-Shortening Curve for Square Plate under Hydrostatic Pressure.

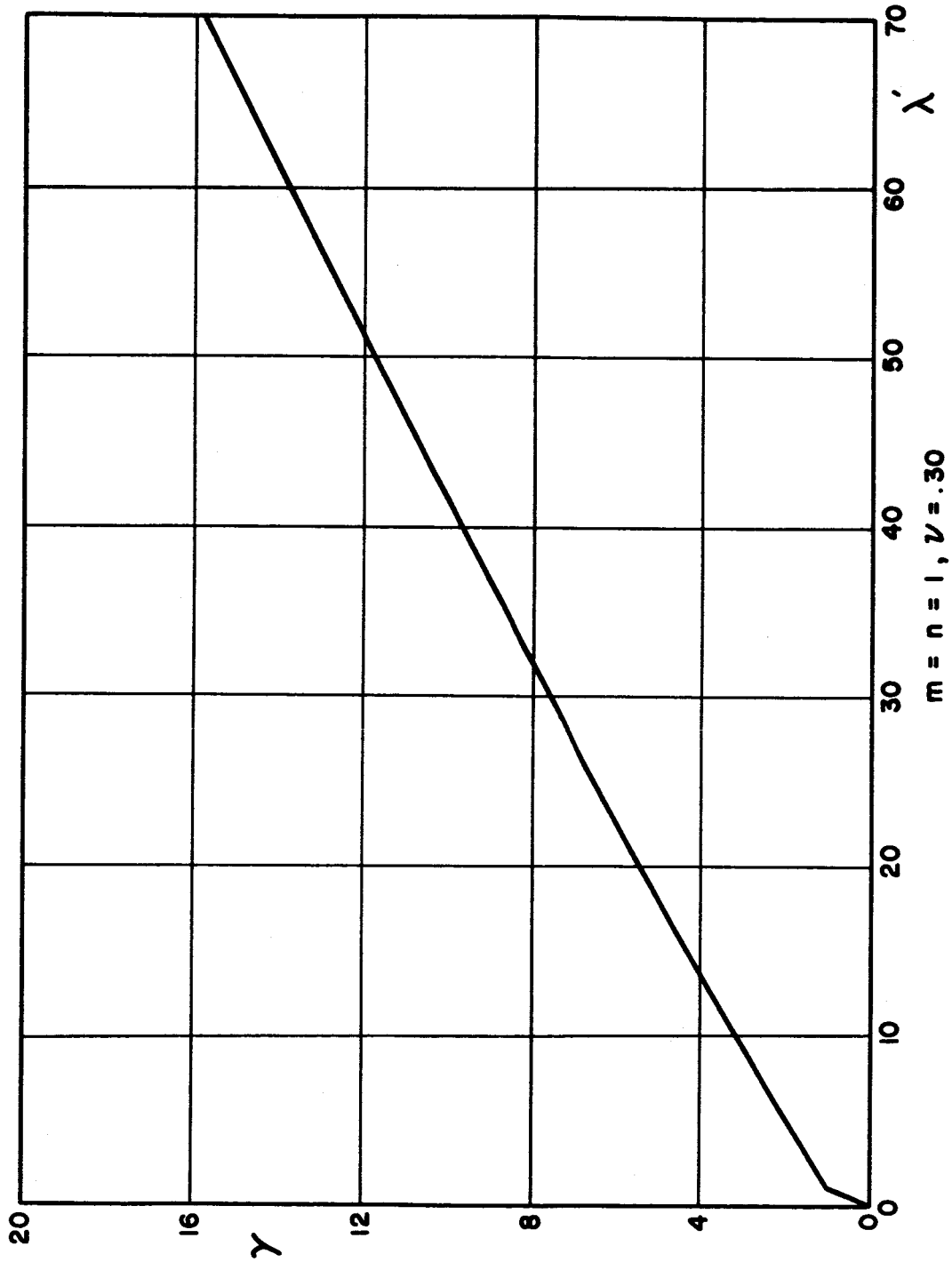

Figure 3b. Nondimensional Load-Shortening Curve for Square Plate under Hydrostatic Pressure (same as Figure 3a but extended range).

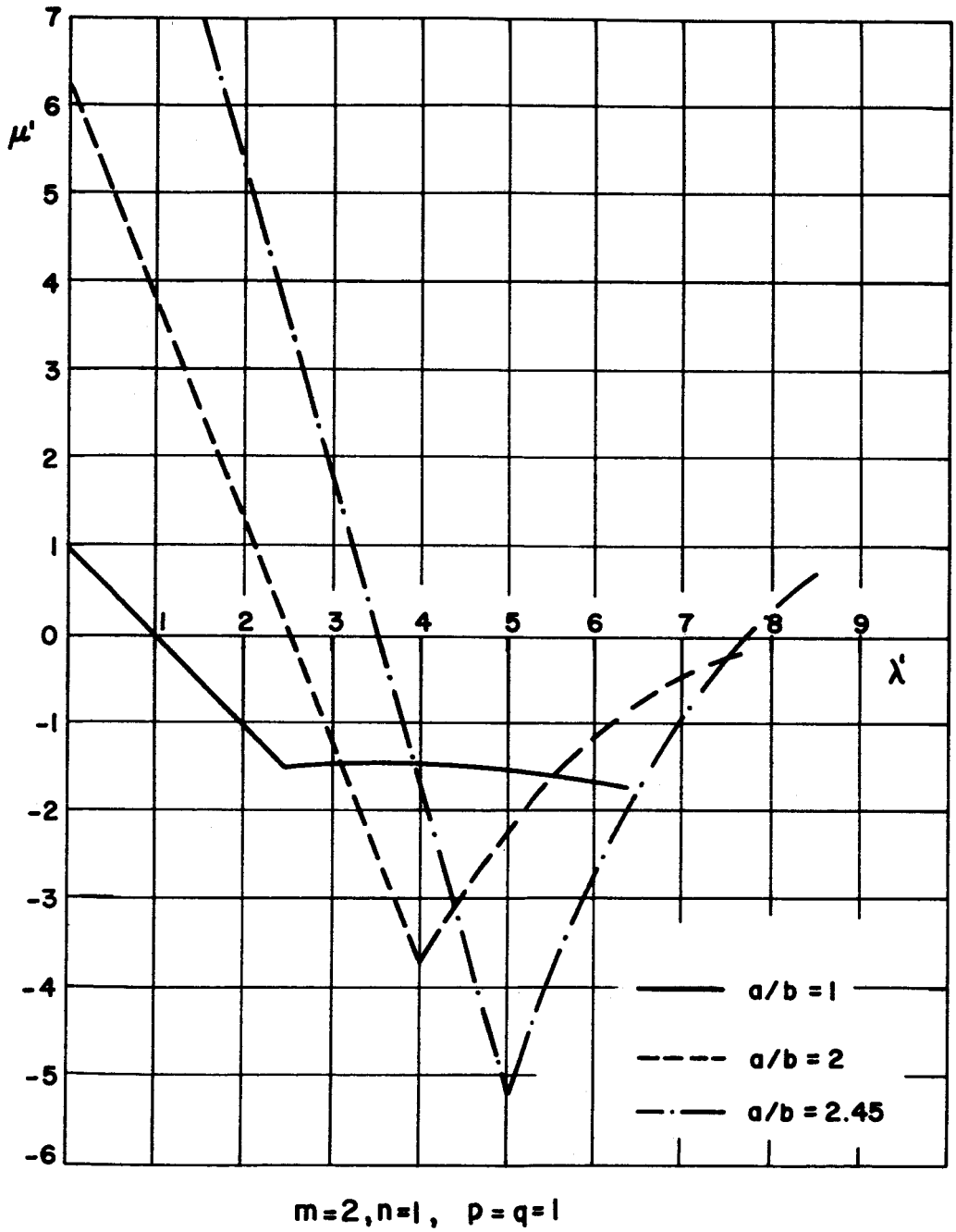

Figure 4. Nondimensional Frequency Squared-Load Curves for Rectangular Plate under Hydrostatic Pressure Second Buckling Mode.

into the second buckling mode ($m = 2$ and $n = 1$) through the application of artificial kinematic constraints which, however, do not restrict the freedom of dynamic vibratory motion. For $m = 2$, $n = 1$, the vibration mode associated with negative μ' corresponds to $p = q = 1$. For all other modes, μ' is positive in the vicinity of the initial instability and up to values of λ' which are of interest to us; hence they are not considered here.

The solid, dashed and dashed-dotted curves represent μ' versus λ' for the $p = q = 1$ vibration mode of plates of aspect ratio 1, 2 and 2.45, respectively. It is noted that μ' remains negative for all values of $\lambda' > 1$ for aspect ratios of 1 and 2, respectively, at least within the limit of the truncated series.* For an aspect ratio of 2.45 μ' becomes positive at $\lambda' = 7.70$; moreover, the truncated series shows satisfactory convergence for the range of values considered. This means that the $m = 2$, $n = 1$ buckling configuration will become stable even after the removal of the artificial kinematic constraints for sufficiently large values of λ'. In this case secondary buckling from the fundamental mode into the second mode may occur; in contrast such secondary buckling is ruled out for a square plate under hydrostatic pressure.

Figures 5, 6 and 7 show the load-shortening curves of the lowest buckling configurations ($m = 1$, $n = 1$ and $m = 2$, $n = 1$) for the plates considered in Figure 4. For a square plate (Figure 5) the edge displacement in the antisymmetric buckling configuration ($m = 2$, $n = 1$) increases with decreasing load when $\lambda' > 7.0$, confirming the previous

* Slow convergence raises doubts as to the reliability of this statement for $a/b = 2$.

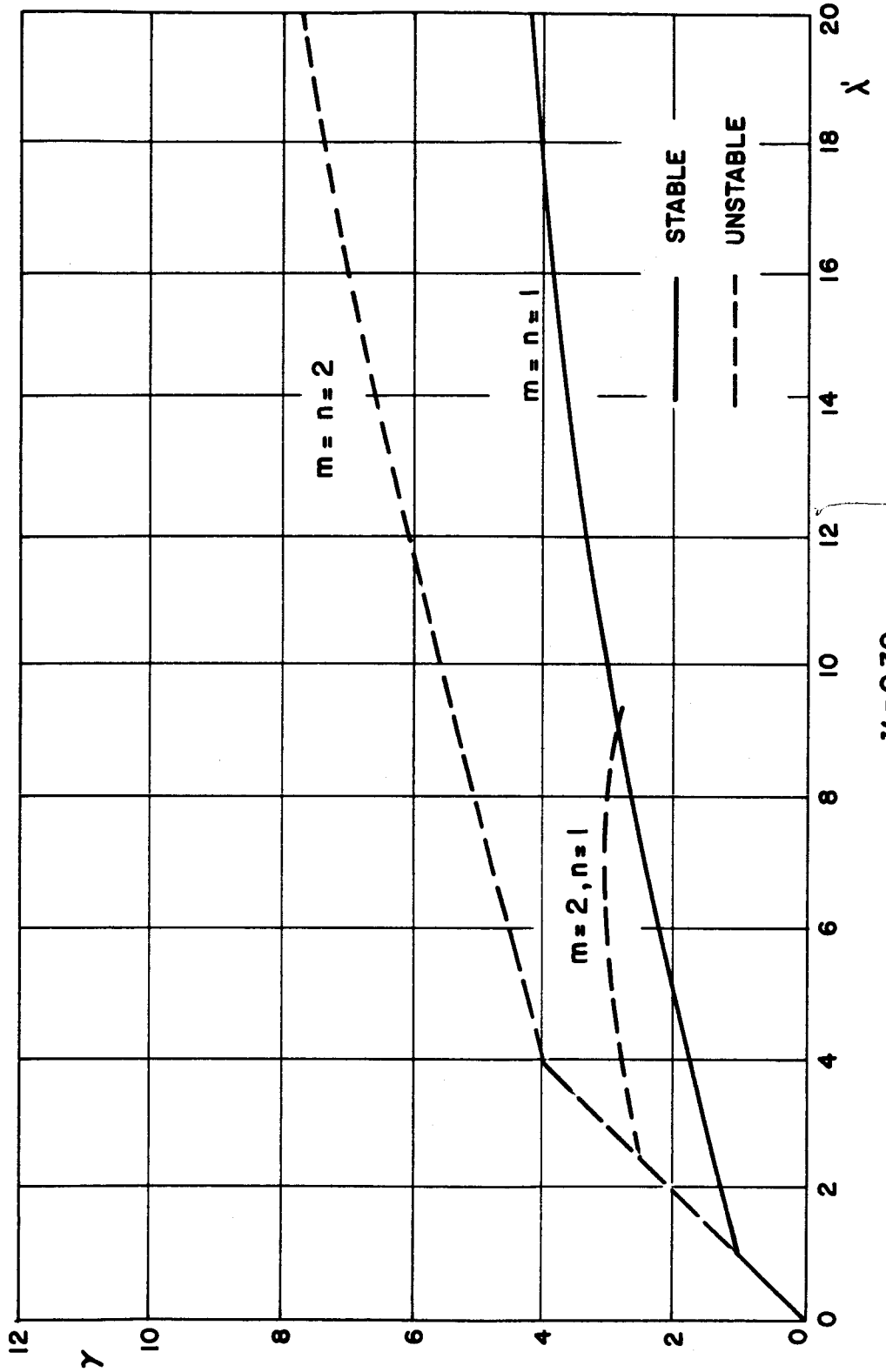

Figure 5. Nondimensional Frequency Squared-Load Curves for Square Plate under Hydrostatic Pressure.

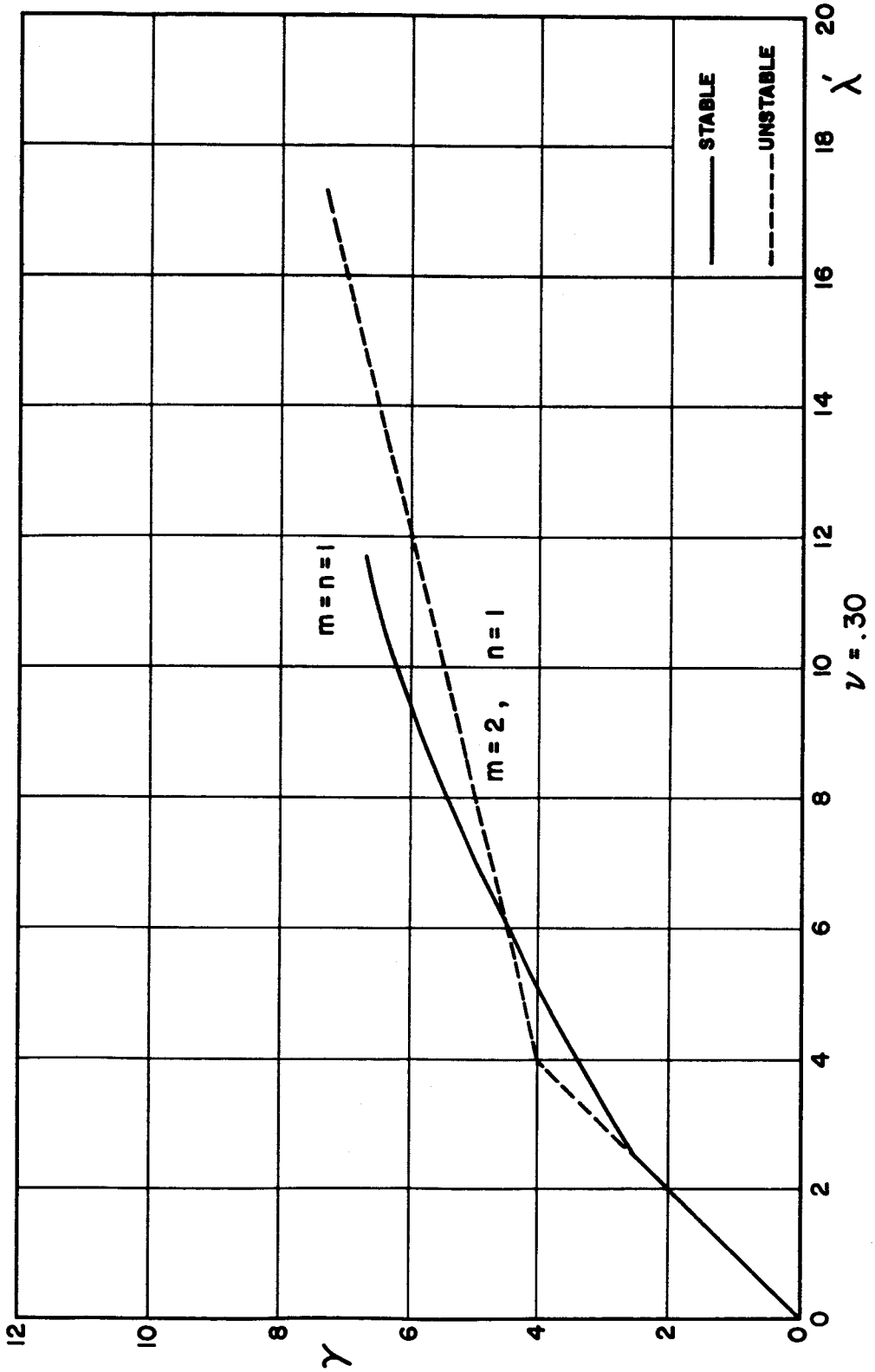

Figure 6. Nondimensional Load-Shortening Curves for Rectangular Plate under Hydrostatic Pressure a/b = 2.

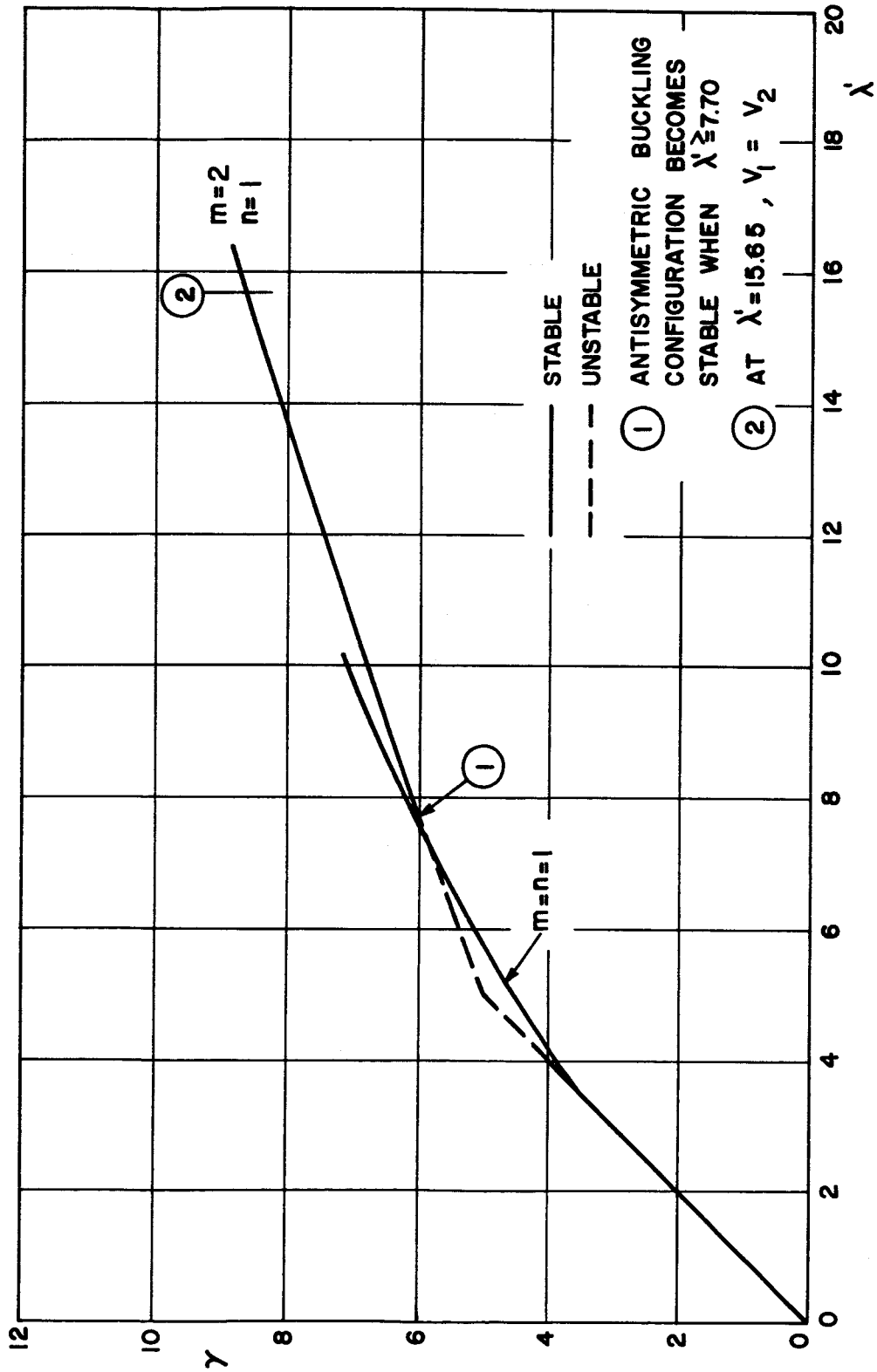

Figure 7. Nondimensional Load-Shortening Curves for Rectangular Plate under Hydrostatic Pressure a/b = 2.45.

conclusion that the antisymmetric buckling configuration for a square plate remains unstable. Figures 6 and 7 treat the rectangular plates of aspect ratio 2 and 2.45, respectively. It is interesting to note that a new equilibrium configuration (not shown) becomes possible at the value of λ' at which the antisymmetric buckling configuration becomes stable. This secondary bifurcation and the unstable character of the new configuration can be shown by considering the first and second variations of the potential energy. The value of λ' associated with equal potential energies for the two stable buckled states is also indicated in Figure 7.

The possibility of secondary buckling from the fundamental mode into a yet higher mode ($m = n = 2$) is treated in Figure 8, which shows the μ' versus λ' curves of a square plate subjected to plane hydrostatic pressure after the plate has been forced to buckle into that mode. Only the two vibration modes $p = q = 1$ and $p = 2, q = 1$ produce negative values of μ'. It is noted that these values remain negative; hence for a square plate the buckling configuration $m = n = 2$ is also unstable. This is confirmed by the load-shortening curves of the $m = n = 1$ and $m = n = 2$ buckling configurations shown in Figure 5. Since the two curves do not intersect the possibility of snap-through from the symmetric ($m = n = 1$) buckling configuration into the antisymmetric ($m = n = 2$) buckling configuration is ruled out.

The behavior of plates subjected to uniaxial edge compression is radically different. This has been treated by Stein[18] and others and is corroborated in Figures 9 and 10. In this case even a square plate exhibits a stable antisymmetric ($m = 2, n = 1$) equilibrium configuration when λ'' becomes sufficiently large. This change-over from

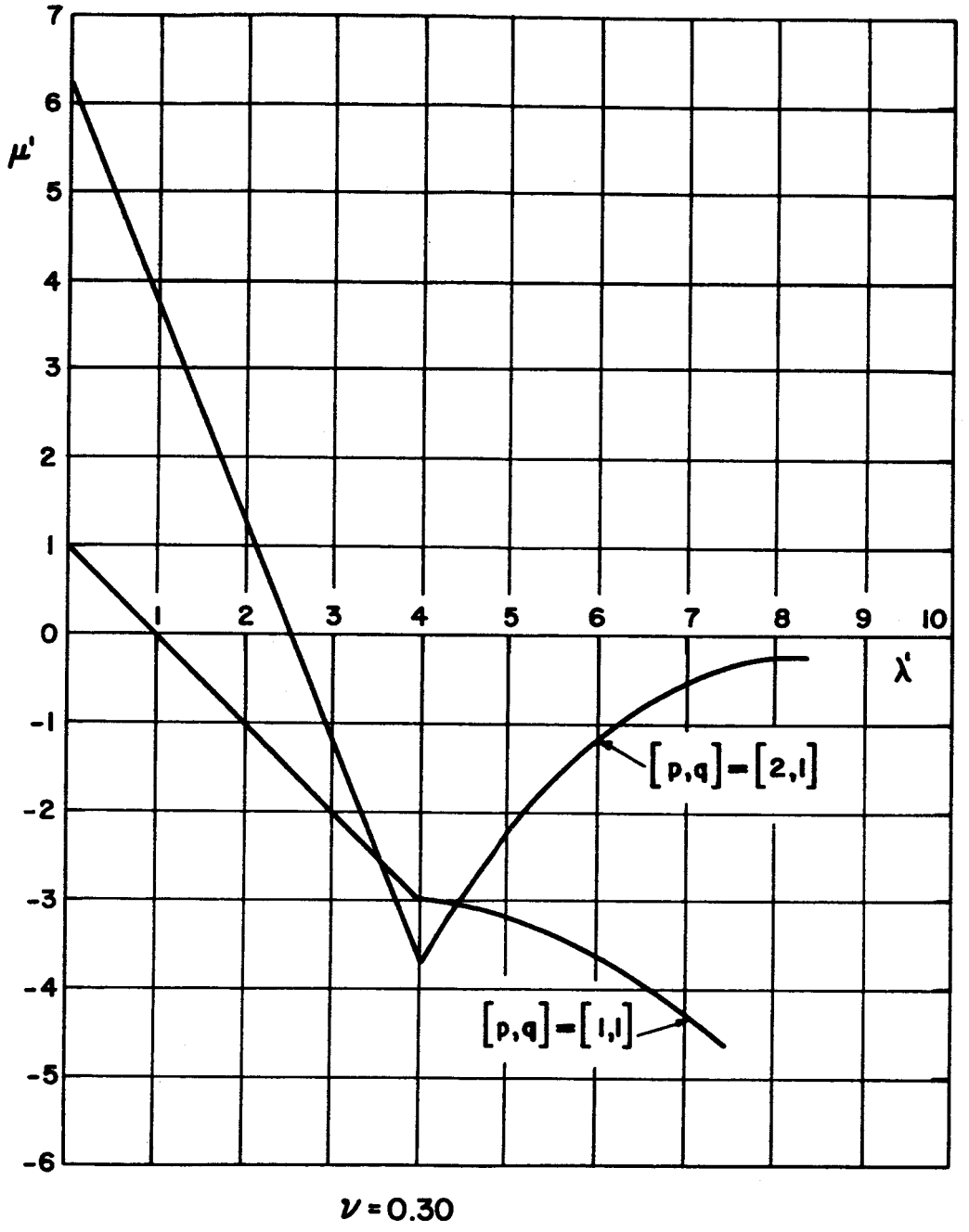

Figure 8. Nondimensional Frequency Squared-Load Curves for Square Plate under Hydrostatic Pressure m = n = 2 Buckling Mode.

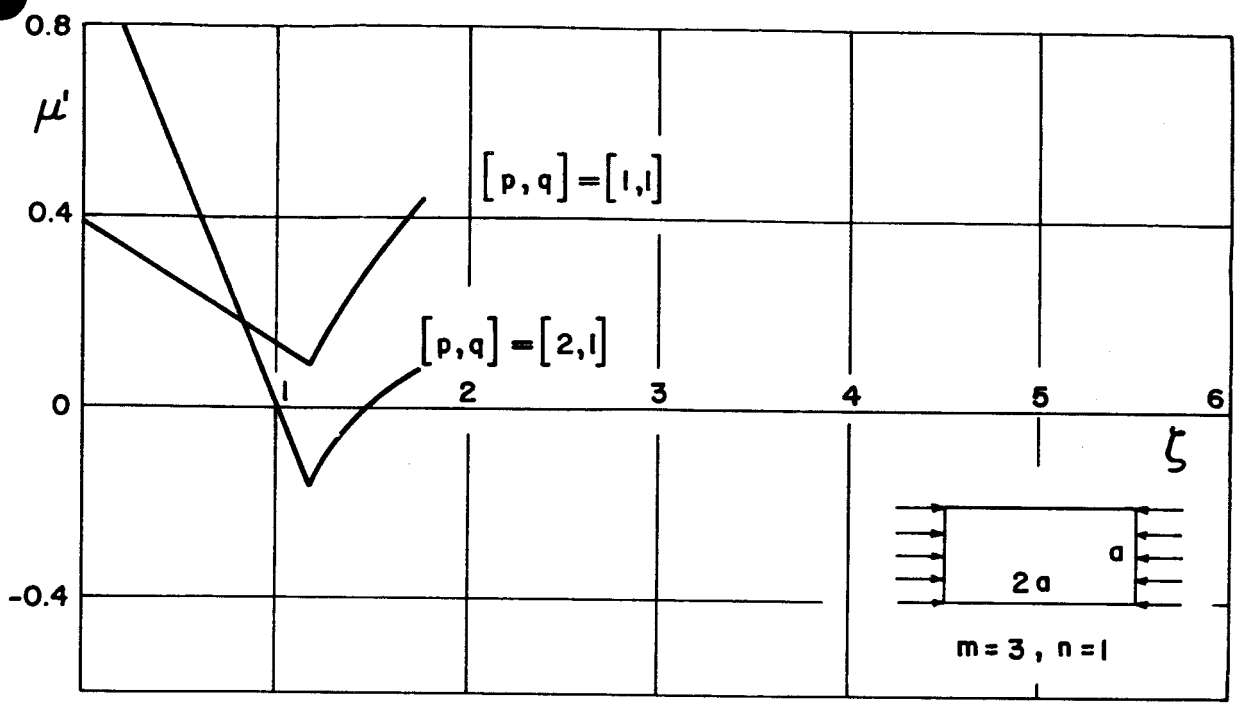

(a) Nondimensional Frequency Squared-Load Curve

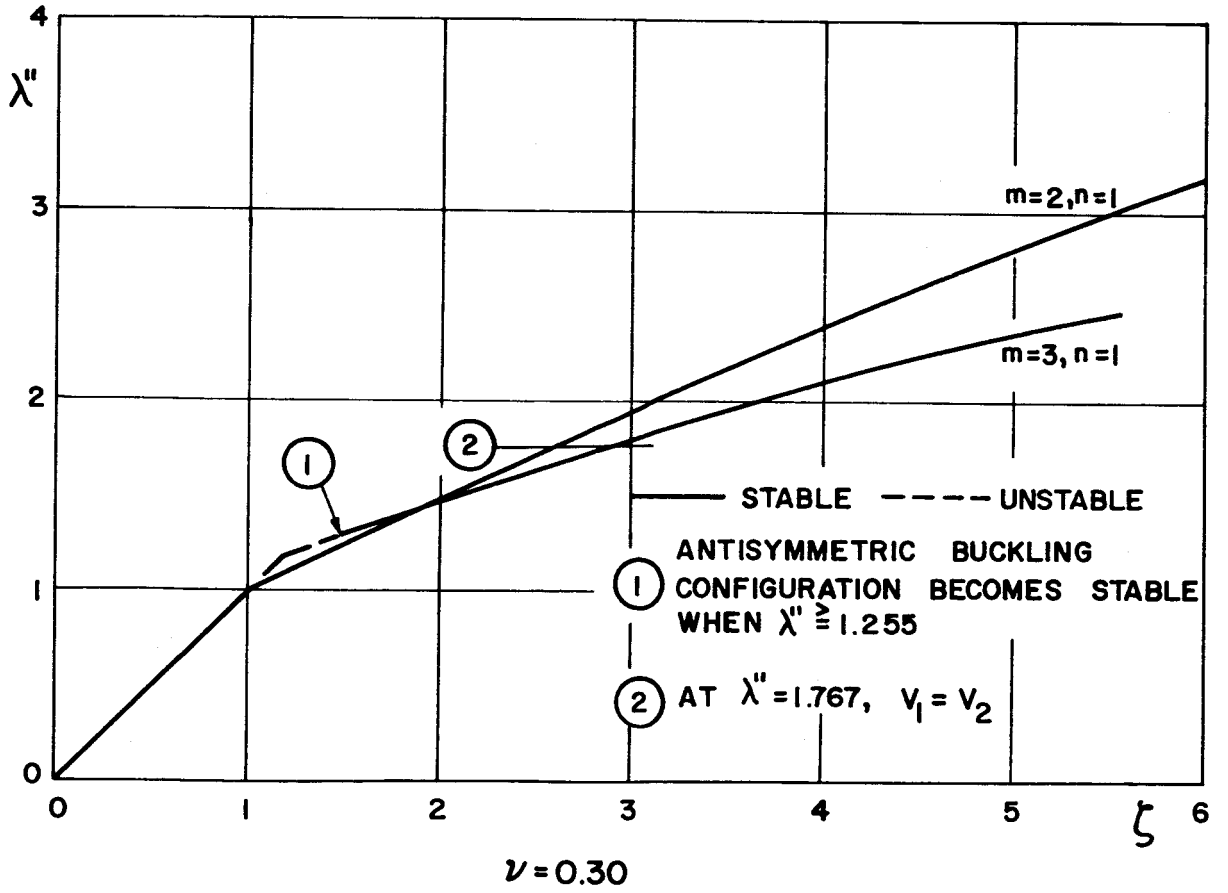

(b) Nondimensional Load-Shortening Curves

Figure 10. Rectangular Plate - Uniaxial Edge Compression a/b = 2.

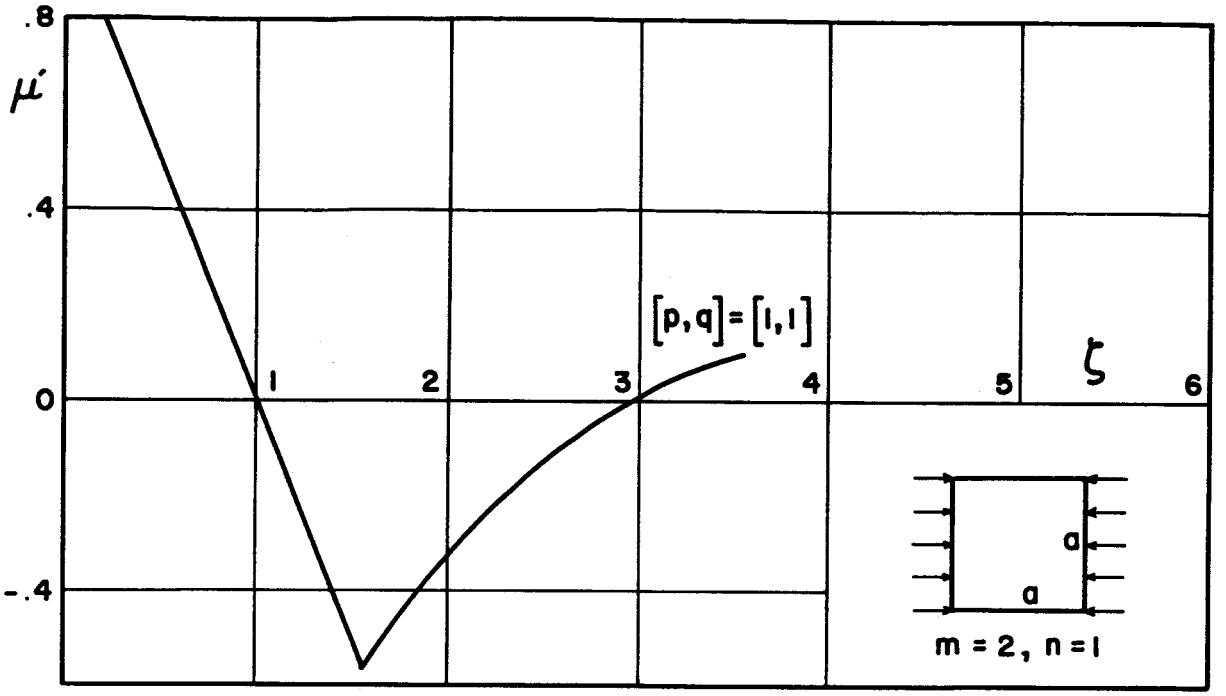

(a) Nondimensional Frequency Squared-Load Curve

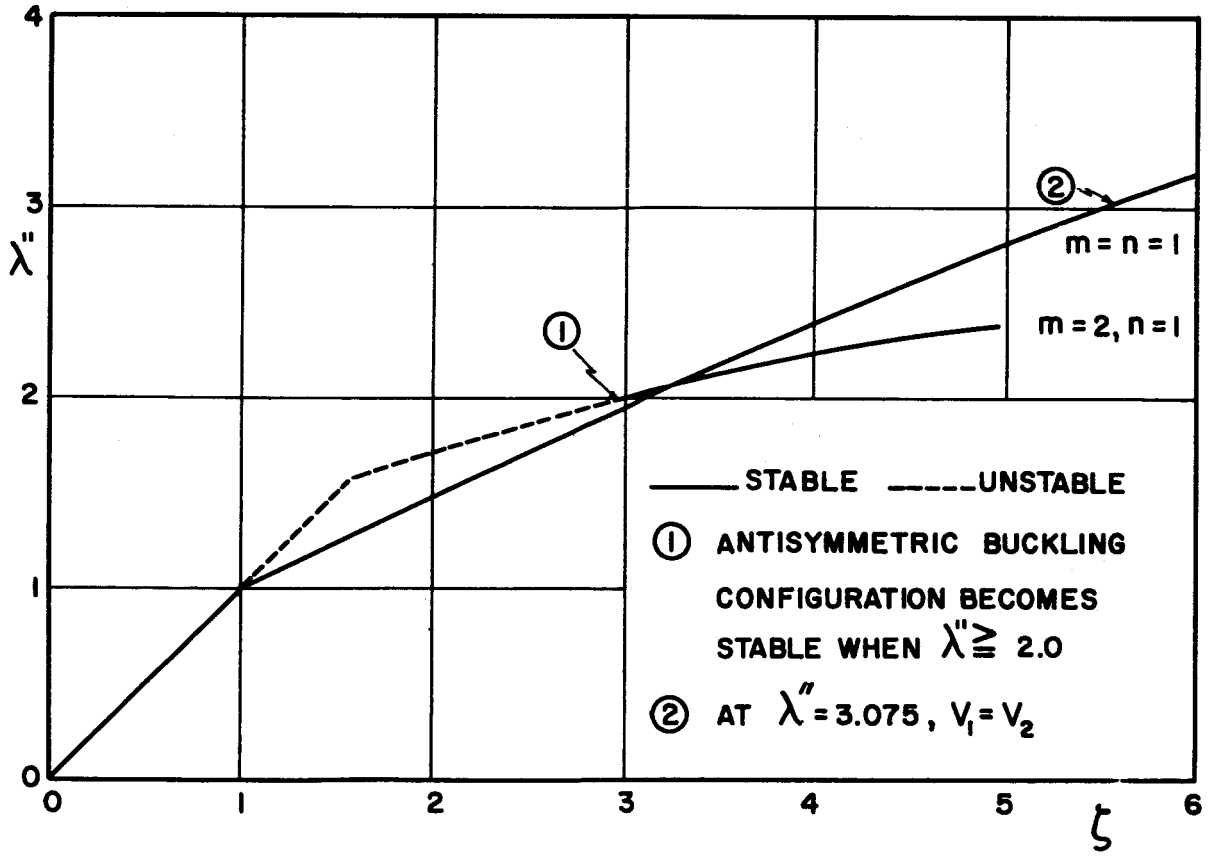

(b) Nondimensional Load-Shortening Curves

Figure 9. Square Plate - Uniaxial Edge Compression.

instability to stability is again accompanied by the emergence of a new unstable configuration (again not indicated in the figures). It is noted also that the values of λ'' so defined (representing lower bounds to secondary buckling) as well as the values of λ'' associated with equal potential energies are very much smaller than in the case of hydrostatic pressure. This is in good qualitative agreement with reported test results.

CHAPTER VI

CONCLUSIONS

It has been demonstrated that perturbation techniques can be used effectively to analyze the dynamic behavior of rectangular plates after they have buckled. The ensuing series show satisfactory convergence for a technically significant range of the load parameter.

Natural frequencies of vibration have been shown to be extremely sensitive to buckling amplitudes, displaying the most pronounced increase in connection with the symmetric vibratory mode. For sufficiently large load parameters this mode, which is primarily extensional, ceases to be associated with the longest period of vibration; however, it becomes more nearly inextensional as buckling proceeds and may therefore again return to its previous fundamental position.

The stability of higher buckling configurations has been investigated by studying the real or imaginary character of the frequencies of vibration about these configurations. The results indicate that all plates under uniaxial edge compression, and rectangular plates of sufficiently large aspect ratio under hydrostatic edge pressure, may eventually exhibit stable secondary buckling modes. The concomitant load parameters represent lower bounds to "secondary buckling loads" which signify the possibility of a sudden snap-through from one buckling configuration into another. This phenomenon had been widely observed before; the present calculations tend to conform with previously reported experimental results.

APPENDIX A

LIST OF FUNCTIONS - HYDROSTATIC EDGE PRESSURE

(1) Static Functions

(a) Deflection

$$W = \varepsilon W^{(1)} + \varepsilon^3 W^{(3)} + \varepsilon^5 W^{(5)} + \cdots$$

in which

$$W^{(1)} = h \sin\frac{m\pi}{a}x \sin\frac{n\pi}{b}y$$

$$W^{(3)} = h\left[A_4 \sin\frac{m\pi}{a}x \sin\frac{3n\pi}{b}y + \bar{A}_4 \sin\frac{3m\pi}{a}x \sin\frac{n\pi}{b}y\right]$$

$$W^{(5)} = h\left[A_{51} \sin\frac{m\pi}{a}x \sin\frac{3n\pi}{b}y + \bar{A}_{51} \sin\frac{3m\pi}{a}x \sin\frac{n\pi}{b}y + A_{52} \sin\frac{3m\pi}{a}x \sin\frac{3n\pi}{b}y\right.$$

$$+ A_{53} \sin\frac{5m\pi}{a}x \sin\frac{n\pi}{b}y + \bar{A}_{53} \sin\frac{m\pi}{a}x \sin\frac{5n\pi}{b}y$$

$$\left. + A_{54} \sin\frac{5m\pi}{a}x \sin\frac{3n\pi}{b}y + \bar{A}_{54} \sin\frac{3m\pi}{a}x \sin\frac{5n\pi}{b}y\right]$$

with

$$A_4 = \frac{Eh^3}{128D} \frac{\left(\frac{m\pi}{a}\right)^4}{\left(\frac{n\pi}{b}\right)^2\left[\left(\frac{m\pi}{a}\right)^2 + \left(\frac{3n\pi}{b}\right)^2\right]}$$

$$\bar{A}_4 = \frac{Eh^3}{128D} \frac{\left(\frac{n\pi}{b}\right)^4}{\left(\frac{m\pi}{a}\right)^2\left[\left(\frac{n\pi}{b}\right)^2 + \left(\frac{3m\pi}{a}\right)^2\right]}$$

$$A_{51} = (A_4)^2\left\{\frac{\left(\frac{n\pi}{b}\right)^2}{(1+\nu)\left[\left(\frac{m\pi}{a}\right)^2 + \left(\frac{n\pi}{b}\right)^2\right]}\left[(25+9\nu) - (24+8\nu)\frac{\left(\frac{n\pi}{b}\right)^2}{\left(\frac{m\pi}{a}\right)^2}\right] + \frac{\left(\frac{m\pi}{a}\right)^2}{\left[\left(\frac{m\pi}{a}\right)^2 + \left(\frac{n\pi}{b}\right)^2\right]}\right.$$

$$\left. - 4 - \frac{\left(\frac{2n\pi}{b}\right)^4}{\left[\left(\frac{m\pi}{a}\right)^2 + \left(\frac{n\pi}{b}\right)^2\right]^2} - \frac{\left(\frac{n\pi}{b}\right)^4}{\left[\left(\frac{2n\pi}{b}\right)^2 + \left(\frac{m\pi}{a}\right)^2\right]^2}\right\} - A_4\bar{A}_4 \frac{\left(\frac{2n\pi}{b}\right)^4}{\left[\left(\frac{m\pi}{a}\right)^2 + \left(\frac{n\pi}{b}\right)^2\right]^2}$$

$$\bar{A}_{51} = (\bar{A}_4)^2\left\{\frac{\left(\frac{m\pi}{a}\right)^2}{(1+\nu)\left[\left(\frac{n\pi}{b}\right)^2 + \left(\frac{m\pi}{a}\right)^2\right]}\left[(25+9\nu) - (24+8\nu)\frac{\left(\frac{m\pi}{a}\right)^2}{\left(\frac{n\pi}{b}\right)^2}\right] + \frac{\left(\frac{n\pi}{b}\right)^2}{\left[\left(\frac{n\pi}{b}\right)^2 + \left(\frac{m\pi}{a}\right)^2\right]}\right.$$

$$\left. - 4 - \frac{\left(\frac{2m\pi}{a}\right)^4}{\left[\left(\frac{n\pi}{b}\right)^2 + \left(\frac{m\pi}{a}\right)^2\right]^2} - \frac{\left(\frac{m\pi}{a}\right)^4}{\left[\left(\frac{2m\pi}{a}\right)^2 + \left(\frac{n\pi}{b}\right)^2\right]^2}\right\} - A_4\bar{A}_4 \frac{\left(\frac{2m\pi}{a}\right)^4}{\left[\left(\frac{n\pi}{b}\right)^2 + \left(\frac{m\pi}{a}\right)^2\right]^2}$$

$$A_{52} = A_4 \frac{Eh^3}{128D} \frac{\left(\frac{n\pi}{b}\right)^4}{\left[\left(\frac{m\pi}{a}\right)^2+\left(\frac{n\pi}{b}\right)^2\right]^2}\left\{1+\frac{\left(\frac{m\pi}{a}\right)^4}{\left[\left(\frac{2n\pi}{b}\right)^2+\left(\frac{m\pi}{a}\right)^2\right]^2}\right\}$$

$$+\bar{A}_4 \frac{Eh^3}{128D} \frac{\left(\frac{m\pi}{a}\right)^4}{\left[\left(\frac{m\pi}{a}\right)^2+\left(\frac{n\pi}{b}\right)^2\right]^2}\left\{1+\frac{\left(\frac{n\pi}{b}\right)^4}{\left[\left(\frac{2m\pi}{a}\right)^2+\left(\frac{n\pi}{b}\right)^2\right]^2}\right\}$$

$$A_{53} = \bar{A}_4 \frac{Eh^3}{128D} \frac{\left(\frac{n\pi}{b}\right)^4}{\left(\frac{m\pi}{a}\right)^2\left[\left(\frac{5m\pi}{a}\right)^2+\left(\frac{n\pi}{b}\right)^2\right]}\left\{1+\frac{3\left(\frac{m\pi}{a}\right)^4}{\left[\left(\frac{2m\pi}{a}\right)^2+\left(\frac{n\pi}{b}\right)^2\right]^2}\right\}$$

$$\bar{A}_{53} = A_4 \frac{Eh^3}{128D} \frac{\left(\frac{m\pi}{a}\right)^4}{\left(\frac{n\pi}{b}\right)^2\left[\left(\frac{5m\pi}{b}\right)^2+\left(\frac{m\pi}{a}\right)^2\right]}\left\{1+\frac{3\left(\frac{n\pi}{b}\right)^4}{\left[\left(\frac{2n\pi}{b}\right)^2+\left(\frac{m\pi}{a}\right)^2\right]^2}\right\}$$

$$A_{54} = -A_4 \frac{Eh^3}{128D} \frac{\left(\frac{n\pi}{b}\right)^4}{\left[\left(\frac{5m\pi}{a}\right)^2+\left(\frac{3n\pi}{b}\right)^2\right]\left[3\left(\frac{m\pi}{a}\right)^2+\left(\frac{n\pi}{b}\right)^2\right]} \frac{\left(\frac{m\pi}{a}\right)^4}{\left[\left(\frac{2m\pi}{a}\right)^2+\left(\frac{n\pi}{b}\right)^2\right]^2}$$

$$\bar{A}_{54} = -A_4 \frac{Eh^3}{128D} \frac{\left(\frac{m\pi}{a}\right)^4}{\left[\left(\frac{5n\pi}{b}\right)^2+\left(\frac{3m\pi}{a}\right)^2\right]\left[3\left(\frac{n\pi}{b}\right)^2+\left(\frac{m\pi}{a}\right)^2\right]} \frac{\left(\frac{n\pi}{b}\right)^4}{\left[\left(\frac{2n\pi}{b}\right)^2+\left(\frac{m\pi}{a}\right)^2\right]^2}$$

(b) Additional Membrane Stresses

$$T_{ij}' = \varepsilon^2 T_{ij}^{(2)} + \varepsilon^4 T_{ij}^{(4)} + \cdots\cdots$$

in which

$$T_{xx}^{(2)} = \frac{Eh^2}{8(1-\nu^2)}\left[\left(\frac{m\pi}{a}\right)^2+\nu\left(\frac{n\pi}{b}\right)^2-(1-\nu^2)\left(\frac{m\pi}{a}\right)^2\cos\frac{2n\pi}{b}y\right]$$

$$T_{yy}^{(2)} = \frac{Eh^2}{8(1-\nu^2)}\left[\left(\frac{n\pi}{b}\right)^2+\nu\left(\frac{m\pi}{a}\right)^2-(1-\nu^2)\left(\frac{n\pi}{b}\right)^2\cos\frac{2m\pi}{a}x\right]$$

$$T_{xy}^{(2)} = 0$$

$$T_{xx}^{(4)} = \frac{Eh^2}{4}\left(\frac{m\pi}{a}\right)^2\Bigg\{ A_4 \cos\frac{2n\pi}{b}y - A_4 \cos\frac{4n\pi}{b}y$$

$$- \frac{\left(\frac{n\pi}{b}\right)^4}{\left[\left(\frac{m\pi}{a}\right)^2+\left(\frac{n\pi}{b}\right)^2\right]^2} 4(A_4+\bar{A}_4)\cos\frac{2m\pi}{a}x\cos\frac{2n\pi}{b}y$$

$$+ \frac{\left(\frac{n\pi}{b}\right)^4}{\left[\left(\frac{2m\pi}{a}\right)^2+\left(\frac{n\pi}{b}\right)^2\right]^2} \bar{A}_4 \cos\frac{4m\pi}{a}x\cos\frac{2n\pi}{b}y$$

$$+ \frac{\left(\frac{n\pi}{b}\right)^4}{\left[\left(\frac{2n\pi}{b}\right)^2+\left(\frac{m\pi}{a}\right)^2\right]^2} 4A_4 \cos\frac{2m\pi}{a}x\cos\frac{4n\pi}{b}y\Bigg\}$$

$$T_{yy}^{(4)} = \frac{Eh^2}{4}\left(\frac{m\pi}{b}\right)^2\Bigg\{ \bar{A}_4 \cos\frac{2m\pi}{a}x - \bar{A}_4 \cos\frac{4m\pi}{a}x$$

$$- \frac{\left(\frac{m\pi}{a}\right)^4}{\left[\left(\frac{m\pi}{a}\right)^2+\left(\frac{n\pi}{b}\right)^2\right]^2} 4(\bar{A}_4+A_4)\cos\frac{2m\pi}{a}x\cos\frac{2n\pi}{b}y$$

$$+ \frac{\left(\frac{m\pi}{a}\right)^4}{\left[\left(\frac{2n\pi}{b}\right)^2+\left(\frac{m\pi}{a}\right)^2\right]^2} A_4 \cos\frac{2m\pi}{a}x\cos\frac{4n\pi}{b}y$$

$$+ \frac{\left(\frac{m\pi}{a}\right)^4}{\left[\left(\frac{2m\pi}{a}\right)^2+\left(\frac{n\pi}{b}\right)^2\right]^2} 4\bar{A}_4 \cos\frac{4m\pi}{a}x\cos\frac{2n\pi}{b}y\Bigg\}$$

$$T_{xy}^{(4)} = \frac{Eh^2}{4}\left(\frac{m\pi}{a}\right)\left(\frac{n\pi}{b}\right)\Bigg\{ - \frac{\left(\frac{m\pi}{a}\right)^2\left(\frac{n\pi}{b}\right)^2}{\left[\left(\frac{m\pi}{a}\right)^2+\left(\frac{n\pi}{b}\right)^2\right]^2} 4(A_4+A_4)\sin\frac{2m\pi}{a}x\sin\frac{2n\pi}{b}y$$

$$+ \frac{\left(\frac{m\pi}{a}\right)^2\left(\frac{n\pi}{b}\right)^2}{\left[\left(\frac{2m\pi}{a}\right)^2+\left(\frac{n\pi}{b}\right)^2\right]^2} 2\bar{A}_4 \sin\frac{4m\pi}{a}x\sin\frac{2n\pi}{b}y$$

$$+ \frac{\left(\frac{m\pi}{a}\right)^2\left(\frac{n\pi}{b}\right)^2}{\left[\left(\frac{2n\pi}{b}\right)^2+\left(\frac{m\pi}{a}\right)^2\right]^2} 2A_4 \sin\frac{2m\pi}{a}x\sin\frac{4n\pi}{b}y\Bigg\}$$

(c) Load Parameter

$$\lambda = \lambda_0 + \varepsilon^2\lambda_2 + \varepsilon^4\lambda_4 + \cdots$$

in which

$$\lambda_0 = \frac{D}{h}\left[\left(\frac{m\pi}{a}\right)^2 + \left(\frac{n\pi}{b}\right)^2\right]$$

$$\lambda_2 = \frac{Eh^2}{16(1-\nu^2)} \frac{1}{\left[\left(\frac{m\pi}{a}\right)^2 + \left(\frac{n\pi}{b}\right)^2\right]} \left\{(3-\nu^2)\left[\left(\frac{m\pi}{a}\right)^4 + \left(\frac{n\pi}{b}\right)^4\right] + 4\nu\left(\frac{m\pi}{a}\right)^2\left(\frac{n\pi}{b}\right)^2\right\}$$

$$\lambda_4 = -\frac{3Eh^2}{16} \frac{1}{\left[\left(\frac{m\pi}{a}\right)^2 + \left(\frac{n\pi}{b}\right)^2\right]} \left[\left(\frac{m\pi}{a}\right)^4 A_4 + \left(\frac{n\pi}{b}\right)^4 \bar{A}_4\right]$$

(d) Additional Membrane Displacements

$$U' = \varepsilon^2 U^{(2)} + \varepsilon^4 U^{(4)} + \cdots$$

$$V' = \varepsilon^2 V^{(2)} + \varepsilon^4 V^{(4)} + \cdots$$

in which

$$U^{(2)} = \frac{h^2}{16\left(\frac{m\pi}{a}\right)}\left[-\left(\frac{m\pi}{a}\right)^2 + \nu\left(\frac{n\pi}{b}\right)^2 + \left(\frac{m\pi}{a}\right)^2 \cos\frac{2n\pi}{b}y\right] \sin\frac{2m\pi}{a}x$$

$$V^{(2)} = \frac{h^2}{16\left(\frac{n\pi}{b}\right)}\left[-\left(\frac{n\pi}{b}\right)^2 + \nu\left(\frac{m\pi}{a}\right)^2 + \left(\frac{n\pi}{b}\right)^2 \cos\frac{2m\pi}{a}x\right] \sin\frac{2n\pi}{b}y$$

$$U^{(4)} = G_1 \sin\frac{2m\pi}{a}x + G_2 \sin\frac{4m\pi}{a}x + G_3 \sin\frac{2m\pi}{a}x \cos\frac{2n\pi}{b}y$$

$$+ G_4 \sin\frac{4m\pi}{a}x \cos\frac{2n\pi}{b}y + G_5 \sin\frac{2m\pi}{a}x \cos\frac{4n\pi}{b}y$$

$$V^{(4)} = \bar{G}_1 \sin\frac{2n\pi}{b}y + \bar{G}_2 \sin\frac{4n\pi}{b}y + \bar{G}_3 \cos\frac{2m\pi}{a}x \sin\frac{2n\pi}{b}y$$

$$+ \bar{G}_4 \cos\frac{2m\pi}{a}x \sin\frac{4n\pi}{b}y + \bar{G}_5 \cos\frac{4m\pi}{a}x \sin\frac{2n\pi}{b}y$$

with

$$G_1 = -\frac{h^2}{16\left(\frac{m\pi}{a}\right)}\left[6\left(\frac{m\pi}{a}\right)^2 + 2\nu\left(\frac{n\pi}{b}\right)^2\right] \bar{A}_4$$

$$\bar{G}_1 = -\frac{h^2}{16\left(\frac{n\pi}{b}\right)}\left[6\left(\frac{n\pi}{b}\right)^2 + 2\nu\left(\frac{m\pi}{a}\right)^2\right] A_4$$

$$G_2 = -\frac{h^2}{16\left(\frac{m\pi}{a}\right)}\left[3\left(\frac{m\pi}{a}\right)^2 - \nu\left(\frac{n\pi}{b}\right)^2\right]\bar{A}_4$$

$$\bar{G}_2 = -\frac{h^2}{16\left(\frac{n\pi}{b}\right)}\left[3\left(\frac{n\pi}{b}\right)^2 - \nu\left(\frac{m\pi}{a}\right)^2\right]A_4$$

$$G_3 = \frac{h^2\left(\frac{m\pi}{a}\right)}{8\left[\left(\frac{m\pi}{a}\right)^2 + \left(\frac{n\pi}{b}\right)^2\right]^2}\left\{\left[-5\left(\frac{n\pi}{b}\right)^4 - 2(1-2\nu)\left(\frac{m\pi}{a}\right)^2\left(\frac{n\pi}{b}\right)^2 - \left(\frac{m\pi}{a}\right)^4\right]A_4 + \left[-\left(\frac{n\pi}{b}\right)^4 + 2(3+2\nu)\left(\frac{m\pi}{a}\right)^2\left(\frac{n\pi}{b}\right)^2 + 3\left(\frac{m\pi}{a}\right)^4\right]\bar{A}_4\right\}$$

$$\bar{G}_3 = \frac{h^2\left(\frac{n\pi}{b}\right)}{8\left[\left(\frac{n\pi}{b}\right)^2 + \left(\frac{m\pi}{a}\right)^2\right]^2}\left\{\left[-5\left(\frac{m\pi}{a}\right)^4 - 2(1-2\nu)\left(\frac{m\pi}{a}\right)^2\left(\frac{n\pi}{b}\right)^2 - \left(\frac{n\pi}{b}\right)^4\right]\bar{A}_4 + \left[-\left(\frac{m\pi}{a}\right)^4 + 2(3+2\nu)\left(\frac{m\pi}{a}\right)^2\left(\frac{n\pi}{b}\right)^2 + 3\left(\frac{n\pi}{b}\right)^4\right]A_4\right\}$$

$$G_4 = \frac{h^2\left(\frac{m\pi}{a}\right)}{8\left[\left(\frac{2m\pi}{a}\right)^2 + \left(\frac{n\pi}{b}\right)^2\right]^2}\left[2\left(\frac{n\pi}{b}\right)^4 + 2(6-\nu)\left(\frac{m\pi}{a}\right)^2\left(\frac{n\pi}{b}\right)^2 + 24\left(\frac{m\pi}{a}\right)^4\right]\bar{A}_4$$

$$\bar{G}_4 = \frac{h^2\left(\frac{n\pi}{b}\right)}{8\left[\left(\frac{2n\pi}{b}\right)^2 + \left(\frac{m\pi}{a}\right)^2\right]^2}\left[2\left(\frac{m\pi}{a}\right)^4 + 2(6-\nu)\left(\frac{m\pi}{a}\right)^2\left(\frac{n\pi}{b}\right)^2 + 24\left(\frac{n\pi}{b}\right)^4\right]A_4$$

$$G_5 = \frac{h^2\left(\frac{m\pi}{a}\right)}{8\left[\left(\frac{2n\pi}{b}\right)^2 + \left(\frac{m\pi}{a}\right)^2\right]^2}\left[20\left(\frac{n\pi}{b}\right)^4 + (8-\nu)\left(\frac{m\pi}{a}\right)^2\left(\frac{n\pi}{b}\right)^2 + \left(\frac{m\pi}{a}\right)^4\right]A_4$$

$$\bar{G}_5 = \frac{h^2\left(\frac{n\pi}{b}\right)}{8\left[\left(\frac{2m\pi}{a}\right)^2 + \left(\frac{n\pi}{b}\right)^2\right]^2}\left[20\left(\frac{m\pi}{a}\right)^4 + (8-\nu)\left(\frac{m\pi}{a}\right)^2\left(\frac{n\pi}{b}\right)^2 + \left(\frac{n\pi}{b}\right)^4\right]\bar{A}_4$$

(2) Dynamic Functions

(A) Static Buckling Configuration m = 1 and n = 1

(i) Vibration Mode p = 1 and q = 1

(a) Deflection

$$w = w^{(0)} + \epsilon^2 w^{(2)} + \epsilon^4 w^{(4)} + \cdots$$

in which

$$w^{(0)} = \sin\frac{\pi}{a}x \sin\frac{\pi}{b}y$$

$$w^{(2)} = 3\left[A_4 \sin\frac{\pi}{a}x \sin\frac{3\pi}{b}y + \bar{A}_4 \sin\frac{3\pi}{a}x \sin\frac{\pi}{b}y \right]$$

$$w^{(4)} = 5\Big[A_{51} \sin\frac{\pi}{a}x \sin\frac{3\pi}{b}y + \bar{A}_{51} \sin\frac{3\pi}{a}x \sin\frac{\pi}{b}y + A_{52} \sin\frac{3\pi}{a}x \sin\frac{3\pi}{b}y + A_{53} \sin\frac{5\pi}{a}x \sin\frac{\pi}{b}y + \bar{A}_{53} \sin\frac{\pi}{a}x \sin\frac{\pi}{b}y + A_{54} \sin\frac{5\pi}{a}x \sin\frac{3\pi}{b}y + \bar{A}_{54} \sin\frac{3\pi}{a}x \sin\frac{5\pi}{b}y \Big]$$

$$+ 2\lambda_2 h \left\{ \frac{\left[\left(\frac{\pi}{a}\right)^2 - 3\left(\frac{\pi}{b}\right)^2\right] A_4}{\left(\frac{2\pi}{b}\right)^2 \left[\left(\frac{\pi}{a}\right)^2 + \left(\frac{3\pi}{b}\right)^2\right] D} \sin\frac{\pi}{a}x \sin\frac{3\pi}{b}y + \frac{\left[\left(\frac{\pi}{b}\right)^2 - 3\left(\frac{\pi}{a}\right)^2\right] \bar{A}_4}{\left(\frac{2\pi}{a}\right)^2 \left[\left(\frac{\pi}{b}\right)^2 + \left(\frac{3\pi}{a}\right)^2\right] D} \sin\frac{3\pi}{a}x \sin\frac{\pi}{b}y \right\}$$

(b) Membrane Stresses

$$t_{ij}' = \epsilon t_{ij}^{(1)} + \epsilon^3 t_{ij}^{(3)} + \cdots$$

in which

$$t_{xx}^{(1)} = \frac{Eh}{4(1-\nu^2)} \left[\left(\frac{\pi}{a}\right)^2 + \nu\left(\frac{\pi}{b}\right)^2 - (1-\nu^2)\left(\frac{\pi}{a}\right)^2 \cos\frac{2\pi}{b}y \right]$$

$$t_{yy}^{(1)} = \frac{Eh}{4(1-\nu^2)} \left[\left(\frac{\pi}{b}\right)^2 + \nu\left(\frac{\pi}{a}\right)^2 - (1-\nu^2)\left(\frac{\pi}{b}\right)^2 \cos\frac{2\pi}{a}x \right]$$

$$t_{xy}^{(1)} = 0$$

$$t_{xx}^{(3)} = Eh\left(\frac{\pi}{a}\right)^2\left\{A_4\cos\frac{2\pi}{b}y - A_4\cos\frac{4\pi}{b}y - \frac{\left(\frac{\pi}{b}\right)^4}{\left[\left(\frac{\pi}{a}\right)^2+\left(\frac{\pi}{b}\right)^2\right]^2}4(A_4+\bar{A}_4)\cos\frac{2\pi}{a}x\cos\frac{2\pi}{b}y\right.$$

$$\left. + \frac{\left(\frac{\pi}{b}\right)^4}{\left[\left(\frac{2\pi}{a}\right)^2+\left(\frac{\pi}{b}\right)^2\right]^2}\bar{A}_4\cos\frac{4\pi}{a}x\cos\frac{2\pi}{b}y + \frac{\left(\frac{\pi}{b}\right)^4}{\left[\left(\frac{2\pi}{b}\right)^2+\left(\frac{\pi}{a}\right)^2\right]^2}4A_4\cos\frac{2\pi}{a}x\cos\frac{4\pi}{b}y\right\}$$

$$t_{yy}^{(3)} = Eh\left(\frac{\pi}{b}\right)^2\left\{\bar{A}_4\cos\frac{2\pi}{a}x - \bar{A}_4\cos\frac{4\pi}{a}x - \frac{\left(\frac{\pi}{a}\right)^4}{\left[\left(\frac{\pi}{a}\right)^2+\left(\frac{\pi}{b}\right)^2\right]^2}4(A_4+\bar{A}_4)\cos\frac{2\pi}{a}x\cos\frac{2\pi}{b}y\right.$$

$$\left. + \frac{\left(\frac{\pi}{a}\right)^4}{\left[\left(\frac{2\pi}{b}\right)^2+\left(\frac{\pi}{a}\right)^2\right]^2}A_4\cos\frac{2\pi}{a}x\cos\frac{4\pi}{b}y + \frac{\left(\frac{\pi}{a}\right)^4}{\left[\left(\frac{2\pi}{a}\right)^2+\left(\frac{\pi}{b}\right)^2\right]^2}4\bar{A}_4\cos\frac{4\pi}{a}x\cos\frac{2\pi}{b}y\right\}$$

$$t_{xy}^{(3)} = Eh\left(\frac{\pi}{a}\right)\left(\frac{\pi}{b}\right)\left\{-\frac{\left(\frac{\pi}{a}\right)^2\left(\frac{\pi}{b}\right)^2}{\left[\left(\frac{\pi}{a}\right)^2+\left(\frac{\pi}{b}\right)^2\right]^2}4(A_4+\bar{A}_4)\sin\frac{2\pi}{a}x\sin\frac{2\pi}{b}y\right.$$

$$\left. + \frac{\left(\frac{\pi}{a}\right)^2\left(\frac{\pi}{b}\right)^2}{\left[\left(\frac{2\pi}{a}\right)^2+\left(\frac{\pi}{b}\right)^2\right]^2}2\bar{A}_4\sin\frac{4\pi}{a}x\sin\frac{2\pi}{b}y + \frac{\left(\frac{\pi}{a}\right)^2\left(\frac{\pi}{b}\right)^2}{\left[\left(\frac{2\pi}{b}\right)^2+\left(\frac{\pi}{a}\right)^2\right]^2}2A_4\sin\frac{2\pi}{a}x\sin\frac{4\pi}{b}y\right\}$$

(c) Frequency Parameter

$$\mu = \mu^{(0)} + \varepsilon^2\mu^{(2)} + \varepsilon^4\mu^{(4)} + \cdots$$

in which

$$\mu^{(0)} = 0$$

$$\mu^{(2)} = \frac{Eh^2}{8(1-\nu^2)}\left\{(3-\nu^2)\left[\left(\frac{\pi}{a}\right)^4+\left(\frac{\pi}{b}\right)^4\right] + 4\nu\left(\frac{\pi}{a}\right)^2\left(\frac{\pi}{b}\right)^2\right\}$$

$$\mu^{(4)} = -\frac{3Eh^2}{4}\left[\left(\frac{\pi}{a}\right)^4A_4 + \left(\frac{\pi}{b}\right)^4\bar{A}_4\right]$$

(ii) Vibration Mode p = 2 and q = 1

(a) Deflection

$$w = w^{(0)} + \varepsilon^2 w^{(2)} + \varepsilon^4 w^{(4)} + \cdots$$

in which

$$w^{(0)} = \sin\frac{2\pi}{a}x \sin\frac{\pi}{b}y$$

$$w^{(2)} = A_{66}\sin\frac{2\pi}{a}x \sin\frac{3\pi}{b}y + A_{68}\sin\frac{4\pi}{a}x \sin\frac{\pi}{b}y + A_{69}\sin\frac{4\pi}{a}x \sin\frac{3\pi}{b}y$$

$$w^{(4)} = A_{324}\sin\frac{2\pi}{a}x \sin\frac{3\pi}{b}y + A_{325}\sin\frac{2\pi}{a}x \sin\frac{5\pi}{b}y + A_{326}\sin\frac{4\pi}{a}x \sin\frac{\pi}{b}y$$
$$+ A_{327}\sin\frac{4\pi}{a}x \sin\frac{3\pi}{b}y + A_{328}\sin\frac{4\pi}{a}x \sin\frac{5\pi}{b}y + A_{329}\sin\frac{6\pi}{a}x \sin\frac{\pi}{b}y$$
$$+ A_{330}\sin\frac{6\pi}{a}x \sin\frac{3\pi}{b}y + A_{331}\sin\frac{6\pi}{a}x \sin\frac{5\pi}{b}y$$

with

$$A_{66} = \frac{Eh^3}{128D}\,\frac{\left\{\dfrac{9(\frac{\pi}{a})^4(\frac{\pi}{b})^4}{[(\frac{\pi}{a})^2+(\frac{2\pi}{b})^2]^2} + \dfrac{25(\frac{\pi}{a})^4(\frac{\pi}{b})^4}{[(\frac{3\pi}{a})^2+(\frac{2\pi}{b})^2]^2} + 4(\frac{\pi}{a})^4\right\}}{(\frac{\pi}{b})^2[7(\frac{\pi}{a})^2+9(\frac{\pi}{b})^2]}$$

$$A_{68} = \frac{Eh^3}{192D}\,\frac{\left\{3(\frac{\pi}{b})^4 + \dfrac{25(\frac{\pi}{a})^4(\frac{\pi}{b})^4}{[(\frac{3\pi}{a})^2+(\frac{2\pi}{b})^2]^2}\right\}}{(\frac{\pi}{a})^2[19(\frac{\pi}{a})^2+(\frac{\pi}{b})^2]}$$

$$A_{69} = -\frac{Eh^3}{64D}\,\frac{\dfrac{(\frac{\pi}{a})^4(\frac{\pi}{b})^4}{[(\frac{3\pi}{a})^2+(\frac{2\pi}{b})^2]^2}}{[3(\frac{\pi}{a})^2+2(\frac{\pi}{b})^2][19(\frac{\pi}{a})^2+9(\frac{\pi}{b})^2]}$$

$$A_{324} = \frac{Eh^3}{128D}\,\frac{(\frac{\pi}{a})^4(\frac{\pi}{b})^4}{(\frac{\pi}{b})^2[7(\frac{\pi}{a})^2+9(\frac{\pi}{b})^2]}\left\{A_4\left[-\frac{16}{(\frac{\pi}{b})^4} - \frac{36}{(\frac{\pi}{a})^4} - \frac{1225}{[(\frac{\pi}{a})^2+(\frac{4\pi}{b})^2]^2}\right.\right.$$
$$\left. - \frac{1225}{[(\frac{3\pi}{a})^2+(\frac{2\pi}{b})^2]^2} - \frac{25}{[(\frac{3\pi}{a})^2+(\frac{4\pi}{b})^2]^2} - \frac{25}{[(\frac{\pi}{a})^2+(\frac{2\pi}{b})^2]^2}\right] + A_4\left[\frac{466}{[(\frac{\pi}{a})^2+(\frac{2\pi}{b})^2]^2}\right.$$
$$\left.\left. + \frac{16}{[(\frac{2\pi}{a})^2+(\frac{\pi}{b})^2]^2}\right] + A_{66}\left[\frac{[(\frac{\pi}{a})^4+(\frac{\pi}{b})^4]}{[(\frac{\pi}{a})^2+(\frac{\pi}{b})^2]}\,\frac{8}{(\frac{\pi}{b})^2(\frac{\pi}{a})^4} + \frac{[(\frac{\pi}{a})^2-(\frac{\pi}{b})^2]}{(1+\nu)[(\frac{\pi}{a})^2+(\frac{\pi}{b})^2]}\,\frac{16}{(\frac{\pi}{a})^2(\frac{\pi}{b})^2}\right.$$

$$+\frac{4}{\left(\frac{\pi}{b}\right)^4}+\frac{4}{\left(\frac{\pi}{a}\right)^4}+\frac{80}{\left[\left(\frac{\pi}{a}\right)^2+\left(\frac{2\pi}{b}\right)^2\right]^2}-\frac{625}{\left[\left(\frac{3\pi}{a}\right)^2+\left(\frac{4\pi}{b}\right)^2\right]^2}-\frac{624}{\left[\left(\frac{3\pi}{a}\right)^2+\left(\frac{2\pi}{b}\right)^2\right]^2}$$

$$-\frac{1}{\left[\left(\frac{3\pi}{a}\right)^2+\left(\frac{4\pi}{b}\right)^2\right]^2}\Bigg]-A_{68}\frac{625}{\left[\left(\frac{3\pi}{a}\right)^2+\left(\frac{2\pi}{b}\right)^2\right]^2}$$

$$+A_{69}\left[\frac{9}{\left(\frac{\pi}{a}\right)^4}+\frac{25}{\left[\left(\frac{3\pi}{a}\right)^2+\left(\frac{2\pi}{b}\right)^2\right]^2}+\frac{49}{\left[\left(\frac{3\pi}{a}\right)^2+\left(\frac{4\pi}{b}\right)^2\right]^2}\right]\Bigg\}$$

$$A_{325}=\frac{Eh^3}{384D}\frac{\left(\frac{\pi}{a}\right)^4\left(\frac{\pi}{b}\right)^4}{\left(\frac{\pi}{b}\right)^2\left[7\left(\frac{\pi}{a}\right)^2+25\left(\frac{\pi}{b}\right)^2\right]}\Bigg\{A_4\left[\frac{8}{\left(\frac{\pi}{b}\right)^4}+\frac{441}{\left[\left(\frac{\pi}{a}\right)^2+\left(\frac{4\pi}{b}\right)^2\right]^2}+\frac{1225}{\left[\left(\frac{3\pi}{a}\right)^2+\left(\frac{4\pi}{b}\right)^2\right]^2}\right.$$

$$\left.+\frac{9}{\left[\left(\frac{\pi}{a}\right)^2+\left(\frac{2\pi}{b}\right)^2\right]^2}+\frac{121}{\left[\left(\frac{3\pi}{a}\right)^2+\left(\frac{2\pi}{b}\right)^2\right]^2}\right]+A_{66}\left[\frac{4}{\left(\frac{\pi}{b}\right)^4}+\frac{225}{\left[\left(\frac{\pi}{a}\right)^2+\left(\frac{4\pi}{b}\right)^2\right]^2}+\frac{49}{\left[\left(\frac{3\pi}{a}\right)^2+\left(\frac{4\pi}{b}\right)^2\right]^2}\right]$$

$$-A_{69}\frac{2401}{\left[\left(\frac{3\pi}{a}\right)^2+\left(\frac{4\pi}{b}\right)^2\right]^2}\Bigg\}$$

$$A_{326}=\frac{Eh^3}{192D}\frac{\left(\frac{\pi}{a}\right)^4\left(\frac{\pi}{b}\right)^4}{\left(\frac{\pi}{a}\right)^2\left[19\left(\frac{\pi}{a}\right)^2+\left(\frac{\pi}{b}\right)^2\right]}\Bigg\{A_4\left[-\frac{36}{\left[\left(\frac{\pi}{a}\right)^2+\left(\frac{\pi}{b}\right)^2\right]^2}-\frac{1346}{\left[\left(\frac{3\pi}{a}\right)^2+\left(\frac{2\pi}{b}\right)^2\right]^2}\right]$$

$$+\bar{A}_4\left[-\frac{36}{\left[\left(\frac{\pi}{a}\right)^2+\left(\frac{\pi}{b}\right)^2\right]^2}-\frac{9}{\left[\left(\frac{5\pi}{a}\right)^2+\left(\frac{2\pi}{b}\right)^2\right]^2}-\frac{441}{\left[\left(\frac{\pi}{a}\right)^2+\left(\frac{2\pi}{b}\right)^2\right]^2}-\frac{6}{\left(\frac{\pi}{a}\right)^4}\right]$$

$$-A_{66}\frac{625}{\left[\left(\frac{3\pi}{a}\right)^2+\left(\frac{2\pi}{b}\right)^2\right]^2}+A_{68}\left[\frac{\left[\left(\frac{\pi}{a}\right)^4+\left(\frac{\pi}{b}\right)^4\right]}{\left[\left(\frac{\pi}{a}\right)^2+\left(\frac{\pi}{b}\right)^2\right]}\frac{12}{\left(\frac{\pi}{a}\right)^2\left(\frac{\pi}{b}\right)^4}-\frac{\left[\left(\frac{\pi}{a}\right)^2-\left(\frac{\pi}{b}\right)^2\right]}{(14)\left[\left(\frac{\pi}{a}\right)^2+\left(\frac{\pi}{b}\right)^2\right]}\frac{24}{\left(\frac{\pi}{a}\right)^2\left(\frac{\pi}{b}\right)^2}\right.$$

$$\left.-\frac{12}{\left(\frac{\pi}{b}\right)^4}-\frac{624}{\left[\left(\frac{3\pi}{a}\right)^2+\left(\frac{2\pi}{b}\right)^2\right]^2}-\frac{81}{\left[\left(\frac{5\pi}{a}\right)^2+\left(\frac{2\pi}{b}\right)^2\right]^2}+\frac{81}{\left[\left(\frac{\pi}{a}\right)^2+\left(\frac{2\pi}{b}\right)^2\right]^2}\right]$$

$$+A_{69}\left[\frac{16}{\left(\frac{\pi}{b}\right)^4}+\frac{25}{\left[\left(\frac{3\pi}{a}\right)^2+\left(\frac{2\pi}{b}\right)^2\right]^2}+\frac{441}{\left[\left(\frac{5\pi}{a}\right)^2+\left(\frac{2\pi}{b}\right)^2\right]^2}\right]\Bigg\}$$

$$A_{327}=\frac{Eh^3}{64D}\frac{\left(\frac{\pi}{a}\right)^4\left(\frac{\pi}{b}\right)^4}{\left[57\left(\frac{\pi}{a}\right)^4+65\left(\frac{\pi}{a}\right)^2\left(\frac{\pi}{b}\right)^2+18\left(\frac{\pi}{b}\right)^4\right]}\Bigg\{A_4\left[\frac{18}{\left(\frac{\pi}{a}\right)^4}+\frac{4}{\left[\left(\frac{\pi}{a}\right)^2+\left(\frac{\pi}{b}\right)^2\right]^2}+\frac{49}{\left[\left(\frac{3\pi}{a}\right)^2+\left(\frac{2\pi}{b}\right)^2\right]^2}\right.$$

$$+\frac{1225}{\left[\left(\frac{3\pi}{a}\right)^2+\left(\frac{4\pi}{b}\right)^2\right]^2}+\frac{25}{\left[\left(\frac{\pi}{a}\right)^2+\left(\frac{2\pi}{b}\right)^2\right]^2}\Bigg]+\bar{A}_4\Bigg[\frac{4}{\left[\left(\frac{\pi}{a}\right)^2+\left(\frac{\pi}{b}\right)^2\right]^2}+\frac{49}{\left[\left(\frac{5\pi}{a}\right)^2+\left(\frac{2\pi}{b}\right)^2\right]^2}$$

$$+\frac{225}{\left[\left(\frac{\pi}{a}\right)^2+\left(\frac{2\pi}{b}\right)^2\right]^2}\Bigg]+A_{66}\Bigg[\frac{9}{\left(\frac{\pi}{a}\right)^4}+\frac{25}{\left[\left(\frac{3\pi}{a}\right)^2+\left(\frac{2\pi}{b}\right)^2\right]^2}+\frac{49}{\left[\left(\frac{3\pi}{a}\right)^2+\left(\frac{4\pi}{b}\right)^2\right]^2}\Bigg]$$

$$+A_{68}\Bigg[\frac{16}{\left(\frac{\pi}{b}\right)^4}+\frac{25}{\left[\left(\frac{3\pi}{a}\right)^2+\left(\frac{2\pi}{b}\right)^2\right]^2}+\frac{441}{\left[\left(\frac{5\pi}{a}\right)^2+\left(\frac{2\pi}{b}\right)^2\right]^2}\Bigg]$$

$$+A_{69}\Bigg\{\frac{\left[\left(\frac{\pi}{a}\right)^4+\left(\frac{\pi}{b}\right)^4\right]\left[12\left(\frac{\pi}{a}\right)^2+8\left(\frac{\pi}{b}\right)^2\right]}{\left[\left(\frac{\pi}{a}\right)^2+\left(\frac{\pi}{b}\right)^2\right]\left(\frac{\pi}{a}\right)^4\left(\frac{\pi}{b}\right)^4}-\frac{8\left[\left(\frac{\pi}{a}\right)^2-\left(\frac{\pi}{b}\right)^2\right]}{(1+\nu)\left[\left(\frac{\pi}{a}\right)^2+\left(\frac{\pi}{b}\right)^2\right]\left(\frac{\pi}{a}\right)^2\left(\frac{\pi}{b}\right)^2}$$

$$+\frac{4}{\left(\frac{\pi}{b}\right)^4}+\frac{4}{\left(\frac{\pi}{a}\right)^4}-\frac{2401}{\left[\left(\frac{3\pi}{a}\right)^2+\left(\frac{4\pi}{b}\right)^2\right]^2}-\frac{2401}{\left[\left(\frac{5\pi}{a}\right)^2+\left(\frac{2\pi}{b}\right)^2\right]^2}-\frac{1}{\left[\left(\frac{5\pi}{a}\right)^2+\left(\frac{4\pi}{b}\right)^2\right]^2}$$

$$+\frac{81}{\left[\left(\frac{\pi}{a}\right)^2+\left(\frac{2\pi}{b}\right)^2\right]^2}\Bigg]\Bigg\}.$$

$$A_{328}=\frac{Eh^3}{192D}\frac{\left(\frac{\pi}{a}\right)^4\left(\frac{\pi}{b}\right)^4}{\left[19\left(\frac{\pi}{a}\right)^4+63\left(\frac{\pi}{a}\right)^2\left(\frac{\pi}{b}\right)^2+50\left(\frac{\pi}{b}\right)^4\right]}\Bigg\{A_4\Bigg[-\frac{9}{\left[\left(\frac{\pi}{a}\right)^2+\left(\frac{2\pi}{b}\right)^2\right]^2}$$

$$-\frac{25}{\left[\left(\frac{3\pi}{a}\right)^2+\left(\frac{4\pi}{b}\right)^2\right]^2}-\frac{49}{\left[\left(\frac{3\pi}{a}\right)^2+\left(\frac{2\pi}{b}\right)^2\right]^2}\Bigg]-A_{66}\frac{1}{\left[\left(\frac{3\pi}{a}\right)^2+\left(\frac{4\pi}{b}\right)^2\right]^2}$$

$$+A_{69}\Bigg[\frac{16}{\left(\frac{\pi}{b}\right)^4}+\frac{49}{\left[\left(\frac{3\pi}{a}\right)^2+\left(\frac{4\pi}{b}\right)^2\right]^2}+\frac{81}{\left[\left(\frac{5\pi}{a}\right)^2+\left(\frac{4\pi}{b}\right)^2\right]^2}\Bigg]\Bigg\}$$

$$A_{329}=\frac{Eh^3}{512D}\frac{\left(\frac{\pi}{a}\right)^4\left(\frac{\pi}{b}\right)^4}{\left(\frac{\pi}{a}\right)^2\left[39\left(\frac{\pi}{a}\right)^2+\left(\frac{\pi}{b}\right)^2\right]}\Bigg\{\bar{A}_4\Bigg[\frac{6}{\left(\frac{\pi}{a}\right)^4}+\frac{16}{\left[\left(\frac{2\pi}{a}\right)^2+\left(\frac{\pi}{b}\right)^2\right]^2}+\frac{49}{\left[\left(\frac{5\pi}{a}\right)^2+\left(\frac{\pi}{b}\right)^2\right]^2}$$

$$+\frac{81}{\left[\left(\frac{3\pi}{a}\right)^2+\left(\frac{2\pi}{b}\right)^2\right]^2}\Bigg]+A_{68}\Bigg[\frac{3}{\left(\frac{\pi}{a}\right)^4}+\frac{441}{\left[\left(\frac{5\pi}{a}\right)^2+\left(\frac{2\pi}{b}\right)^2\right]^2}\Bigg]-A_{69}\frac{2401}{\left[\left(\frac{5\pi}{a}\right)^2+\left(\frac{2\pi}{b}\right)^2\right]^2}\Bigg\}$$

$$A_{330}=\frac{Eh^3}{192D}\frac{\left(\frac{\pi}{a}\right)^4\left(\frac{\pi}{b}\right)^4}{\left[104\left(\frac{\pi}{a}\right)^4+50\left(\frac{\pi}{a}\right)^2\left(\frac{\pi}{b}\right)^2+9\left(\frac{\pi}{b}\right)^4\right]}\Bigg\{\bar{A}_4\Bigg[-\frac{9}{\left[\left(\frac{5\pi}{a}\right)^2+\left(\frac{2\pi}{b}\right)^2\right]^2}$$

$$- \frac{9}{\left[\left(\frac{3\pi}{a}\right)^2+\left(\frac{2\pi}{b}\right)^2\right]^2}\Bigg] - A_{68}\frac{81}{\left[\left(\frac{5\pi}{a}\right)^2+\left(\frac{2\pi}{b}\right)^2\right]^2}$$

$$+ A_{69}\left[\frac{9}{\left(\frac{\pi}{a}\right)^4} + \frac{441}{\left[\left(\frac{5\pi}{a}\right)^2+\left(\frac{2\pi}{b}\right)^2\right]^2} + \frac{81}{\left[\left(\frac{5\pi}{a}\right)^2+\left(\frac{4\pi}{b}\right)^2\right]^2}\right]\Bigg\}$$

$$A_{331} = \frac{Eh^3}{128D}\frac{\left(\frac{\pi}{a}\right)^4\left(\frac{\pi}{b}\right)^4}{\left[156\left(\frac{\pi}{a}\right)^4+217\left(\frac{\pi}{a}\right)^2\left(\frac{\pi}{b}\right)^2+75\left(\frac{\pi}{b}\right)^4\right]}\left\{-A_{69}\frac{1}{\left[\left(\frac{5\pi}{a}\right)^2+\left(\frac{4\pi}{b}\right)^2\right]^2}\right\}$$

(b) Membrane Stresses

$$t'_{ij} = \varepsilon t_{ij}^{(1)} + \varepsilon^3 t_{ij}^{(3)} + \cdots$$

in which

$$t_{xx}^{(1)} = \frac{Eh}{4}\left\{\frac{36\left(\frac{\pi}{a}\right)^2\left(\frac{\pi}{b}\right)^4}{\left[\left(\frac{\pi}{a}\right)^2+\left(\frac{2\pi}{b}\right)^2\right]^2}\cos\frac{\pi}{a}x\cos\frac{2\pi}{b}y + \frac{4\left(\frac{\pi}{a}\right)^2\left(\frac{\pi}{b}\right)^4}{\left[\left(\frac{3\pi}{a}\right)^2+\left(\frac{2\pi}{b}\right)^2\right]^2}\cos\frac{3\pi}{a}x\cos\frac{2\pi}{b}y\right\}$$

$$t_{yy}^{(1)} = \frac{Eh}{4}\left\{\left(\frac{\pi}{b}\right)^2\cos\frac{\pi}{a}x - \left(\frac{\pi}{b}\right)^2\cos\frac{3\pi}{a}x - \frac{9\left(\frac{\pi}{a}\right)^4\left(\frac{\pi}{b}\right)^2}{\left[\left(\frac{\pi}{a}\right)^2+\left(\frac{2\pi}{b}\right)^2\right]^2}\cos\frac{\pi}{a}x\cos\frac{2\pi}{b}y\right.$$

$$\left. + \frac{9\left(\frac{\pi}{a}\right)^4\left(\frac{\pi}{b}\right)^2}{\left[\left(\frac{3\pi}{a}\right)^2+\left(\frac{2\pi}{b}\right)^2\right]^2}\cos\frac{3\pi}{a}x\cos\frac{2\pi}{b}y\right\}$$

$$t_{xy}^{(1)} = \frac{Eh}{4}\left\{-\frac{18\left(\frac{\pi}{a}\right)^3\left(\frac{\pi}{b}\right)^3}{\left[\left(\frac{\pi}{a}\right)^2+\left(\frac{2\pi}{b}\right)^2\right]^2}\sin\frac{\pi}{a}x\sin\frac{2\pi}{b}y + \frac{6\left(\frac{\pi}{a}\right)^3\left(\frac{\pi}{b}\right)^3}{\left[\left(\frac{3\pi}{a}\right)^2+\left(\frac{2\pi}{b}\right)^2\right]^2}\sin\frac{3\pi}{a}x\sin\frac{2\pi}{b}y\right\}$$

$$t_{xx}^{(3)} = \frac{Eh}{4}\left(\frac{\pi}{a}\right)^2\left\{\frac{\left(\frac{\pi}{b}\right)^4}{\left[\left(\frac{\pi}{a}\right)^2+\left(\frac{2\pi}{b}\right)^2\right]^2}\left(100A_4 - 100\bar{A}_4 + 4A_{66}\right)\cos\frac{\pi}{a}x\cos\frac{2\pi}{b}y\right.$$

$$+ \frac{\left(\frac{\pi}{b}\right)^4}{\left[\left(\frac{\pi}{a}\right)^2+\left(\frac{4\pi}{b}\right)^2\right]^2}\left(-784A_4 - 400A_{66}\right)\cos\frac{\pi}{a}x\cos\frac{4\pi}{b}y$$

$$\left. + \frac{\left(\frac{\pi}{b}\right)^4}{\left[\left(\frac{3\pi}{a}\right)^2+\left(\frac{2\pi}{b}\right)^2\right]^2}\left(-196A_4 - 100A_{66} - 100A_{68} + 4A_{69}\right)\cos\frac{3\pi}{a}x\cos\frac{2\pi}{b}y\right.$$

$$+\frac{\left(\frac{\pi}{b}\right)^4}{\left[\left(\frac{3\pi}{a}\right)^2+\left(\frac{4\pi}{b}\right)^2\right]^2}\left(400A_4+16A_{66}-784A_{69}\right)\cos\frac{3\pi}{a}x\cos\frac{4\pi}{b}y$$

$$+\frac{\left(\frac{\pi}{b}\right)^4}{\left[\left(\frac{5\pi}{a}\right)^2+\left(\frac{2\pi}{b}\right)^2\right]^2}\left(4\bar{A}_4+36A_{68}-196A_{69}\right)\cos\frac{5\pi}{a}x\cos\frac{2\pi}{b}y$$

$$+\frac{\left(\frac{\pi}{b}\right)^4}{\left[\left(\frac{5\pi}{a}\right)^2+\left(\frac{4\pi}{b}\right)^2\right]^2}16A_{69}\cos\frac{5\pi}{a}x\cos\frac{4\pi}{b}y\Bigg\}$$

$$t_{yy}^{(3)}=\frac{Eh}{4}\left(\frac{\pi}{b}\right)^2\Bigg\{A_4\cos\frac{\pi}{a}x+A_{68}\cos\frac{3\pi}{a}x-\left(\bar{A}_4+A_{68}\right)\cos\frac{5\pi}{a}x$$

$$+\frac{\left(\frac{\pi}{a}\right)^4}{\left[\left(\frac{\pi}{a}\right)^2+\left(\frac{2\pi}{b}\right)^2\right]^2}\left(25A_4-25\bar{A}_4+A_{66}\right)\cos\frac{\pi}{a}x\cos\frac{2\pi}{b}y$$

$$+\frac{\left(\frac{\pi}{a}\right)^4}{\left[\left(\frac{\pi}{a}\right)^2+\left(\frac{4\pi}{b}\right)^2\right]^2}\left(-49A_4-25A_{66}\right)\cos\frac{\pi}{a}x\cos\frac{4\pi}{b}y$$

$$+\frac{\left(\frac{\pi}{a}\right)^4}{\left[\left(\frac{3\pi}{a}\right)^2+\left(\frac{2\pi}{b}\right)^2\right]^2}\left(-441A_4-225A_{66}-225A_{68}+9A_{69}\right)\cos\frac{3\pi}{a}x\cos\frac{2\pi}{b}y$$

$$+\frac{\left(\frac{\pi}{a}\right)^4}{\left[\left(\frac{3\pi}{a}\right)^2+\left(\frac{4\pi}{b}\right)^2\right]^2}\left(225A_4+9A_{66}-441A_{69}\right)\cos\frac{3\pi}{a}x\cos\frac{4\pi}{b}y$$

$$+\frac{\left(\frac{\pi}{a}\right)^4}{\left[\left(\frac{5\pi}{a}\right)^2+\left(\frac{2\pi}{b}\right)^2\right]^2}\left(25\bar{A}_4+225A_{68}-1225A_{69}\right)\cos\frac{5\pi}{a}x\cos\frac{2\pi}{b}y$$

$$+\frac{\left(\frac{\pi}{a}\right)^4}{\left[\left(\frac{5\pi}{a}\right)^2+\left(\frac{4\pi}{b}\right)^2\right]^2}\left(25A_{69}\right)\cos\frac{5\pi}{a}x\cos\frac{4\pi}{b}y\Bigg\}$$

$$t_{xy}^{(3)}=\frac{Eh}{4}\left(\frac{\pi}{a}\right)\left(\frac{\pi}{b}\right)\Bigg\{\frac{\left(\frac{\pi}{a}\right)^2\left(\frac{\pi}{b}\right)^2}{\left[\left(\frac{\pi}{a}\right)^2+\left(\frac{2\pi}{b}\right)^2\right]^2}\left(50A_4-50\bar{A}_4+2A_{66}\right)\sin\frac{\pi}{a}x\sin\frac{2\pi}{b}y$$

$$+\frac{(\frac{\pi}{a})^2(\frac{\pi}{b})^2}{[(\frac{\pi}{a})^2+(\frac{4\pi}{b})^2]^2}(-196A_4-100A_{66})\sin\frac{\pi}{a}x\sin\frac{4\pi}{b}y$$

$$+\frac{(\frac{\pi}{a})^2(\frac{\pi}{b})^2}{[(\frac{3\pi}{a})^2+(\frac{2\pi}{b})^2]^2}(-294A_4-150A_{66}-150A_{68}+6A_{69})\sin\frac{3\pi}{a}x\sin\frac{2\pi}{b}y$$

$$+\frac{(\frac{\pi}{a})^2(\frac{\pi}{b})^2}{[(\frac{3\pi}{a})^2+(\frac{4\pi}{b})^2]^2}(300A_4+12A_{66}-588A_{69})\sin\frac{3\pi}{a}x\sin\frac{4\pi}{b}y$$

$$+\frac{(\frac{\pi}{a})^2(\frac{\pi}{b})^2}{[(\frac{5\pi}{a})^2+(\frac{2\pi}{b})^2]^2}(10\bar{A}_4+90A_{68}-490A_{69})\sin\frac{5\pi}{a}x\sin\frac{2\pi}{b}y$$

$$+\frac{(\frac{\pi}{a})^2(\frac{\pi}{b})^2}{[(\frac{5\pi}{a})^2+(\frac{4\pi}{b})^2]}(20A_{69})\sin\frac{5\pi}{a}x\sin\frac{4\pi}{b}y\Bigg\}$$

(c) Frequency Parameter

$$\lambda=\lambda^{(0)}+\varepsilon^2\lambda^{(2)}+\varepsilon^4\lambda^{(4)}+\cdots$$

in which

$$\lambda^{(0)}=\frac{D}{h}\,3(\frac{\pi}{a})^2\left[(\frac{2\pi}{a})^2+(\frac{\pi}{b})^2\right]$$

$$\lambda^{(2)}=\frac{Eh^2}{16}\Bigg\{-\frac{[(\frac{\pi}{a})^4+(\frac{\pi}{b})^4][(\frac{2\pi}{a})^2+(\frac{\pi}{b})^2]}{[(\frac{\pi}{a})^2+(\frac{\pi}{b})^2]}+\frac{6(\frac{\pi}{a})^2(\frac{\pi}{b})^2[(\frac{\pi}{a})^2-(\frac{\pi}{b})^2]}{(1+\nu)[(\frac{\pi}{a})^2+(\frac{\pi}{b})^2]}$$

$$+4[(\frac{\pi}{a})^4+(\frac{\pi}{b})^4]+\frac{(\frac{\pi}{a})^4(\frac{\pi}{b})^4}{[(\frac{3\pi}{a})^2+(\frac{2\pi}{b})^2]^2}+\frac{81(\frac{\pi}{a})^4(\frac{\pi}{b})^4}{[(\frac{\pi}{a})^2+(\frac{2\pi}{b})^2]^2}\Bigg\}$$

$$\lambda^{(4)}=\frac{Eh}{16}\Bigg\{A_4\Big[-5(\frac{\pi}{a})^4+\frac{9(\frac{\pi}{a})^6}{[(\frac{\pi}{a})^2+(\frac{\pi}{b})^2]}-\frac{450(\frac{\pi}{a})^4(\frac{\pi}{b})^4}{[(\frac{\pi}{a})^2+(\frac{2\pi}{b})^2]^2}-\frac{98(\frac{\pi}{a})^4(\frac{\pi}{b})^4}{[(\frac{3\pi}{a})^2+(\frac{2\pi}{b})^2]^2}\Big]$$

$$+\bar{A}_4\Big[9(\frac{\pi}{b})^4+\frac{9(\frac{\pi}{a})^2(\frac{\pi}{b})^4}{[(\frac{\pi}{a})^2+(\frac{\pi}{b})^2]}+\frac{450(\frac{\pi}{a})^4(\frac{\pi}{b})^4}{[(\frac{\pi}{a})^2+(\frac{2\pi}{b})^2]^2}\Big]+A_{66}\Big[-4(\frac{\pi}{a})^4$$

$$- \frac{9(\frac{\pi}{a})^4(\frac{\pi}{b})^4}{[(\frac{\pi}{a})^2+(\frac{2\pi}{b})^2]^2} - \frac{25(\frac{\pi}{a})^4(\frac{\pi}{b})^4}{[(\frac{3\pi}{a})^2+(\frac{2\pi}{b})^2]^2}] - A_{168}\left[3(\frac{\pi}{b})^4 + \frac{25(\frac{\pi}{a})^4(\frac{\pi}{b})^4}{[(\frac{3\pi}{a})^2+(\frac{2\pi}{b})^2]^2}\right]$$

$$+ A_{169} \frac{(\frac{\pi}{a})^4(\frac{\pi}{b})^4}{[(\frac{3\pi}{a})^2+(\frac{2\pi}{b})^2]^2} \Big\}$$

(B) Static Buckling Configuration m = 2 and n = 1

(i) Vibration Mode p = 1 and q = 1

(a) Deflection

$$w = w^{(0)} + \varepsilon^2 w^{(2)} + \cdots$$

in which

$$w^{(0)} = \sin\frac{\pi}{a}x \sin\frac{\pi}{b}y$$

$$w^{(2)} = A_{162}\sin\frac{3\pi}{a}x \sin\frac{\pi}{b}y - A_{164}\sin\frac{3\pi}{a}x \sin\frac{3\pi}{b}y + A_{166}\sin\frac{\pi}{a}x \sin\frac{3\pi}{b}y$$

$$+ A_{168}\sin\frac{5\pi}{a}x \sin\frac{\pi}{b}y + A_{169}\sin\frac{5\pi}{a}x \sin\frac{3\pi}{b}y$$

with

$$A_{162} = \frac{Eh^3}{128D} \frac{-3(\frac{\pi}{b})^4 - \frac{225(\frac{\pi}{a})^4(\frac{\pi}{b})^4}{[(\frac{\pi}{a})^2+(\frac{2\pi}{b})^2]^2}}{(\frac{\pi}{a})^2[6(\frac{\pi}{a})^2+(\frac{\pi}{b})^2]}$$

$$A_{164} = \frac{Eh^3}{384D} \frac{-\frac{81(\frac{\pi}{a})^4(\frac{\pi}{b})^4}{[(\frac{\pi}{a})^2+(\frac{2\pi}{b})^2]^2}}{[(\frac{\pi}{a})^2+(\frac{\pi}{b})^2][2(\frac{\pi}{a})^2+3(\frac{\pi}{b})^2]}$$

$$A_{166} = \frac{Eh^3}{128D} \frac{(\frac{\pi}{a})^4(\frac{\pi}{b})^4\left\{\frac{225}{[(\frac{\pi}{a})^2+(\frac{2\pi}{b})^2]^2} + \frac{49}{[(\frac{3\pi}{a})^2+(\frac{2\pi}{b})^2]^2} + \frac{4}{(\frac{\pi}{b})^4}\right\}}{(\frac{\pi}{b})^2[-2(\frac{\pi}{a})^2+9(\frac{\pi}{b})^2]}$$

$$A_{168} = \frac{Eh^3}{384D} \frac{(\frac{\pi}{a})^4(\frac{\pi}{b})^4\left\{\frac{3}{(\frac{\pi}{a})^4} + \frac{49}{[(\frac{3\pi}{a})^2+(\frac{2\pi}{b})^2]^2}\right\}}{(\frac{\pi}{a})^2[22(\frac{\pi}{a})^2+(\frac{\pi}{b})^2]}$$

$$A_{169} = \frac{Eh^3}{128D} \frac{(\frac{\pi}{a})^4(\frac{\pi}{b})^4\left\{-\frac{1}{[(\frac{3\pi}{a})^2+(\frac{2\pi}{b})^2]^2}\right\}}{[3(\frac{\pi}{a})^2+(\frac{\pi}{b})^2][22(\frac{\pi}{a})^2+9(\frac{\pi}{b})^2]}$$

(b) Membrane Stresses

$$t_{ij}' = \varepsilon t_{ij}^{(1)} + \varepsilon^3 t_{ij}^{(3)} + \cdots$$

in which

$$t_{xx}^{(1)} = \frac{Eh}{4}\left[-\frac{36(\frac{\pi}{a})^2(\frac{\pi}{b})^4}{[(\frac{\pi}{a})^2+(\frac{2\pi}{b})^2]^2}\cos\frac{\pi}{a}x\cos\frac{2\pi}{b}y + \frac{4(\frac{\pi}{a})^2(\frac{\pi}{b})^4}{[(\frac{3\pi}{a})^2+(\frac{2\pi}{b})^2]^2}\cos\frac{3\pi}{a}x\cos\frac{2\pi}{b}y\right]$$

$$t_{yy}^{(1)} = \frac{Eh}{4}\left[-\frac{9(\frac{\pi}{a})^4(\frac{\pi}{b})^2}{[(\frac{\pi}{a})^2+(\frac{2\pi}{b})^2]^2}\cos\frac{\pi}{a}x\cos\frac{2\pi}{b}y - (\frac{\pi}{b})^2\cos\frac{3\pi}{a}x\right.$$

$$\left. + \frac{9(\frac{\pi}{a})^4(\frac{\pi}{b})^2}{[(\frac{3\pi}{a})^2+(\frac{2\pi}{b})^2]^2}\cos\frac{3\pi}{a}x\cos\frac{2\pi}{b}y + (\frac{\pi}{b})^2\cos\frac{\pi}{a}x\right]$$

$$t_{xy}^{(1)} = \frac{Eh}{4}\left[-\frac{18(\frac{\pi}{a})^3(\frac{\pi}{b})^3}{[(\frac{\pi}{a})^2+(\frac{2\pi}{b})^2]^2}\sin\frac{\pi}{a}x\sin\frac{2\pi}{b}y + \frac{6(\frac{\pi}{a})^3(\frac{\pi}{b})^3}{[(\frac{3\pi}{a})^2+(\frac{2\pi}{b})^2]^2}\sin\frac{3\pi}{a}x\sin\frac{2\pi}{b}y\right]$$

$$t_{xx}^{(3)} = \frac{Eh}{4}(\frac{\pi}{a})^2\left\{\frac{(\frac{\pi}{b})^4}{[(\frac{\pi}{a})^2+(\frac{2\pi}{b})^2]^2}(4A_{14}-100A_{62}-36A_{164}+100A_{166})\cos\frac{\pi}{a}x\cos\frac{2\pi}{b}y\right.$$

$$+ \frac{(\frac{\pi}{b})^4}{[(\frac{\pi}{a})^2+(\frac{4\pi}{b})^2]^2}(-400A_{14}+1296A_{164}-784A_{166})\cos\frac{\pi}{a}x\cos\frac{4\pi}{b}y$$

$$+ \frac{(\frac{\pi}{b})^4}{[(\frac{3\pi}{a})^2+(\frac{2\pi}{b})^2]^2}(-100A_{14}-196A_{166}-196A_{168}+4A_{169})\cos\frac{3\pi}{a}x\cos\frac{2\pi}{b}y$$

$$\left. + \frac{(\frac{\pi}{b})^4}{[(\frac{3\pi}{a})^2+(\frac{4\pi}{b})^2]^2}(16A_{14}+400A_{166}-1936A_{169})\cos\frac{3\pi}{a}x\cos\frac{4\pi}{b}y\right.$$

$$+\frac{\left(\frac{\pi}{b}\right)^4}{\left[\left(\frac{5\pi}{a}\right)^2+\left(\frac{2\pi}{b}\right)^2\right]^2}\left(-196\bar{A}_{14}+4A_{162}+324A_{164}\right)\cos\frac{5\pi}{a}x\cos\frac{2\pi}{b}y$$

$$+\frac{\left(\frac{\pi}{b}\right)^4}{\left[\left(\frac{5\pi}{a}\right)^2+\left(\frac{4\pi}{b}\right)^2\right]^2}\left(-144A_{164}\right)\cos\frac{5\pi}{a}x\cos\frac{4\pi}{b}y$$

$$+\frac{\left(\frac{\pi}{b}\right)^4}{\left[\left(\frac{7\pi}{a}\right)^2+\left(\frac{2\pi}{b}\right)^2\right]^2}\left(100\bar{A}_{14}+36A_{168}-484A_{169}\right)\cos\frac{7\pi}{a}x\cos\frac{2\pi}{b}y$$

$$+\frac{\left(\frac{\pi}{b}\right)^4}{\left[\left(\frac{7\pi}{a}\right)^2+\left(\frac{4\pi}{b}\right)^2\right]^2}\left(16A_{169}\right)\cos\frac{7\pi}{a}x\cos\frac{2\pi}{b}y\Bigg\}$$

$$t_{yy}^{(3)}=\frac{Eh}{4}\left(\frac{\pi}{b}\right)^2\Bigg\{A_{162}\cos\frac{\pi}{a}x+A_{168}\cos\frac{3\pi}{a}x+\left(\bar{A}_{14}-A_{162}\right)\cos\frac{5\pi}{a}x$$

$$-\left(\bar{A}_{14}+A_{168}\right)\cos\frac{7\pi}{a}x+\frac{\left(\frac{\pi}{a}\right)^2}{\left[\left(\frac{\pi}{a}\right)^2+\left(\frac{2\pi}{b}\right)^2\right]^2}\left(A_{14}-25A_{162}-9A_{164}+25A_{166}\right)\cos\frac{\pi}{a}x\cos\frac{2\pi}{b}y$$

$$+\frac{\left(\frac{\pi}{a}\right)^4}{\left[\left(\frac{\pi}{a}\right)^2+\left(\frac{4\pi}{b}\right)^2\right]^2}\left(-25A_{14}+81A_{164}-49A_{166}\right)\cos\frac{\pi}{a}x\cos\frac{4\pi}{b}y$$

$$+\frac{\left(\frac{\pi}{a}\right)^4}{\left[\left(\frac{3\pi}{a}\right)^2+\left(\frac{2\pi}{b}\right)^2\right]^2}\left(-225A_{14}-441A_{166}-441A_{168}+9A_{169}\right)\cos\frac{3\pi}{a}x\cos\frac{2\pi}{b}y$$

$$+\frac{\left(\frac{\pi}{a}\right)^4}{\left[\left(\frac{3\pi}{a}\right)^2+\left(\frac{4\pi}{b}\right)^2\right]^2}\left(9A_{14}+225A_{166}-1089A_{169}\right)\cos\frac{3\pi}{a}x\cos\frac{4\pi}{b}y$$

$$+\frac{\left(\frac{\pi}{a}\right)^4}{\left[\left(\frac{5\pi}{a}\right)^2+\left(\frac{2\pi}{b}\right)^2\right]^2}\left(-1225\bar{A}_{14}+25A_{162}+2025A_{164}\right)\cos\frac{5\pi}{a}x\cos\frac{2\pi}{b}y$$

$$+\frac{\left(\frac{\pi}{a}\right)^4}{\left[\left(\frac{5\pi}{a}\right)^2+\left(\frac{4\pi}{b}\right)^2\right]^2}\left(-225A_{164}\right)\cos\frac{5\pi}{a}x\cos\frac{4\pi}{b}y$$

$$+\frac{\left(\frac{\pi}{a}\right)^4}{\left[\left(\frac{7\pi}{a}\right)^2+\left(\frac{2\pi}{b}\right)^2\right]^2}\left(1225\bar{A}_{14}+441A_{168}-5929A_{169}\right)\cos\frac{7\pi}{a}x\cos\frac{2\pi}{b}y$$

$$+\frac{\left(\frac{\pi}{a}\right)^4}{\left[\left(\frac{7\pi}{a}\right)^2+\left(\frac{4\pi}{b}\right)^2\right]^2}\left(49A_{169}\right)\cos\frac{7\pi}{a}x\cos\frac{4\pi}{b}y\Bigg\}$$

$$t_{xy}^{(3)}=\frac{Eh}{4}\left(\frac{\pi}{a}\right)\left(\frac{\pi}{b}\right)\Bigg\{\frac{\left(\frac{\pi}{a}\right)^2\left(\frac{\pi}{b}\right)^2}{\left[\left(\frac{\pi}{a}\right)^2+\left(\frac{2\pi}{b}\right)^2\right]^2}\left(2A_{14}-50A_{162}-18A_{164}+50A_{166}\right)\sin\frac{\pi}{a}x\sin\frac{2\pi}{b}y$$

$$+\frac{\left(\frac{\pi}{a}\right)^2\left(\frac{\pi}{b}\right)^2}{\left[\left(\frac{\pi}{a}\right)^2+\left(\frac{4\pi}{b}\right)^2\right]^2}\left(-100A_{14}+324A_{164}-196A_{166}\right)\sin\frac{\pi}{a}x\sin\frac{4\pi}{b}y$$

$$+\frac{\left(\frac{\pi}{a}\right)^2\left(\frac{\pi}{b}\right)^2}{\left[\left(\frac{3\pi}{a}\right)^2+\left(\frac{2\pi}{b}\right)^2\right]}\left(-150A_{14}-294A_{166}-294A_{168}+6A_{169}\right)\sin\frac{3\pi}{a}x\sin\frac{2\pi}{b}y$$

$$+\frac{\left(\frac{\pi}{a}\right)^2\left(\frac{\pi}{b}\right)^2}{\left[\left(\frac{3\pi}{a}\right)^2+\left(\frac{4\pi}{b}\right)^2\right]^2}\left(12A_{14}+300A_{166}-1452A_{169}\right)\sin\frac{3\pi}{a}x\sin\frac{4\pi}{b}y$$

$$+\frac{\left(\frac{\pi}{a}\right)^2\left(\frac{\pi}{b}\right)^2}{\left[\left(\frac{5\pi}{a}\right)^2+\left(\frac{2\pi}{b}\right)^2\right]^2}\left(-490\bar{A}_{14}+10A_{162}+810A_{164}\right)\sin\frac{5\pi}{a}x\sin\frac{2\pi}{b}y$$

$$+\frac{\left(\frac{\pi}{a}\right)^2\left(\frac{\pi}{b}\right)^2}{\left[\left(\frac{5\pi}{a}\right)^2+\left(\frac{4\pi}{b}\right)^2\right]^2}\left(-180A_{164}\right)\sin\frac{5\pi}{a}x\sin\frac{4\pi}{b}y$$

$$+\frac{\left(\frac{\pi}{a}\right)^2\left(\frac{\pi}{b}\right)^2}{\left[\left(\frac{7\pi}{a}\right)^2+\left(\frac{2\pi}{b}\right)^2\right]^2}\left(350\bar{A}_{14}+126A_{168}-1694A_{169}\right)\sin\frac{7\pi}{a}x\sin\frac{2\pi}{b}y$$

$$+\frac{\left(\frac{\pi}{a}\right)^2\left(\frac{\pi}{b}\right)^2}{\left[\left(\frac{7\pi}{a}\right)^2+\left(\frac{4\pi}{b}\right)^2\right]}\left(28A_{169}\right)\sin\frac{7\pi}{a}x\sin\frac{4\pi}{b}y$$

with

$$A_{14}=\frac{Eh^3}{128D}\frac{16\left(\frac{\pi}{a}\right)^4}{\left(\frac{\pi}{b}\right)^2\left[\left(\frac{2\pi}{a}\right)^2+\left(\frac{3\pi}{b}\right)^2\right]}\qquad \bar{A}_{14}=\frac{Eh^3}{128D}\frac{\left(\frac{\pi}{b}\right)^4}{\left(\frac{2\pi}{a}\right)^2\left[\left(\frac{\pi}{b}\right)^2+\left(\frac{6\pi}{a}\right)^2\right]}$$

(c) Frequency Parameter

$$\mu = \mu^{(0)} + \varepsilon^2 \mu^{(2)} + \varepsilon^4 \mu^{(4)} + \cdots$$

in which

$$\mu^{(0)} = -3\left(\frac{\pi}{a}\right)^2 \frac{D}{h}\left[\left(\frac{\pi}{a}\right)^2 + \left(\frac{\pi}{b}\right)^2\right]$$

$$\mu^{(2)} = -\frac{Eh^2}{16(1-\nu^2)} \frac{\left[\left(\frac{\pi}{a}\right)^2 + \left(\frac{\pi}{b}\right)^2\right]}{\left[4\left(\frac{\pi}{a}\right)^2 + \left(\frac{\pi}{b}\right)^2\right]} \left\{(3-\nu^2)\left[16\left(\frac{\pi}{a}\right)^4 + \left(\frac{\pi}{b}\right)^4\right] + 16\nu\left(\frac{\pi}{a}\right)^2\left(\frac{\pi}{b}\right)^2\right\}$$

$$+ \frac{Eh^2}{8(1-\nu^2)}\left[4\left(\frac{\pi}{a}\right)^4 + \left(\frac{\pi}{b}\right)^4 + 5\nu\left(\frac{\pi}{a}\right)^2\left(\frac{\pi}{b}\right)^2\right] + \frac{Eh^2}{16}\left\{4\left(\frac{\pi}{a}\right)^4 + 4\left(\frac{\pi}{b}\right)^4 + \frac{\left(\frac{\pi}{a}\right)^4\left(\frac{\pi}{b}\right)^4}{\left[\left(\frac{3\pi}{a}\right)^2 + \left(\frac{2\pi}{b}\right)^2\right]^2}\right.$$

$$\left. + \frac{81\left(\frac{\pi}{a}\right)^4\left(\frac{\pi}{b}\right)^4}{\left[\left(\frac{\pi}{a}\right)^2 + \left(\frac{2\pi}{b}\right)^2\right]^2}\right\}$$

$$\mu^{(4)} = \frac{Eh^2}{16}\left\{\frac{3\left[\left(\frac{\pi}{a}\right)^2 + \left(\frac{\pi}{b}\right)^2\right]\left[16\left(\frac{\pi}{a}\right)^4 A_{14} + \left(\frac{\pi}{b}\right)^4 \bar{A}_{14}\right]}{\left[\left(\frac{2\pi}{a}\right)^2 + \left(\frac{\pi}{b}\right)^2\right]} - \left(\frac{\pi}{a}\right)^4 (8A_{14} + 4A_{166})\right.$$

$$- \left(\frac{\pi}{b}\right)^4 (3A_{162} + A_{168}) + \frac{9\left(\frac{\pi}{a}\right)^4\left(\frac{\pi}{b}\right)^4}{\left[\left(\frac{\pi}{a}\right)^2 + \left(\frac{2\pi}{b}\right)^2\right]^2}(-2A_{14} + 25A_{162} + 9A_{164} - 25A_{166})$$

$$\left. + \frac{\left(\frac{\pi}{a}\right)^4\left(\frac{\pi}{b}\right)^4}{\left[\left(\frac{3\pi}{a}\right)^2 + \left(\frac{2\pi}{b}\right)^2\right]^2}(-50A_{14} - 49A_{168} - 49A_{166} + A_{169})\right\}$$

(ii) Vibration Mode p = 2, q = 1

(a) Deflection

$$w = w^{(0)} + \varepsilon^2 w^{(2)} + \varepsilon^4 w^{(4)} + \cdots$$

in which

$$w^{(0)} = \sin\frac{2\pi}{a}x \sin\frac{\pi}{b}y$$

$$w^{(2)} = 3\left[A_{14}\sin\frac{2\pi}{a}x \sin\frac{3\pi}{b}y + \bar{A}_{14}\sin\frac{6\pi}{a}x \sin\frac{\pi}{b}y\right]$$

$$w^{(4)} = 5\left[A_{151}\sin\frac{2\pi}{a}x\sin\frac{3\pi}{b}y + \bar{A}_{151}\sin\frac{6\pi}{a}x\sin\frac{\pi}{b}y + A_{152}\sin\frac{6\pi}{a}x\sin\frac{3\pi}{b}y\right.$$

$$+ A_{153}\sin\frac{10\pi}{a}x\sin\frac{\pi}{b}y + \bar{A}_{153}\sin\frac{2\pi}{a}x\sin\frac{\pi}{b}y + A_{154}\sin\frac{10\pi}{a}x\sin\frac{3\pi}{b}y$$

$$\left. + \bar{A}_{154}\sin\frac{6\pi}{a}x\sin\frac{5\pi}{b}y\right]$$

$$+ 2\lambda_2' h\left\{\frac{\left[\left(\frac{2\pi}{a}\right)^2 - 3\left(\frac{\pi}{b}\right)^2\right]A_{14}}{\left(\frac{2\pi}{b}\right)^2\left[\left(\frac{2\pi}{a}\right)^2 + \left(\frac{3\pi}{b}\right)^2\right]D}\sin\frac{2\pi}{a}x\sin\frac{3\pi}{b}y + \frac{\left[\left(\frac{\pi}{b}\right)^2 - 3\left(\frac{2\pi}{a}\right)^2\right]\bar{A}_{14}}{\left(\frac{4\pi}{a}\right)^2\left[\left(\frac{\pi}{b}\right)^2 + \left(\frac{6\pi}{a}\right)^2\right]D}\sin\frac{6\pi}{a}x\sin\frac{\pi}{b}y\right\}$$

with

$$\lambda_2' = \frac{Eh^2}{16(1-\nu^2)}\frac{1}{\left[\left(\frac{2\pi}{a}\right)^2 + \left(\frac{\pi}{b}\right)^2\right]}\left\{(3-\nu^2)\left[\left(\frac{2\pi}{a}\right)^4 + \left(\frac{\pi}{b}\right)^4\right] + 4\nu\left(\frac{2\pi}{a}\right)^2\left(\frac{\pi}{b}\right)^2\right\}$$

$$A_{151} = (A_{51})_{\substack{m=2\\n=1}} \qquad \bar{A}_{151} = (\bar{A}_{51})_{\substack{m=2\\n=1}}$$

$$A_{152} = (A_{52})_{\substack{m=2\\n=1}}$$

$$A_{153} = (A_{53})_{\substack{m=2\\n=1}} \qquad \bar{A}_{153} = (\bar{A}_{53})_{\substack{m=2\\n=1}}$$

$$A_{154} = (A_{54})_{\substack{m=2\\n=1}} \qquad \bar{A}_{154} = (\bar{A}_{54})_{\substack{m=2\\n=1}}$$

(b) Membrane Stresses

$$t_{ij}' = \varepsilon t_{ij}^{(1)} + \varepsilon^3 t_{ij}^{(3)} + \cdots$$

in which

$$t_{xx}^{(1)} = \frac{Eh}{4(1-\nu^2)}\left[\left(\frac{2\pi}{a}\right)^2 + \nu\left(\frac{\pi}{b}\right)^2 - (1-\nu^2)\left(\frac{2\pi}{a}\right)^2\cos\frac{2\pi}{b}y\right]$$

$$t_{yy}^{(1)} = \frac{Eh}{4(1-\nu^2)}\left[\left(\frac{\pi}{b}\right)^2 + \nu\left(\frac{2\pi}{a}\right)^2 - (1-\nu^2)\left(\frac{\pi}{b}\right)^2\cos\frac{4\pi}{a}x\right]$$

$$t_{xy}^{(1)} = 0$$

$$t_{xx}^{(3)} = Eh\left(\frac{2\pi}{a}\right)^2\left\{A_{14}\cos\frac{2\pi}{b}y - A_{14}\cos\frac{4\pi}{b}y - \frac{\left(\frac{\pi}{b}\right)^4}{\left[\left(\frac{2\pi}{a}\right)^2 + \left(\frac{\pi}{b}\right)^2\right]^2}4(A_{14} + \bar{A}_{14})\cos\frac{4\pi}{a}x\cos\frac{2\pi}{b}y\right.$$

$$+\frac{\left(\frac{\pi}{b}\right)^4}{\left[\left(\frac{4\pi}{a}\right)^2+\left(\frac{\pi}{b}\right)^2\right]^2}\bar{A}_{14}\cos\frac{8\pi}{a}x\cos\frac{2\pi}{b}y+\frac{\left(\frac{\pi}{b}\right)^4}{\left[\left(\frac{2\pi}{b}\right)^2+\left(\frac{2\pi}{a}\right)^2\right]^2}4A_{14}\cos\frac{4\pi}{a}x\cos\frac{4\pi}{b}y\Bigg\}$$

$$t_{yy}^{(3)}=Eh\left(\frac{\pi}{b}\right)^2\Bigg\{\bar{A}_{14}\cos\frac{4\pi}{a}x-\bar{A}_{14}\cos\frac{8\pi}{a}x-\frac{\left(\frac{2\pi}{a}\right)^4}{\left[\left(\frac{2\pi}{a}\right)^2+\left(\frac{\pi}{b}\right)^2\right]^2}4\left(\bar{A}_{14}+A_{14}\right)\cos\frac{4\pi}{a}x\cos\frac{2\pi}{b}y$$

$$+\frac{\left(\frac{2\pi}{a}\right)^4}{\left[\left(\frac{2\pi}{b}\right)^2+\left(\frac{2\pi}{a}\right)^2\right]^2}A_{14}\cos\frac{4\pi}{a}x\cos\frac{4\pi}{b}y+\frac{\left(\frac{2\pi}{a}\right)^4}{\left[\left(\frac{4\pi}{a}\right)^2+\left(\frac{\pi}{b}\right)^2\right]^2}4\bar{A}_{14}\cos\frac{8\pi}{a}x\cos\frac{2\pi}{b}y\Bigg\}$$

$$t_{xy}^{(3)}=Eh\left(\frac{2\pi}{a}\right)\left(\frac{\pi}{b}\right)\Bigg\{-\frac{\left(\frac{2\pi}{a}\right)^2\left(\frac{\pi}{b}\right)^2}{\left[\left(\frac{2\pi}{a}\right)^2+\left(\frac{\pi}{b}\right)^2\right]^2}4\left(A_{14}+\bar{A}_{14}\right)\sin\frac{4\pi}{a}x\sin\frac{2\pi}{b}y$$

$$+\frac{\left(\frac{2\pi}{a}\right)^2\left(\frac{\pi}{b}\right)^2}{\left[\left(\frac{4\pi}{a}\right)^2+\left(\frac{\pi}{b}\right)^2\right]^2}2\bar{A}_{14}\sin\frac{8\pi}{a}x\sin\frac{2\pi}{b}y+\frac{\left(\frac{2\pi}{a}\right)^2\left(\frac{\pi}{b}\right)^2}{\left[\left(\frac{2\pi}{b}\right)^2+\left(\frac{2\pi}{a}\right)^2\right]^2}2A_{14}\sin\frac{4\pi}{a}x\sin\frac{4\pi}{b}y\Bigg\}$$

(c) Frequency Parameter

$$\mathcal{M}=\mathcal{M}^{(0)}+\varepsilon^2\mathcal{M}^{(2)}+\varepsilon^4\mathcal{M}^{(4)}+\cdots$$

in which

$$\mathcal{M}^{(0)}=0$$

$$\mathcal{M}^{(2)}=\frac{Eh^2}{8(1-\nu^2)}\left\{(3-\nu^2)\left[\left(\frac{2\pi}{a}\right)^4+\left(\frac{\pi}{b}\right)^4\right]+4\nu\left(\frac{2\pi}{a}\right)^2\left(\frac{\pi}{b}\right)^2\right\}$$

$$\mathcal{M}^{(4)}=-\frac{3Eh^2}{4}\left[\left(\frac{2\pi}{a}\right)^4A_{14}+\left(\frac{\pi}{b}\right)^4\bar{A}_{14}\right]$$

(3) General Algebraic Expressions for ${}_{pq}\mu^{(o)}$ and ${}_{pq}\mu^{(2)}$

$$ {}_{pq}M^{(o)} = \frac{D}{h}\left[\left(\frac{p\pi}{a}\right)^2+\left(\frac{q\pi}{b}\right)^2\right]\left\{\left[\left(\frac{p\pi}{a}\right)^2+\left(\frac{q\pi}{b}\right)^2\right]-\left[\left(\frac{m\pi}{a}\right)^2+\left(\frac{n\pi}{b}\right)^2\right]\right\} $$

$$ {}_{pq}M^{(2)} = -\frac{Eh^2}{16(1-\nu^2)}\frac{\left[\left(\frac{p\pi}{a}\right)^2+\left(\frac{q\pi}{b}\right)^2\right]}{\left[\left(\frac{m\pi}{a}\right)^2+\left(\frac{n\pi}{b}\right)^2\right]}\left\{(3-\nu^2)\left[\left(\frac{m\pi}{a}\right)^4+\left(\frac{n\pi}{b}\right)^4\right]+4\nu\left(\frac{m\pi}{a}\right)^2\left(\frac{n\pi}{b}\right)^2\right\} $$

$$ +\frac{Eh^2}{8(1-\nu^2)}\left\{\left[p^2m^2\left(\frac{\pi}{a}\right)^4+q^2n^2\left(\frac{\pi}{b}\right)^4\right]+\nu\left[\left(p^2n^2+q^2m^2\right)\left(\frac{\pi^2}{ab}\right)^2\right]\right\} $$

$$ +\frac{Eh^2}{16}\left\{\left[p^2m^2\left(\frac{\pi}{a}\right)^4\delta_n^q+q^2n^2\left(\frac{\pi}{b}\right)^4\delta_m^p\right]+\frac{(pn-qm)^4\left(\frac{\pi^2}{ab}\right)^4}{\left[(p+m)^2\left(\frac{\pi}{a}\right)^2+(q+n)^2\left(\frac{\pi}{b}\right)^2\right]^2}\right. $$

$$ +\frac{(pn+qm)^4\left(\frac{\pi^2}{ab}\right)^4}{\left[(p+m)^2\left(\frac{\pi}{a}\right)^2+(q-n)^2\left(\frac{\pi}{b}\right)^2\right]^2}\left(1+\delta_n^q\right)+\frac{(pn+qm)^4\left(\frac{\pi^2}{ab}\right)^4}{\left[(p-m)^2\left(\frac{\pi}{a}\right)^2+(q+n)^2\left(\frac{\pi}{b}\right)^2\right]^2}\left(1+\delta_m^p\right) $$

$$ \left.+\frac{(pn-qm)^4\left(\frac{\pi^2}{ab}\right)^4}{\left[(p-m)^2\left(\frac{\pi}{a}\right)^2+(q-n)^2\left(\frac{\pi}{b}\right)^2\right]^2}\left(1+\delta_m^p+\delta_n^q\right)\right\} $$

APPENDIX B

VIBRATIONS OF A SIMPLY SUPPORTED RECTANGULAR PLATE UNDER UNIAXIAL EDGE COMPRESSION

This problem concerns itself with the vibrations of a simply supported rectangular plate which is subjected to prescribed total edge thrusts at $x = 0$ and $x = a$. The differential equation governing the static deflection of the plate is again

$$D\Delta\Delta W - h(\lambda t^{o}_{ij} + T'_{ij})W_{,ij} = 0 \tag{B.1}$$

in which

$$t^{o}_{ij} = \begin{bmatrix} -1 & 0 \\ 0 & 0 \end{bmatrix} \tag{B.2}$$

$$T'_{ij} = \frac{1}{2} \left\langle W_{,i} W_{,j} \right\rangle \tag{B.3}$$

The operator (B.3) is identified with the same set of equations as in the main body of the paper, except for a change in the boundary conditions. That is, instead of $U'(a,y)$ and $V'(x,b)$ vanishing, the new boundary conditions read

$$U'(a,y) = k_1 \tag{B.4}$$

$$V'(x,b) = k_2 \tag{B.5}$$

in which k_1 and k_2 are determined from

$$\int_0^b T'_{xx}(a,y)dy = 0 \tag{B.6}$$

$$\int_0^a T'_{yy}(x,b)dx = 0 \tag{B.7}$$

Alternately, the previous set of boundary conditions may be used and two uniform additional tensile stresses, one in the x direction and the

other in the y direction, may be superimposed so as to satisfy Equations (B.6) and (B.7). In the dynamic case, this problem has the same differential equation and same boundary conditions as in the main body of the paper except t^{o}_{ij} takes the form of Equation (B.2). The method of solution for this problem is the same perturbation method presented in Chapter III and hence it is not repeated here.

The general algebraic expressions for the static deflection, the static additional membrane stresses, the load parameter and the static additional membrane displacements are as follows:

$$W = \epsilon W^{(1)} + \epsilon^3 W^{(3)} + \ldots . \tag{B.8}$$

$$T'_{ij} = \epsilon^2 T^{(2)}_{ij} + \epsilon^4 T^{(4)}_{ij} + \ldots . \tag{B.9}$$

$$\lambda = \lambda_o + \epsilon^2 \lambda + \epsilon^4 \lambda + \ldots . \tag{B.10}$$

$$U' = \epsilon^2 \left\{ \frac{h^2}{16(\frac{m\pi}{a})} \left[-(\frac{m\pi}{a})^2 + \nu(\frac{n\pi}{b})^2 + (\frac{m\pi}{a})^2 \cos \frac{2n\pi}{b} y \right] \sin \frac{2m\pi}{a} x - \frac{(\frac{m\pi}{a})^2 h^2}{8} x \right\}$$

$$+ \ldots . \tag{B.11}$$

$$V' = \epsilon^2 \left\{ \frac{h^2}{16(\frac{n\pi}{b})} \left[-(\frac{n\pi}{b})^2 + \nu(\frac{m\pi}{a})^2 + (\frac{n\pi}{b})^2 \cos \frac{2m\pi}{a} x \right] \sin \frac{2n\pi}{b} y - \frac{(\frac{n\pi}{b})^2 h^2}{8} y \right\}$$

$$+ \ldots . \tag{B.12}$$

in which

$$W^{(1)} = h \sin \frac{m\pi}{a} x \sin \frac{n\pi}{b} y$$

$$W^{(3)} = h(B_4 \sin \frac{m\pi}{a} x \sin \frac{3n\pi}{b} y + \bar{B}_4 \sin \frac{3m\pi}{a} x \sin \frac{n\pi}{b} y)$$

$$T^{(2)}_{xx} = - \frac{Eh^2}{8} (\frac{m\pi}{a})^2 \cos \frac{2n\pi}{b} y$$

$$T^{(2)}_{yy} = - \frac{Eh^2}{8} (\frac{n\pi}{b})^2 \cos \frac{2m\pi}{a} x$$

$$T^{(2)}_{xy} = 0$$

$$T_{xx}^{(4)} = \frac{Eh^2}{4}\left(\frac{m\pi}{a}\right)^2\left\{B_4\cos\frac{2n\pi}{b}y - B_4\cos\frac{4n\pi}{b}y - \frac{4\left(\frac{n\pi}{b}\right)^4}{\left[\left(\frac{m\pi}{a}\right)^2+\left(\frac{n\pi}{b}\right)^2\right]^2}(B_4+\bar{B}_4)\right.$$

$$\cos\frac{2m\pi}{a}x\cos\frac{2n\pi}{b}y + \frac{\left(\frac{n\pi}{b}\right)^4}{\left[\left(\frac{2m\pi}{a}\right)^2+\left(\frac{n\pi}{b}\right)^2\right]^2}\bar{B}_4\cos\frac{4m\pi}{a}x\cos\frac{2n\pi}{b}y$$

$$\left. + \frac{4\left(\frac{n\pi}{b}\right)^4}{\left[\left(\frac{2n\pi}{b}\right)^2+\left(\frac{m\pi}{a}\right)^2\right]^2}B_4\cos\frac{2m\pi}{a}x\cos\frac{4n\pi}{b}y\right\}$$

$$T_{yy}^{(4)} = \frac{Eh^2}{4}\left(\frac{n\pi}{b}\right)^2\left\{\bar{B}_4\cos\frac{2m\pi}{a}x - \bar{B}_4\cos\frac{4m\pi}{a}x - \frac{4\left(\frac{m\pi}{a}\right)^4}{\left[\left(\frac{m\pi}{a}\right)^2+\left(\frac{n\pi}{b}\right)^2\right]^2}(B_4+\bar{B}_4)\right.$$

$$\cos\frac{2m\pi}{a}x\cos\frac{2n\pi}{b}y + \frac{\left(\frac{m\pi}{a}\right)^4}{\left[\left(\frac{m\pi}{a}\right)^2+\left(\frac{2n\pi}{b}\right)^2\right]^2}B_4\cos\frac{2m\pi}{a}x\cos\frac{4n\pi}{b}y$$

$$\left. + \frac{4\left(\frac{m\pi}{a}\right)^4}{\left[\left(\frac{2m\pi}{a}\right)^2+\left(\frac{n\pi}{b}\right)^2\right]^2}\bar{B}_4\cos\frac{4m\pi}{a}x\cos\frac{2n\pi}{b}y\right\}$$

$$T_{xy}^{(4)} = \frac{Eh^2}{4}\left(\frac{m\pi}{a}\right)\left(\frac{n\pi}{b}\right)\left\{ - \frac{4\left(\frac{m\pi}{a}\right)^2\left(\frac{n\pi}{b}\right)^2}{\left[\left(\frac{m\pi}{a}\right)^2+\left(\frac{n\pi}{b}\right)^2\right]^2}(B_4+\bar{B}_4)\sin\frac{2m\pi}{a}x\sin\frac{2n\pi}{b}y\right.$$

$$+ \frac{2\left(\frac{m\pi}{a}\right)^2\left(\frac{n\pi}{b}\right)^2}{\left[\left(\frac{2m\pi}{a}\right)^2+\left(\frac{n\pi}{b}\right)^2\right]^2}\bar{B}_4\sin\frac{4m\pi}{a}x\sin\frac{2n\pi}{b}y + \frac{2\left(\frac{m\pi}{a}\right)^2\left(\frac{n\pi}{b}\right)^2}{\left[\left(\frac{m\pi}{a}\right)^2+\left(\frac{2n\pi}{b}\right)^2\right]^2}B_4$$

$$\left.\sin\frac{2m\pi}{a}x\sin\frac{4n\pi}{b}y\right\}$$

$$\lambda_o = \frac{D}{h}\left[\frac{(\frac{m\pi}{a})^2+(\frac{n\pi}{b})^2}{(\frac{m\pi}{a})}\right]^2$$

$$\lambda_2 = \frac{Eh^2}{16}\left[\frac{(\frac{m\pi}{a})^4+(\frac{n\pi}{b})^4}{(\frac{m\pi}{a})^2}\right]$$

$$\lambda_4 = -\frac{3Eh^2}{16}\left[\frac{(\frac{m\pi}{a})^4 B_4 + (\frac{n\pi}{b})^4 \bar{B}_4}{(\frac{m\pi}{a})^2}\right]$$

$$B_4 = \frac{3(1-\nu^2)(\frac{m\pi}{a})^4}{64(\frac{n\pi}{b})^2[(\frac{m\pi}{a})^2+5(\frac{n\pi}{b})^2]}$$

$$\bar{B}_4 = \frac{6(1-\nu^2)(\frac{n\pi}{b})^4}{64[9(\frac{m\pi}{a})^4-(\frac{n\pi}{b})^4]}$$

Note that λ now becomes the ratio of the prescribed compression to that required for the initial instability. Let ζ be the ratio of the edge displacement caused by the prescribed edge compression to that required for the initial instability; then ζ is related to λ by

$$\zeta = \frac{\lambda u^o + \frac{1}{b}\int_o^b U'(a,y)dy}{\lambda_o u^o} \qquad (B.13)$$

The λ versus ζ curve is now the load-shortening curve. The lowest buckling mode is given by $m = a/b$ and $n = 1$.

The general algebraic expressions for the deflection and the frequency parameter of the vibration mode $p = q = 1$ about the buckled configuration $m = n = 1$ are

$$w = h \sin\frac{\pi}{a}x \sin\frac{\pi}{b}y + \epsilon^2 3h(B_{14}\sin\frac{\pi}{a}x \sin\frac{3\pi}{b}y + \bar{B}_{14}\sin\frac{3\pi}{a}x \sin\frac{\pi}{b}y)$$

$$+ \ldots.$$

$$\mu = \epsilon^2 \frac{Eh^2}{8}\left[\left(\frac{\pi}{a}\right)^4 + \left(\frac{\pi}{b}\right)^4\right] - \epsilon^4 \frac{3Eh^2}{4}\left[\left(\frac{\pi}{a}\right)^4 B_{14} + \left(\frac{\pi}{b}\right)^4 \bar{B}_{14}\right] + \ldots.$$

in which

$$B_{14} = \frac{3(1-\nu^2)\left(\frac{\pi}{a}\right)^4}{64\left(\frac{\pi}{b}\right)^2\left[\left(\frac{\pi}{a}\right)^2+5\left(\frac{\pi}{b}\right)^2\right]}$$

$$\bar{B}_{14} = \frac{6(1-\nu^2)\left(\frac{\pi}{b}\right)^4}{64\left[9\left(\frac{\pi}{a}\right)^4-\left(\frac{\pi}{b}\right)^4\right]}$$

The general expressions for the frequency parameter of the vibration modes $p = 1, q = 1$ and $p = 2, q = 1$ about the buckled configuration $m = 2, n = 1$ are

$$_{11}\mu = \frac{D}{h}\left[-3\left(\frac{\pi}{a}\right)^4 + \frac{3}{4}\left(\frac{\pi}{b}\right)^4 + \epsilon^2 \frac{Eh^2}{16}\left\{\frac{15}{4}\left(\frac{\pi}{b}\right)^4 + \frac{\left(\frac{\pi}{a}\right)^4\left(\frac{\pi}{b}\right)^4}{\left[\left(\frac{3\pi}{a}\right)^2+\left(\frac{2\pi}{b}\right)^2\right]^2}\right.\right.$$

$$+ \left.\frac{81\left(\frac{\pi}{a}\right)^4\left(\frac{\pi}{b}\right)^4}{\left[\left(\frac{\pi}{a}\right)^2+\left(\frac{2\pi}{b}\right)^2\right]^2}\right\} + \epsilon^4\frac{Eh^2}{16}\left\{\left(\frac{\pi}{a}\right)^4(4B_{24}-4B_{66})+\left(\frac{\pi}{b}\right)^4\left(\frac{3}{4}\bar{B}_{24}+3B_{62}-3B_{68}\right)\right.$$

$$+ \frac{9\left(\frac{\pi}{a}\right)^4\left(\frac{\pi}{b}\right)^4}{\left[\left(\frac{\pi}{a}\right)^2+\left(\frac{2\pi}{b}\right)^2\right]^2}\left(-2B_{24}+25B_{62}+9B_{64}-25B_{66}\right)$$

$$+ \left.\frac{\left(\frac{\pi}{a}\right)^4\left(\frac{\pi}{b}\right)^4}{\left[\left(\frac{3\pi}{a}\right)^2+\left(\frac{2\pi}{b}\right)^2\right]^2}\left(-50B_{24}-49B_{68}-49B_{66}+B_{69}\right)\right\} + \ldots.$$

$$_{21}\mu = \epsilon^2 \frac{Eh^2}{8}\left[\left(\frac{2\pi}{a}\right)^4 + \left(\frac{\pi}{b}\right)^4\right] - \epsilon^4 \frac{3Eh^2}{4}\left[\left(\frac{2\pi}{a}\right)^4 B_{24} + \left(\frac{\pi}{b}\right)^4 \bar{B}_{24}\right] + \ldots.$$

in which

$$B_{24} = \frac{3(1-\nu^2)(\frac{\pi}{a})^4}{4(\frac{\pi}{b})^2[4(\frac{\pi}{a})^2+5(\frac{\pi}{b})^2]}$$

$$\bar{B}_{24} = \frac{3(1-\nu^2)(\frac{\pi}{b})^4}{32[144(\frac{\pi}{a})^4-(\frac{\pi}{b})^4]}$$

$$B_{62} = \frac{3(1-\nu^2)}{4[48(\frac{\pi}{a})^4-2(\frac{\pi}{b})^4]}\{-3(\frac{\pi}{b})^4 - \frac{225(\frac{\pi}{a})^4(\frac{\pi}{b})^4}{[(\frac{\pi}{a})^2+(\frac{2\pi}{b})^2]}\}$$

$$B_{64} = \frac{-3(1-\nu^2)}{4[48(\frac{\pi}{a})^4 + 144(\frac{\pi}{a})^2(\frac{\pi}{b})^2 + 78(\frac{\pi}{b})^4]}\{\frac{81(\frac{\pi}{a})^4(\frac{\pi}{b})^4}{[(\frac{\pi}{a})^2+(\frac{2\pi}{b})^2]^2}\}$$

$$B_{66} = \frac{3(1-\nu^2)}{4[16(\frac{\pi}{a})^2(\frac{\pi}{b})^2 + 80(\frac{\pi}{b})^4]}\{\frac{225(\frac{\pi}{a})^4(\frac{\pi}{b})^4}{[(\frac{\pi}{a})^2+(\frac{2\pi}{b})^2]^2} + \frac{49(\frac{\pi}{a})^4(\frac{\pi}{b})^4}{[(\frac{3\pi}{a})^2+(\frac{2\pi}{b})^2]^2} + 4(\frac{\pi}{a})^4\}$$

$$B_{68} = \frac{3(1-\nu^2)}{4[528(\frac{\pi}{a})^4 - 6(\frac{\pi}{b})^4]}\{\frac{49(\frac{\pi}{a})^4(\frac{\pi}{b})^4}{[(\frac{3\pi}{a})^2+(\frac{2\pi}{b})^2]^2} + 3(\frac{\pi}{b})^4\}$$

$$B_{69} = \frac{-3(1-\nu^2)}{4[528(\frac{\pi}{a})^4 + 400(\frac{\pi}{a})^2(\frac{\pi}{b})^2 + 74(\frac{\pi}{b})^4]}\{\frac{(\frac{\pi}{a})^4(\frac{\pi}{b})^4}{[(\frac{3\pi}{a})^2+(\frac{2\pi}{b})^2]}\}$$

The general expressions for the frequency parameter of the vibration modes $p = 1\ q = 1$, $p = 2\ q = 1$, $p = 2\ q = 2$ and $p = 3\ q = 1$ about the buckled configuration $m = 3,\ n = 1$ are

$$_{11}\mu = \frac{D}{h}[-8(\frac{\pi}{a})^4 + \frac{8}{9}(\frac{\pi}{b})^4] + \epsilon^2\frac{Eh^2}{16}\{\frac{35}{9}(\frac{\pi}{b})^4 + \frac{(\frac{\pi}{a})^4(\frac{\pi}{b})^4}{[(\frac{2\pi}{a})^2+(\frac{\pi}{b})^2]^2} + \frac{16(\frac{\pi}{a})^4(\frac{\pi}{b})^4}{[(\frac{\pi}{a})^2+(\frac{\pi}{b})^2]^2}\}$$

$$+ \ldots.$$

$$21^{\mu} = \frac{D}{h}\left[-20\left(\frac{\pi}{a}\right)^4 + \frac{5}{9}\left(\frac{\pi}{b}\right)^4\right] + \epsilon^2 \frac{Eh^2}{16}\left\{\left(\frac{641}{128} - \frac{4}{9}\right)\left(\frac{\pi}{b}\right)^4 + \frac{\left(\frac{\pi}{a}\right)^4\left(\frac{\pi}{b}\right)^4}{\left[\left(\frac{4\pi}{a}\right)^2+\left(\frac{2\pi}{b}\right)^2\right]^2}\right.$$

$$\left. + \frac{625\left(\frac{\pi}{a}\right)^4\left(\frac{\pi}{b}\right)^4}{\left[\left(\frac{2\pi}{a}\right)^2+\left(\frac{2\pi}{b}\right)^2\right]^2}\right\} + \epsilon^4 \frac{Eh^2}{16}\left\{\left(\frac{\pi}{a}\right)^4(72B_{34}-36B_{166})+\left(\frac{\pi}{b}\right)^4\left(\frac{4}{3}\bar{B}_{34}+3B_{162}-3B_{167}\right)\right.$$

$$+ \frac{\left(\frac{\pi}{a}\right)^4\left(\frac{\pi}{b}\right)^4}{\left[\left(\frac{\pi}{a}\right)^2+\left(\frac{2\pi}{b}\right)^2\right]^2}\left(-450B_{34}-1225B_{166}+1225B_{166}-625B_{164}\right)$$

$$\left. + \frac{\left(\frac{\pi}{a}\right)^4\left(\frac{\pi}{b}\right)^4}{\left[\left(\frac{5\pi}{a}\right)^2+\left(\frac{2\pi}{b}\right)^2\right]^2}\left(-162B_{34}-121B_{166}-121B_{167}-B_{169}\right)\right\} + \ldots.$$

$$22^{\mu} = \frac{D}{h}\left[-20\left(\frac{\pi}{a}\right)^4 + 24\left(\frac{\pi}{a}\right)^2\left(\frac{\pi}{b}\right)^2 - \frac{140}{9}\left(\frac{\pi}{b}\right)^4\right] + \epsilon^2 \frac{Eh^2}{16}\left\{-36\left(\frac{\pi}{a}\right)^4 - \frac{4}{9}\left(\frac{\pi}{b}\right)^4\right.$$

$$\left. + \frac{256\left(\frac{\pi}{a}\right)^4\left(\frac{\pi}{b}\right)^4}{\left[\left(\frac{5\pi}{a}\right)^2+\left(\frac{3\pi}{b}\right)^2\right]^2} + \frac{4096\left(\frac{\pi}{a}\right)^4\left(\frac{\pi}{b}\right)^4}{\left[\left(\frac{5\pi}{a}\right)^2+\left(\frac{\pi}{b}\right)^2\right]^2} + \frac{4096\left(\frac{\pi}{a}\right)^4\left(\frac{\pi}{b}\right)^4}{\left[\left(\frac{\pi}{a}\right)^2+\left(\frac{3\pi}{b}\right)^2\right]^2} + \frac{256\left(\frac{\pi}{a}\right)^4\left(\frac{\pi}{b}\right)^4}{\left[\left(\frac{\pi}{a}\right)^2+\left(\frac{\pi}{b}\right)^2\right]^2}\right\}$$

$$+ \ldots.$$

$$31^{\mu} = \epsilon^2 \frac{Eh^2}{8}\left[\left(\frac{3\pi}{a}\right)^4+\left(\frac{\pi}{b}\right)^4\right] - \epsilon^4 \frac{3Eh^2}{4}\left[\left(\frac{3\pi}{a}\right)^4 B_{34} + \left(\frac{\pi}{b}\right)^4 \bar{B}_{34}\right] + \ldots.$$

in which

$$B_{34} = \frac{243(1-\nu^2)\left(\frac{\pi}{a}\right)^4}{64\left(\frac{\pi}{b}\right)^2\left[9\left(\frac{\pi}{a}\right)^2 + 5\left(\frac{\pi}{b}\right)^2\right]}$$

$$\bar{B}_{34} = \frac{3(1-\nu^2)\left(\frac{\pi}{b}\right)^4}{32\left[729\left(\frac{\pi}{a}\right)^4-\left(\frac{\pi}{b}\right)^4\right]}$$

$$B_{162} = \frac{3(1-\nu^2)}{4[132(\frac{\pi}{a})^4 - \frac{4}{3}(\frac{\pi}{b})^4]} \{- \frac{1225(\frac{\pi}{a})^4(\frac{\pi}{b})^4}{[(\frac{\pi}{a})^2+(\frac{2\pi}{b})^2]^2} - 3(\frac{\pi}{b})^4\}$$

$$B_{164} = \frac{3(1-\nu^2)}{4[132(\frac{\pi}{a})^4 + 256(\frac{\pi}{a})^2(\frac{\pi}{b})^2 + \frac{236}{4}(\frac{\pi}{b})^4} \{\frac{625(\frac{\pi}{a})^4(\frac{\pi}{b})^4}{[(\frac{\pi}{a})^2+(\frac{2\pi}{b})^2]^2}\}$$

$$B_{166} = \frac{3(1-\nu^2)}{4[64(\frac{\pi}{a})^2(\frac{\pi}{b})^2 + 80(\frac{\pi}{b})^4]} \{36(\frac{\pi}{a})^4 + \frac{1225(\frac{\pi}{a})^4(\frac{\pi}{b})^4}{[(\frac{\pi}{a})^2+(\frac{2\pi}{b})^2]^2} + \frac{121(\frac{\pi}{a})^4(\frac{\pi}{b})^4}{[(\frac{5\pi}{a})^2+(\frac{2\pi}{b})^2]^2}\}$$

$$B_{167} = \frac{3(1-\nu^2)}{4[3540(\frac{\pi}{a})^4 - \frac{20}{3}(\frac{\pi}{b})^4]} \{\frac{121(\frac{\pi}{a})^4(\frac{\pi}{b})^4}{[(\frac{5\pi}{a})^2+(\frac{2\pi}{b})^2]^2} + 3(\frac{\pi}{b})^4\}$$

$$B_{169} = \frac{3(1-\nu^2)}{4[3540(\frac{\pi}{a})^4 + 1024(\frac{\pi}{a})^2(\frac{\pi}{b})^2 + \frac{220}{3}(\frac{\pi}{b})^4]} \{- \frac{(\frac{\pi}{a})^4(\frac{\pi}{b})^4}{[(\frac{5\pi}{a})^2+(\frac{2\pi}{b})^2]^2}\}$$

For the cases of $a = b$ and $a = 2b$ results are shown in Figures 9 and 10.

REFERENCES

1. Willers, F. A. "Eigenschwingungen gedrückter Kreisplatten," Zeitschrift für angewandte Mathematik und Mechanik, Vol. 20, (1940), p. 37.

2. Massonnet, Ch. "Les Relations entre les Modes Normaux de Vibration et la Stabilité des Systèmes Elastiques," Bulletin des Cours et des Laboratoires d'Essais des Constructions du Génie Civil, Université de Liege, Vol. 1, 1940.

3. Lurie, H. "Lateral Vibrations as Related to Structural Stability," J. Appl. Mech., Vol. 19, No. 2, (June 1952), pp. 195-204.

4. Bolotin, V. V. Dynamische Stabilitat elastischer Systeme (German Ed.), 1956.

5. Bryan, G. H. "On the Stability of a Plane Plate under Thrusts in Its Own Plane with Application on the Buckling of the Sides of a Ship," Proc. London Math. Soc., (1891), p. 54.

6. Timoshenko, S. Theory of Elastic Stability, McGraw Hill Book Company, Inc., New York, 1936.

7. von Kármán, T. "Festigkeitsprobleme im Maschinenbau," Encylkopädie der Mathematischen Wissenshaften, Vol. IV, 4, Teubner, Leipzig, (1910), pp. 348-352.

8. Cox, H. L. Buckling of Thin Plates in Compression, Aero Research Comm., Report No. 1554, 1933.

9. Marguerre, K. Apparent Width of the Plate in Compression, NACA TM 833, 1937.

10. Levy, S. Bending of Rectangular Plates with Large Deflections, NACA TR 737, 1942.

11. Friedrichs, K. O. and Stoker, J. J. "Buckling of the Circular Plate Beyond the Critical Thrust," J. Appl. Mech., Vol. 9, (1942).

12. Friedrichs, K. O. and Stoker, J. J. "The Nonlinear Boundary Value Problem of the Buckled Plate," Amer. J. of Math., Vol. 63, (1941), pp. 839-888.

13. Alexeev, S. A. "The Postcritical Behavior of Flexible Elastic Plate," Appl. Math. and Mech. (U.S.S.R.), Vol. XX, No. 6, (1956), pp. 673-679.

14. Masur, E. F. "On the Analysis of Buckled Plates," Proc. of the Third U.S. National Congress of Applied Mechanics, (1958), pp. 411-417.

15. Schuman, L. and Back, G. Strength of Rectangular Flat Plates Under Edge Compression, NACA TR 356, 1936.

16. Ramberg, W., McPherson, A.E. and Levy, S. Experimental Study of Deformation and of Effective Width in Axially Loaded Sheet Stringer Panels, NACA TN 684, 1939.

17. Ojalvo, M. and Hull, F. H. "Effective Width of Thin Rectangular Plates," Proc. ASCE, Vol. 84, EM 3 Mech. Div., (July 1958), p. 1718.

18. Stein, M. "Behavior of Buckled Rectangular Plates," Proc. ASCE, Vol. 86, EM 2 Mech. Div., April 1960.

19. Koiter, W. T. De meedragende breedte bij groote overschrijding ker knikspanning voor verschillende inklemming der plaatranden, (The Effective Width of Flat Plates for Various Longitudinal Edge Conditions at Loads Far Beyond the Buckling Load), Rep. S. 287, National Luctvaartlaboratorium, Amsterdam, Dec., 1943.

20. Bisplinghoff, R. L. and Pian, T. H. H. "On the Vibration of Thermally Buckled Bars and Plates," Ninth International Congress for Applied Mechanics, Vol. 7, (1956), pp. 307-318.

21. Shulman, Y. On the Vibration of Thermally Stressed Plates in the Pre-buckling and Post-buckling States, Mass. Inst. of Tech., TR 25-25, Jan. 1958.

22. Herzog, B. and Masur E. F. Frequencies and Modes of Vibration of Vibration of Buckled Circular Plates, NASA TN D-2245, Feb. 1964.

23. Reissner, E. "On Transverse Vibrations of Thin Shallow Shells," Quart. Appl. Math., Vol. 13, (1955), pp. 169-176.

24. Courant, R. and Hilbert, D. Methods of Mathematical Physics, Vol. I (English Ed.), Interscience Publishers, Inc., New York, (1953), p. 281.

25. Tsien, H. S. "A Theory for the Buckling of Thin Shells," J. Aero. Sci., Vol. 9, No. 10, (Aug. 1942), pp. 373-384.

26. Friedrichs, K. O. "On the Minimum Buckling Load for Spherical Shells," Theodore von Karman Anniversary Volume, Cal. Inst. Tech., Pasadena, (1941), pp. 258-272.

27. Panov, D. U. and Feodossiev, V. I. "On the Equilibrium and Loss of Stability of Sloping Shells for Large Deflections," Prikladnaya Matematika i Mekhanika, Vol. 12, (1948), p. 389.

28. Trubert, M. R. P. and Nash, W. A. "Effect of Membrane Forces on Lateral Vibrations of Rectangular Plates," Developments in Mechanics, Vol. I, Plenum Press, New York, 1961.